GRS

Modelling the re-saturation of bentonite in final repositories in crystalline rock

Final Report

**Gesellschaft für Anlagen-
und Reaktorsicherheit
(GRS) mbH**

Modelling the re-saturation of bentonite in final repositories in crystalline rock

Final Report

Klaus-Peter Kröhn

März 2004

Abstract

Bentonite plays an important role in the design of underground repositories for toxic and radioactive waste. The hydrophilic properties of bentonite appear to be ideally suited for minimising any contact of water with the waste. However, the behaviour of bentonite at changing water contents is a very complex phenomenon which may be influenced by hydraulic, mechanical, thermal and chemical processes. Therefore, the prediction of the re-saturation process requires a numerical model. The investigations documented here aim at a re-saturation model in the context of long-term safety analyses. For this reason, such models has to be as simple as possible.

A comprehensive discussion of the microstructure of bentonite as well as the processes which might be relevant to re-saturation forms a base for providing a sound conceptual model. Applying these fundamentals to the already existing models reveals some severe deficiencies. In particular, they do not contain the central process of hydration of the clay minerals and they do not account for the hydration of water vapour in the pore space. Thus, new conceptual models are developed for the re-saturation via liquid water as well as via water vapour.

Checking these models states a major problem since the measurement of a control parameter, as e. g. the water content, requires a lot of effort. Thus, only few uptake experiments deal with the dynamics of the water content distribution in a bentonite sample. But they are of different geometrical and/or physical complexity and furthermore, they do not provide a sufficient resolution of the water content in space and in time concurrantly. Even much less investigated is the matter of re-saturation via water vapour alone. In accompanying experiments this gap is bridged and a basis for checking the new re-saturation models as well as the already existing models is created.

Additionally, the uptake experiments with water vapour show a high relevance of re-saturation via water vapour. In fact, it cannot be excluded that the main water transport mechanism is gas diffusion of vapour in the air of the pore space and that there is no two-phase flow taking place at all during re-saturation.

Table of contents

1   Introduction

In crystalline rock water is always present. Therefore, the metallic waste containers of an underground repository in this kind of host rock must be protected against a corrosive attack of the water. The geotechnical barrier between the containers and the host rock is meant to reduce the detrimental effects of water by delaying and minimising water flow in the near-field of a repository. Bentonite is considered for this purpose as a material for the backfilling and sealing of emplacement galleries and boreholes. As soon as the bentonite, which is brought in in air-dry condition, comes into contact with water, the process of re-saturation begins. The clay minerals absorb the water, swell and thereby reduce the pore volume, which also drastically reduces permeability. Incoming water is thereby stored to a certain extent in the bentonite, and the influx of further water is hindered very effectively. In fully re-saturated bentonite, the water moves very slowly due to the low permeability and also in very small volumes due to the low porosity. These characteristics make bentonite appear an ideal material for geotechnical barriers.

However, the behaviour of bentonite at changing water contents is a very complex phenomenon which may be influenced by hydraulic, mechanical, thermal and chemical processes. These processes are coupled by a range of parameters and equations of state. Some of these couplings are highly non-linear and some are still not fully understood today despite year-long and substantial research. A comprehensive and universally valid description of the processes is therefore difficult. Nevertheless, the relevant characteristics of the bentonite have to be registered so that they can be duly considered in long-term safety analyses.

The following study is restricted to the re-saturation of an initially dry or partially saturated bentonite, which represents a decisive partial aspect of the performance of bentonite barriers. By far the majority of studies of this issue were made using the US bentonite type MX-80. Here, most of the latest literature comes form Sweden. This is why the investigations summarised in this report are closely related to the conditions prevailing at the Swedish Äspö Hard Rock Laboratory.

The simulation of the re-saturation process requires a thorough description with a numerical model. So far, efforts in this respect have been aimed at covering as many of the complex coupled physical processes as possible by a model, with the result that these models

became very intricate by nature. On the other hand, a re-saturation model should be as simple as possible in the context of long-term safety analyses. The studies documented here thus represent the various attempts to come up with simple but satisfactory model-based descriptions of the re-saturation behaviour in bentonite and to validate these by way of re-saturation experiments. The results permit a completely different assessment of the relevance of the processes involved in re-saturation than previously assumed. However, these alternative interpretations have yet to be confirmed for non-isothermal conditions and increased pressures.

The first step on the way to new models is to develop an idea of the individual and coupled processes that may play a role in re-saturation. For this purpose, Chapter 2 contains a description of the microstructure of the bentonite, and a comprehensive conceptual model in the form of a FEP list (Features, Events and Processes) is given in Chapter 3. Chapter 4 contains a compilation of the currently used thermal-hydraulic-mechanical (THM) codes for the simulation of the uptake of water in the bentonite as well as an analysis of the processes considered in these codes. Since the analysis has identified some deficiencies in the codes, new, simplified re-saturation models are developed in chapters 5 to 7, namely the "advection model" for the re-saturation with liquid and the "vapour diffusion model" for the re-saturation with vapour. A first test of the advection model on a published experiment and a comparison with the results of the well-known empirical "diffusion law" are already presented here. Re-saturation experiments carried out at GRS and the corresponding results are described in Chapter 8. The experiments allow an in-depth insight into the dynamics of the hydraulic processes during re-saturation, especially since mechanical and thermal effects are largely excluded due to the simple experimental conditions. They furthermore provide the basis for the determination of a further parameter needed for the diffusion model. In Chapter 9, the new models are verified with the help of the laboratory results. Conclusions and an outlook can be found in Chapter 10. Details on some special aspects of the issue of re-saturation are compiled in the appendices.

2   Microstructure of bentonite

2.1   Composition of bentonite MX-80

The main component of MX-80 bentonite is the clay mineral montmorillonite. This mineral alone is responsible for the swelling of bentonite. Montmorillonite belongs to the smectite group of highly expandable clay minerals. The criterion to be assigned to such a group is the similarity both in molecular structure and with regard to re-saturation and sorption behaviour. The typical composition of MX-80 bentonite is: 65-75 % montmorillonite, 10-14 % quartz, 5-9 % feldspar, 3-5 % carbonate, 2-4 % mica and chlorite as well as 1-3 % heavy minerals [45].

2.2   Microstructure of montmorillonite

Chemically, montmorillonite is a layered alumosilicate. The two fundamental elements of this mineral are the tetrahedral and the octahedral compounds. At the centre of the tetrahedrons (T) is a Si^{4+} cation. The corners of the tetrahedrons are formed by oxygen atoms. Similarly, the octahedrons (O) are formed by one central Al^{3+} cation and six O or OH anions. These fundamental elements and the structure of a montmorillonite at various scales are shown in Fig. 2.1.

Tetrahedrons as well as octahedrons are each linked by common oxygen ions to form a level layer structure called "sheet". Octahedron and tetrahedron sheets are in turn linked by common ions. In the case of montmorillonite, an O sheet is linked to a T sheet at its top and bottom. Such a TOT layer forms the so-called elementary layer or lamella. Due to the ratio of tetrahedron and octahedron sheets, one also speaks of a 2:1 structure of the montmorillonite.

The elementary layer of a montmorillonite can approximately be seen as a circular disc with an average diameter of about 300 nm and a layer thickness of about one nanometre [17]. In the elementary layer, part of the Al^{3+} ions are replaced by divalent metal ions, e. g. Mg^{2+}. This results in the negative charging of this layer.
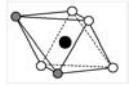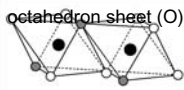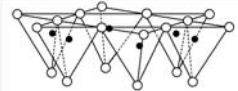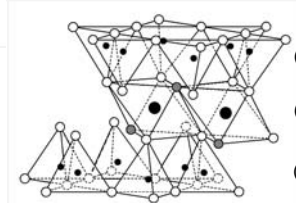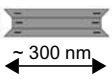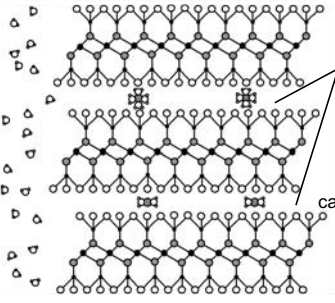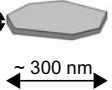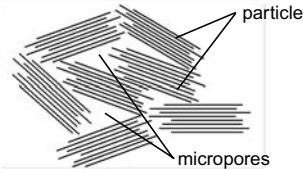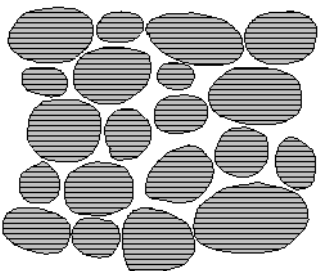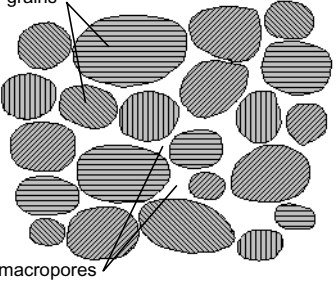
level	detailed representation	symbolic representation
atoms and molecules	octahedral element tetrahedral element octahedron sheet (O) tetrahedron sheet (T)	O^{2-} OH^- Al^{3+} Si^{4+} (T) (O)
elementary layer or lamella	(T) Si^{4+} partly replaced by Al^{3+} (O) Al^{3+} partly replaced by Fe^{2+}, Mg^{2+} (T)	~ 1 nm ~ 300 nm
particle or stack of lamellae	interlayer or interlamellar space thickness: up to 1 nm depending on the amount of hydrated water O OH Si OH Al(Mg) O Si cations +H_2O 3 - 20 lamellae depending on the interlayer cation	~3 to 40 nm ~ 300 nm
grain	3d-view 2d-representation particle micropores	~ 0.1 mm
macro-structure	grains in natural bentonite beds grains in bentonite powder grains macropores	

Fig. 2.1 The structure of montmorillonite on different scales.

lamella view after [22], particle view after [29], 3d grain view after [49] and view of the macrostructure after [45].

The elementary layers combine in stacks to form clay particles, with the lamellae being separated from each other by the so-called interlayer or interlamellar space. In a dry bentonite cations are found in the interlayer, e. g. Na^+, Mg^{2+}, Ca^{2+} or K^+. Depending on the respective interlayer cation, between three and twenty elementary layers can accumulate to form particles.

Gas cannot enter the interlamellar space even though there exists a measurable interlayer volume. Upon the entrance of water, however, water molecules deposit around the interlayer cations, which means that the interlayer ions become hydrated. This widens the interlamellar space. Depending on the amount of hydrated water, the interlayer have thicknesses of up to one nanometre. The maximum absorbable amount of water depends on the kind of interlayer cations. A detailed description of the hydration steps is given in Appendix C. As regards diffusion processes, the movement of water in the interlamellar space is negligible.

In the natural bentonite deposits, the clay particles are always arranged in the same preferred orientation owing to their genesis, which leads to a clear anisotropy of the material. The bentonite is broken up by the production process, with ensuing grain formation and arbitrary orientation of the grains. Therefore one can expect a rather more isotropic material behaviour in the compacted bentonite. The grain size of industrially processed bentonite powder is between 0.1 and 2 mm [34], [45], [46].

Due to the microstructure of the bentonite, the overall pore space is divided into two different types: first, the free space between the grains like in a classic porous medium, and second, the free volumes within the clay grains which ensue from the fact that the clay particles are irregularly arranged within the grains. However, no formal distinction of these two kinds will be made in the following.

3   General conceptual model of re-saturation

3.1   Phenomenological description

For the following considerations, the simplified assumption is made that the cavity of the underground workings V_G - as shown in Fig. 3.1 - consists exclusively of the following three volumes:

$$V_G = V_B + V_b + V_o \qquad\qquad (3.1)$$

V_G -   volume of the underground workings [m^3],
V_B -   cask volume [m^3],
V_b -   bentonite volume [m^3] and
V_o -   open volume [m^3].
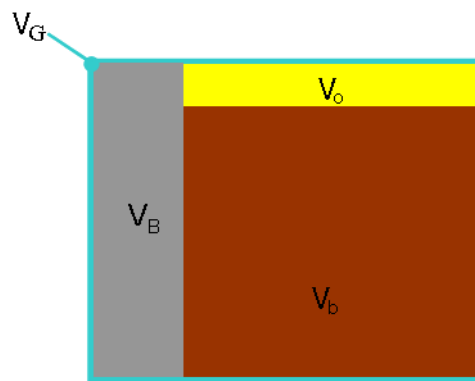
Fig. 3.1   Characteristic volumes in a bentonite for the phenomenological description

In this context, the open volume describes the volume which is not filled for technical reasons when the bentonite is put into place. The volume of the underground workings is in principle variable. For the following phenomenological description of re-saturation, however, it is assumed as being constant.

As soon as unsaturated bentonite gets into contact with water, its structure changes with the uptake of the liquid. As a result of the hydration of water molecules between the elementary layers of the clay minerals - in the so-called interlayer - the elementary layers are pushed apart and the clay minerals expand. For a phenomenological description of re-saturation it is therefore expedient to divide the bentonite volume V_b again into three areas:

$$V_b = V_s + V_i + V_p \qquad\qquad (3.2)$$

V_s - volume of the solid fraction on the bentonite [m^3],

V_i - volume of the interlayer [m^3] and

V_P - pore volume [m^3].

During re-saturation, four characteristic conditions can be observed, which are sketched in Figure 3.2 and are explained in more detail below:

- Condition I: condition at fitting
- Condition II: start of bentonite restraining
- Condition III: maximum swelling
- Condition IV: maximum re-saturation
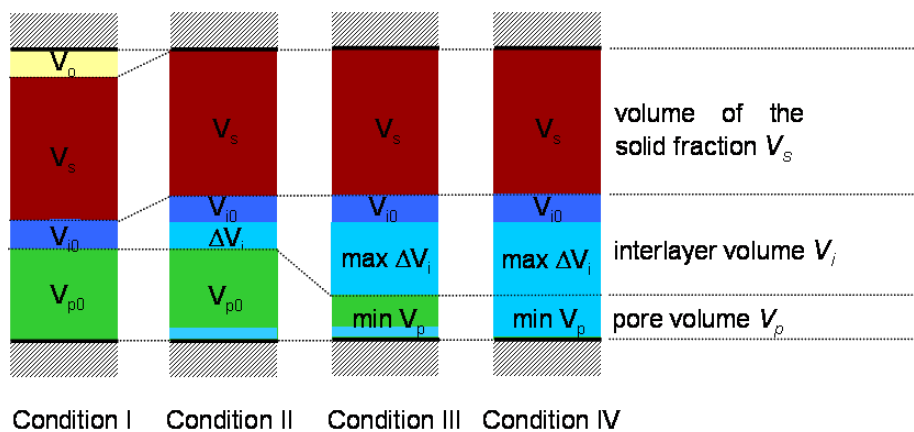
Fig. 3.2 Volume changes during the re-saturation of bentonite

Condition I is the situation immediately following the fitting of the bentonite. The degree of initial compaction determines the size of the initial pore volume V_{p0}. There has not yet been any contact with liquid water. In this condition, due to the humidity of the ambient air, there is already hydrated water present in the bentonite. This condition of the bentonite is also referred to as "air-dry". The interlayer therefore have an initial volume V_{i0} which corresponds to the amount of water that has already been absorbed. The same applies - albeit to a lesser extent - to oven-dry bentonite. Even after drying of the bentonite

at 105 °C until its constant weight is reached there still remains a certain, albeit small amount of hydrated water in the bentonite. Here as well as in the following, the term "amount" is used synonymously with the term "mass".

The water in the interlamellar space is nearly immobile. From the charging density of a smectite and the dimensions of an elementary cell in the SiO_4 tetrahedron layer it is possible to estimate the density of the hydrated water in the interlayer. In Appendix C, density values are derived in this way. According to these values, the density of the water in the interlayer differs only slightly from the density of the unbound water and is therefore equated here in first-order approximation.

Entering water will transform the bentonite from Condition I to Condition II. The water is absorbed from the pore space, enters the interlayer through hydration and there occupies an additional volume ΔV_i. In this context, the ratio of the process velocities of flow and hydration determines the amount of water remaining in the pore volume. The volume of entering water is shown in light blue in Figure 3.2 in order to distinguish it from the hydrated water - shown in dark blue - contained in the bentonite in Condition I.

For simplification, it is assumed that the bentonite will initially swell into the open volume without reducing the pore volume. This means that the open volume V_o will decrease by the same degree that the volume of the interlayer increases. Condition II is the situation in which the open volume has just completely disappeared. Each further swelling is hindered by the restraint of the bentonite in the volume of the underground workings and is therefore related to the build-up of a swelling pressure.

For the transition from Condition II to Condition III, the flow of water through the pore space has to continue. Furthermore, the driving force of hydration - the gradient in the chemical potential between the pore water and the water in the interlayer - has to keep up as well. Under these conditions, the accumulation of water in the interlayer continues and subsequently reduces the pore volume since the interlayer water and the solid fraction in the bentonite can be considered as incompressible. The pore volume does, however, not disappear completely. At the end of hydration, there remains a pore volume of the size min V_p. The reaching of this minimum porosity marks Condition III.

If re-saturation only takes place via water vapour and not via liquid water, Condition III is at the same time also the end condition of the re-saturation process. The pore volume is then filled with air that is saturated with vapour. In the case of re-saturation via liquid water, the bentonite can absorb more water in its pores until Condition IV - the condition of full saturation of the bentonite with water - has been reached. However, since the residual porosity of saturated bentonite is only a few percent, the differences of water content between Condition III and Condition IV is small.

3.2 Description as a FEP list

3.2.1 Structure of the list

In order to come from the qualitative consideration of the re-saturation of the bentonite to a quantitative description, it is necessary to identify the physical processes that play a role in re-saturation. Here it soon becomes obvious that these processes influence each other in many ways and thereby form a complex network of interdependencies. The first step on the way to a mathematical model therefore consists of creating a conceptual model of the re-saturation of the bentonite used as sealing material in underground repositories.

The conceptual model is represented in the form of a list of features, events and processes (FEPs) that are relevant in connection with re-saturation. Starting point of the FEP list is a compilation of the central FEPs that are relevant for the description of re-saturation. These FEPs are ranked in the upper levels of a hierarchical structure of FEPs. This, however, is not an expression of the highest priority of these FEPs but the result of a previous arrangement process in which the number of FEPs at the top level was minimised.

The FEPs of one level may be dependent on further FEPs on the next lower level. Depending on how far these dependencies are pursued, there will be more or fewer FEP levels. To avoid repetition, FEPs that influence more than one other FEP are placed at the top level. This way, a FEP may also be dependent of another FEP at a higher level and thus allow recursions.

10

The FEPs at the top level are divided into three groups:

- volumes,
- variables and
- processes.

Each FEP of the top level is briefly explained in a special sub-chapter. These sub-chapters also contain in tabular form the dependencies on other FEPs. To illustrate the mutual dependencies of the FEPs, the table also indicates the level of each individual FEP and some of the most important conditional equations.

Each FEP may be dependent on another FEP of the top level. Where this is so, it is shown by bold print and by italics. This makes it possible to do without a further break-down of the dependencies at these points.

When the FEP list was compiled, FEPs were identified which are not considered in the conceptual model because they are either of subordinated relevance or have not yet been sufficiently investigated. With a view to a possible re-assessment of the relevance or new research results, however, these FEPs are nevertheless included in the list, where they are marked by being printed in grey.

It should generally be noted here that the FEP list that is presented cannot claim to be a lastingly valid conceptual model but merely mirrors the current state of knowledge. Moreover, the break-down of the FEPs is done with a view to the concrete aim of re-saturation of a bentonite buffer in a repository. In this respect, the following compilation provides a possibility to enter into the complex physical coherences of bentonite re-saturation. Updating the FEP list to the latest state of knowledge and adding special problems if necessary also allows it to be used for the development or for checking purposes of new mathematical and numerical models.

3.2.2   Volumes

The initial condition considered here is Condition II as described in Chapter 3.1. The open volume thus has just disappeared, but is considered indirectly by switching from the actual initial dry density of Condition I to a reduced initial density of Condition II. The cavity of the underground workings V_G is filled completely by the volume of the waste casks V_B and the bentonite volume V_b.

For the FEP list it is necessary to have a more differentiated description of the bentonite than in the phenomenological consideration. The contemplated volumes are compiled in the following and are graphically represented for clarification in Fig. 3.3:

V_b -   bentonite volume; $V_b = V_q + V_p + V_{nq}$

V_q -   grain volume of the clay minerals; $V_q = V_s + V_i$

V_s -   solid-materials volume of the expandable material

V_i -   interlayer volume

V_{nq} -   grain volume of the non-expandable material

V_p -   pore volume
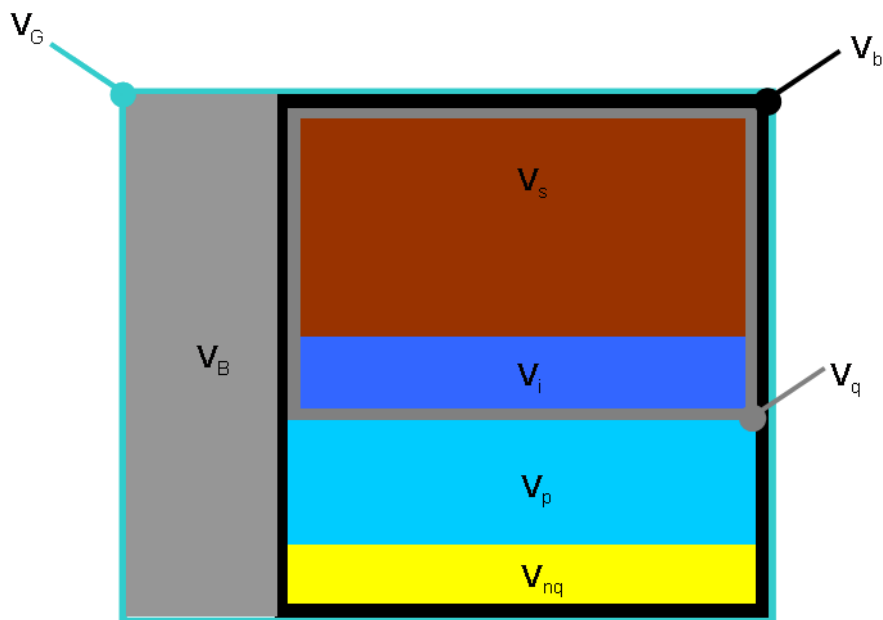
Fig. 3.3   Volumes in the bentonite

In the following, the FEPs

- pore volume,
- grain volume of the clay minerals,
- grain volume of the non-expandable material, and
- bentonite volume

are described.

3.2.2.1   Pore volume

The pore volume results from the difference between the bentonite volume and the sum of the grain volumes of the clay minerals and the non-expandable minerals. The volume of the non-expandable minerals may change through dissolution or precipitation. Salts that have entered the bentonite with the solution may also be precipitated as they remain in the pore water during hydration. These salts are then counted among the non-expandable minerals. These effects are, however, the subject of current research and are therefore not considered. Under these conditions, V_{nq} = const. applies.

Tab. 3.1   FEPs influencing the pore volume

Level	FEP	Formula
1	Pore volume	$V_p = V_b - V_q - V_{nq}$
2	***Bentonite volume (see Tab. 3.3)***	V_b
2	***Grain volume of the clay minerals (see Tab. 3.2)***	V_q
2	Grain volume of the non-expandable materials	V_{nq}

3.2.2.2   Grain volume of the clay minerals

The volume of clay minerals is composed of the volume of solid matter of the clay minerals and the volume of the interlayer. The latter is changeable due to the hydration. Heat expansion and remineralisation are neglected.

Tab. 3.2   FEPs influencing the grain volume of the clay minerals

Level	FEP	Formula
1	Grain volume of the clay minerals	$V_q = V_s + V_i$
2	Solid matter volume	V_s
2	Interlayer water volume	V_i
3	Initial water content	
3	*Hydratation (see Tab. 3.8)*	
2	Heat-induced deformation	
3	*Temperature (see Tab. 3.7)*	
3	Thermal expansion coefficient	
2	Remineralisation	

3.2.2.3   Bentonite volume

As the bentonite always fills the entire volume of the underground workings minus the volume of the waste casks emplaced, changes in the underground workings or the waste casks will also always have an effect on the bentonite volume. Changes in the volume of the underground workings ensue from displacements of the rock. Changes in the cask volume may occur when the structural integrity of the waste casks is lost due to corrosion. In contrast to the swelling of the bentonite into any additionally accessible volume that may open up as a result of the failure of casks, the extrusion of bentonite into possibly existing fractures can be neglected. The same applies to changes in the volumes of the casks due to a growing layer of corrosion.

3.2.3   Variables

The following variables form FEPs of the top level:

- amount of water in the pore volume
- saturation
- gas pressure
- temperature.

Tab. 3.3   FEPs influencing the bentonite volume

Level	FEP	Formula
1	Bentonite volume	$V_b = V_G - V_B$
2	Volume of the underground workings	$V_G = V_{G0} + \Delta V_B$
3	Initial volume of the underground workings	V_{G0}
3	Displacement of the rock	ΔV_G
4	Mechanical deformation of the rock	
4	Deformation through heat-up	
4	Supporting effect of the bentonite	
2	Cask volume	$V_B = V_{B0} + \Delta V_B$
3	Initial volume of the casks	V_{B0}
3	*Volume decrease through **corrosion** (s.Tab. 3.11)*	
3	Volume increase through cask failure	
2	*Extrusion volume into the fractures*	

3.2.3.1   Amount of water in the pore volume

Water in the pore volume may be present in liquid or gaseous form. In the following, the term "water" shall mean both conditions. Gaseous water shall be referred to as "vapour", and this shall also apply when the partial vapour pressure is below the partial saturation pressure. Hydration and corrosion are processes that extract water from the pore volume. The assumption is that these processes also occur when the water in the pore volume is exclusively in the form of vapour. Water may also be extracted from the liquid phase by precipitation and the dissolution of minerals. However, these two effects will not be considered any further following Chapter 3.2.2.1.

Owing to the low heat expansion coefficient for liquid water, it is also possible to leave heat-induced expansion unconsidered. The balancing of the amount of water in the pore volume can thus be simplified in the expression

$$m_w(t) = m_{w0} + \int_t (\dot{m}_{w\ ein} - \dot{m}_{w\ aus} - \dot{m}_{w\ hyd} - \dot{m}_{w\ kor})dt \qquad (3.3)$$

in accordance with Figure 3.4.
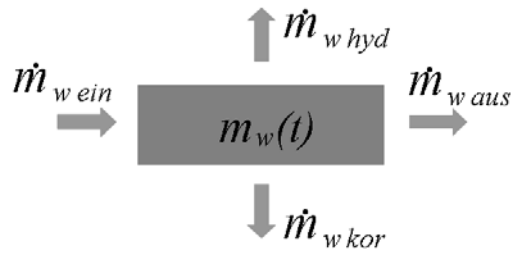
Fig. 3.4   Mass balance of the pore water

Tab. 3.4   FEPs influencing the amount of water in the pore volume

Level	FEP	Formula
1	Amount of water in the pore volume	see equation 3.3
2	Initial amount of water	$m_{w\,0}$
2	***Water transport in the pore volume (see Tab. 3.9)***	$\dot{m}_{w\,ein}, \dot{m}_{w\,aus}$
2	Water extraction through ***hydration (see Tab. 3.8)***	$\dot{m}_{w\,hyd}$
2	Water consumption through ***corrosion (see Tab. 3.11)***	$\dot{m}_{w\,kor}$
2	Water consumption through precipitation	
2	Water consumption through mineral dissolution	
2	Expansion of the liquid water through heat-up	
3	***Temperature (see Tab. 3.7)***	
3	Thermal expansion coefficient	

3.2.3.2   Saturation

As in the classic two-phase flow theory, saturation S_l is used here to refer to the volumetric fraction of the liquid phase in the pore volume. This FEP is an indicator of whether the water is present in the pore volume in one or in two phases. If both phases are present, the saturation influences the water transport via the constitutive relations of the two-phase flow.

The amount of the liquid phase ensues from the amount of water in the pore volume minus the water that is present in the form of vapour. For $0 < S_l < 1$ the assumption applies that the air in a pore is saturated with vapour to the maximum, in line with the equilibrium saturation of the solution. In this case, the amount of vapour is a function of the pressure, the temperature and the pore volume. Unless there is liquid water in the pore volume, the relative humidity can also assume values lower than 1.

Tab. 3.5   FEPs influencing saturation

Level	FEP	Formula
1	Saturation	$S_l = V_l/V_p$
2	*Pore volume (see Tab. 3.1)*	V_p
2	Volume of the liquid phase	V_l
3	Density of the liquid phase	
4	Composition of solution	
3	Amount of the liquid phase	
4	*Amount of water in the pore volume (see Tab. 3.4)*	
4	*Temperature (see Tab. 3.7)*	
4	*Gas pressure (see Tab. 3.6)*	
4	*Pore volume (see Tab. 3.1)*	

3.2.3.3   Gas pressure

Assuming that the body of bentonite considered is fully enclosed by water, the gas in the pore volume is confined by a layer of re-saturated bentonite. In this case, the gas could only escape if the gas pressure were to rise above the swelling pressure and thereby cause microcracks in the bentonite. Research is currently going on into the mechanisms playing a role in this context. For this reason, the related FEPs are not broken down any further neither here nor in the description of the FEP "Gas transport in the pore volume".

An increase in gas pressure may occur as a result of various different effects:

- gas production through corrosion,
- temperature increase, and
- compression through progressing re-saturation.

Counteracting an increase are:

- transport of dissolved gas in liquid water,
- transport of gas through microcracks, and
- possible cask failure.

Tab. 3.6 FEPs influencing gas pressure in the pore volume

Level	FEP
1	Gas pressure
2	Initial amount of gas
2	Gas production through ***corrosion (see Tab. 3.11)***
2	***Temperature (see Tab. 3.7)***
2	***Pore volume (see Tab. 3.1)***
2	***Amount of water in the pore volume (see Tab. 3.4)***
2	Additional volume due to cask failure
2	***Gas transport in the pore volume (see Tab. 3.10)***

If the assumption of the complete enclosure in liquid does not apply, the gas in the pore volume of the bentonite can escape through pathways in the host rock. If such a pathway leads to a part of the mine that has not yet been re-saturated, the gas pressure in the bentonite will be approximately the gas pressure prevailing in the mine. If the pathway ends in an aquifer, a gas pressure that corresponds to the hydrostatic water pressure will first have to build up before the gas leaves the pore volume in the bentonite.

3.2.3.4 Temperature

The transient temperature distribution in the bentonite is mainly governed by heat sources and heat transfer. Heat propagation through flow-induced transport is neglected due to the low fluid velocities. In the same way, temperature changes through phase transitions play a subordinate role due to the low transition flows.

Tab. 3.7   FEPs influencing the temperature in the pore volume

Level	FEP
1	Temperature
2	Initial temperature
2	Thermal boundary conditions
2	Heat sources
2	Heat conduction
2	Fluid-coupled heat transport
2	Phase transitions

3.2.4 Processes

The following processes form FEPs of the top level:

- hydration
- water transport in the pore volume
- gas transport in the pore volume
- corrosion.

3.2.4.1 Hydration

Hydration is understood here as the flow of water from the pore volume into the interlayer of the clay minerals. In the following, the associated flow rate is also referred to as "hydration rate". Hydration is driven by a gradient in the chemical potential between the water in the pore volume and the water in the interlayers. Potential difference and hydration are

linked by a proportionality factor a that is not described in this context any further. The chemical potential of the water in the interlamellar space increases with the amount of hydrated water. Provided the pores are filled at least partly with water, the chemical potential of the water in the pore volume is governed by the composition of the solution. If there is only vapour in the pore space, the chemical potential of the water in the gas phase is proportional to the relative humidity [28]. At 100 % saturation with vapour, the chemical potential corresponds to the potential of the liquid water.

Under constant conditions in the pore volume, a bentonite body thus gets closer with time to a state of equilibrium in which the chemical potentials of pore and interlayer water are the same. This is why the theoretically imaginable condition of complete dryness does not exist under natural conditions. A certain amount of water will always enter the bentonite in form of the atmospheric humidity and will hydrate there. One therefore speaks of "air-dry" bentonite with a "natural" water content when a bentonite has been exposed for some time to normal room temperature and atmospheric humidity.

In the state of equilibrium, the whole of the liquid water of the pore volume has transferred to the interlayer unless there is more water present than the interlayer can absorb. The maximum amount of water that can be absorbed by the interlayer depends on the interlayer cations of the clay minerals and on the volume available for swelling. If the bentonite is highly compacted and fixed, there is not enough room available for swelling, so that hydration will already end before all theoretically available hydration positions of the water molecules are occupied [45]. In this case, however, there principally remains a certain residual pore volume $V_{p\,min}$ that cannot be further reduced. At the end of hydration, the water fills the maximum interlayer volume $V_{i\,max}$.

The flow into the interlayer may be limited by the fact that the flow of the water into the pore volume is slower than the hydration. In this case, the hydration rate is not governed by the potential difference but by the water flow in the pore volume $\dot{m}_l = \mathbf{J_l} \cdot A$. Since it is not clear whether the diffusion of water molecules in the interlayer has any noticeable effect on the level of the hydration rate, this FEP is not considered.

The composition of cations in the interlayer change by ion exchange with a solution in the pore volume. This effect is, however, neglected here.

Tab. 3.8   FEPs influencing hydration

Level	FEP	Formula
1	Hydration $\dot{m}_{w\ hyd} = 0$ for $V_i = V_{i\ max}$ $\dot{m}_{w\ hyd} = a\Delta\Pi_{chem}$ for $V_i < V_{i\ max}$ and for $\mathbf{J_l}A > a\Delta\Pi_{chem}$ $\dot{m}_{w\ hyd} = \mathbf{J_l}A$ for $V_i < V_{i\ max}$ and for $\mathbf{J_l}A < a\Delta\Pi_{chem}$	
2	Differences in the chemical potential	$\Delta\Pi_{chem} = \Pi_{chem\ p} - \Pi_{chem\ i}$
3	Chemical potential of the pore water	$\Pi_{chem\ p}$
4	Composition of solution	
4	Relative humidity	$r_h \leq 1$ for $S_l=0$ and $r_h=1$ for $S_l>0$
5	*Saturation (see Tab. 3.5)*	
3	Chemical potential of the interlayer water	$\Pi_{chem\ i}$
4	Bentonite type	
5	Ion exchange	
4	Water content in the interlayer	
4	Diffusion in the interlayer	
2	Maximum size of the interlayer volume	$V_{i\ max} = V_b - V_s - V_{p\ min}$
3	*Bentonite volume (see Tab. 3.3)*	V_b
3	Solid matter volume	V_s
3	Minimum pore volume	$V_{p\ min}$
2	*Water transport in the pore volume (see Tab. 3.9)*	J_l

3.2.4.2   Water transport in the pore volume

In the following, the propagation of the liquid water as well as of the vapour in the pore volume are considered.

As soon as an unsaturated bentonite gets into contact with water, the water is absorbed by the bentonite. The water moves within the pores of the bentonite and is driven by capillary forces and hydraulic pressure. The air in the pore volume is displaced by the liquid water and gets pressurised if it cannot leave the bentonite unhindered. As a consequence, the pressure of the gas phase hinders liquid from entering the bentonite. The water is additionally driven by the suction resulting from the gradient in the chemical potential until it reaches the interlayer and hydrates [49]. Thus the hydration extracts water from the pore volume.

The vapour flow is described by a diffusive process. The associated coefficient of the free, binary gas diffusion $D_g{}^w{}_{bin}$ is pressure- and temperature-dependent. However, with decreasing pore radius, the influence of Knudsen diffusion is getting increasingly stronger until binary diffusion no longer plays a role. Knudsen diffusion solely depends on the pore radius and the molecular weight. The relevance of the respective diffusion process ensues from the ratio between the pore diameter d and the mean free path length of the gas molecules λ. For more details on the determination of the effective vapour diffusion coefficient, see Appendix A.

At the interface between liquid and gaseous phase, the gas is always saturated with vapour. If the vapour is transported away from this boundary surface by a gradient of the partial vapour pressure, the phase transition acts as a sink for the liquid and as vapour source for the gas. In a reverse effect, the condensation of water acts as a source for the liquid and as a sink for the gas. It has to be noted in this context that owing to the small volumes of the pores one can assume in principle a local atmosphere of saturated water vapour when gas and water are simultaneously present in the pores [15].

Tab. 3.9 FEPs influencing water transport in the pore volume

Level	FEP	Formula
1	Water transport in the pore volume	$\mathbf{J_l} = \mathbf{J_l^w} + \mathbf{J_g^w}$
2	Liquid water flow	$\mathbf{J_l^w} = S_l \rho_l \mathbf{v_l}$
3	*Saturation (see Tab. 3.5)*	S_l
3	Density	ρ_l
3	Flow velocity	$\mathbf{v_l} = -\dfrac{k_{rl}}{\eta_l}\mathbf{k} \cdot \nabla p_l$
4	Hydraulic pressure gradient	∇p_l
5	Hydraulic boundary conditions	
5	Sources/Sinks	
6	*Corrosion (see Tab. 3.11)*	
6	*Hydration (see Tab. 3.8)*	
6	Phase transitions	
5	Suction	
6	Capillary pressure	
6	*Pressure induced by hydration (see Tab. 3.8)*	
5	*Gas pressure (see Tab. 3.6)*	
4	Absolute permeability	$\mathbf{k} = \mathrm{f}(V_p)$
4	Relative permeability	$k_{rl} = \mathrm{f}(S_l)$
4	Viscosity	$\eta = \mathrm{f}(T)$
2	Vapour flow	$\mathbf{J_g^w} = S_g \varPhi \tau D_g^w \nabla \rho_g^w$
3	Partial density gradient $\nabla \rho_g^w \cong \rho_g \nabla X_g^w$; $X_g^w = \dfrac{m_g^w}{m_g}$, $\rho_g = \dfrac{p_g M_g}{RT}$	
4	Hydraulic boundary conditions	
4	Sources/Sinks	
5	*Corrosion (see Tab. 3.11)*	
5	*Hydration (see Tab. 3.8)*	
5	Phase transitions	

Tab. 3.9 FEPs influencing water transport in the pore volume

Level	FEP	Formula
3	Diffusion coefficient $D_g^w = D_{g\,bin}^w$ for $d > \lambda$ $D_g^w = f(D_{g\,bin}^w, D_{g\,knud}^w)$ for $d \approx \lambda$ $D_g^w = D_{g\,knud}^w$ for $d < \lambda$	
4	Coefficient of binary gas diffusion $D_{g\,bin}^w = D_{g\,0}^w \dfrac{p_g}{p_{g0}} \left(\dfrac{T}{T_0}\right)^{\theta}$	
5	*Gas pressure (see Tab. 3.6)*	p_g
5	*Temperature (see Tab. 3.7)*	T
4	Coefficient of Knudsen diffusion $D_{g\,knud}^w = \dfrac{1}{3}\sqrt{\dfrac{8R}{\pi M_w}}\,d\,\sqrt{T}$	
5	Pore diameter	d
5	*Temperature (see Tab. 3.7)*	T
3	Porosity	Φ
3	Tortuosity	τ
4	*Pore volume (see Tab. 3.1)*	V_p
4	*Bentonite volume (see Tab. 3.3)*	V_b
3	*Gas saturation (see Tab. 3.5)*	$S_g = 1 - S_l$

3.2.4.3   Gas transport in the pore volume

Gas movement in the bentonite is possible

- as gas flow in the pore volume due to pressure differences resulting from
  - gas production,
  - temperature changes or
  - compression of the gas due to the progressing saturation front,

- as fast flow through the saturated area of the bentonite, if the bentonite fractures upon exceeding a critical gas pressure and temporarily opens up new flow paths, and

- as transport process of gases dissolved in the liquid.

There are different transport processes for the different states of saturation. The state of partial saturation with water (S_l<1) has to be differentiated from state of full saturation with water (S_l =1).

If water and gas coexist in the pore volume, the gas becomes dissolved at the interface between the two phases. Here, one can assume in good approximation that there will be a persistent equilibrium of solution. The mass fraction of dissolved gas in the liquid phase ensues from Henry's law and depends on the temperature and the pressure in the gas phase. Owing to the assumption of the instantaneous solution equilibrium, the pore water acts like a storage medium for the gas. Transport in the liquid phase does not take place under partially saturated conditions.

Assuming that flow of the gas phase is faster than all other processes involved in the re-saturation, it is possible to do without a calculation of this flow. It will then suffice to restrict oneself to considering gas pressure and the amount of gas in the state of equilibrium.

In an area of complete saturation with water, the assumption of an instantaneous solution equilibrium has no longer any relevance. The dynamics of the diffusive and the advective transports of dissolved gas in the liquid phase have to be considered. But the amount of gas transported is so small that this FEP is only relevant for the investigation of long periods.

Tab. 3.10 FEPs influencing gas transport in the pore volume

Level	FEP	Formula
1	Gas transport in the pore volume	$\mathbf{J_g} = \mathbf{J_l^a} + \mathbf{J_g^a}$
2	Flow in the gas phase (SI<1)	$\mathbf{J_g^a}$
3	Gas flow in the pore volume	
3	Gas flow in pressure-induced cracks	
2	Gas transport in the solution (S_l=1)	$\mathbf{J_l^a} = \mathbf{J_{l\,adv}^a} + \mathbf{J_{l\,dif}^a}$
3	Advective gas transport	$\mathbf{J_{l\,adv}^a} = \mathbf{J_l^w} X_l^a$
4	***Water transport in the pore volume (see Tab. 3.9)***	$\mathbf{J_l^w}$
4	Mass fraction of gas dissolved in the water	X_l^a
3	Diffusive-dispersive gas transport	$\mathbf{J_{l\,dif}^a} = \Phi \rho_l D_l^a \nabla X_l^a$
4	Porosity	Φ
4	Density of the liquid phase	ρ_l
4	Diffusion/Dispersion coefficient	D_l^a
5	***Pore volume (see Tab. 3.1)***	
5	***Bentonite volume (see Tab. 3.3)***	
4	Gradient of the gas fraction in the water	∇X_l^a
3	Boundary conditions	
4	Henry's coefficient	
5	***Temperature (see Tab. 3.7)***	
4	***Gas pressure (see Tab. 3.6)***	
2	***Saturation (see Tab. 3.5)***	

3.2.4.4 Corrosion

With corrosion processes, a distinction is made between aerobic and anaerobic corrosion. Aerobic corrosion in the repository can be left aside due to the limited supply of oxygen. As soon as any incoming water gets into contact with the metals of the waste casks, anaerobic corrosion and, as a consequence thereof, the chemical conversion of water sets in. This results in solid corrosion products and the generation of considerable amounts of gas. This is why corrosion is understood here as a phenomenon which represents on the one hand a sink for the pore water with a corresponding flow rate $\dot{m}_{kor}$ and which on the other hand leads to gas production at the rate $\dot{m}_g$. The flow rate for the water sink is linearly proportional to the gas production rate.

The process of corrosion can be started both by liquid water and by water vapour. Here, the assumption is that the surface-related corrosion rate r_l for liquid water is higher than the rate $r_{g\ max}$ for vapour under vapour-saturated conditions. If the pore water is used up faster due to the corrosion than can be replaced through the water transport in the pore volume, the corrosion rate and therefore the gas production is governed by the water transport.

Tab. 3.11   FEPs influencing corrosion

Level	FEP	Formula
1	Corrosion	$\dot{m}_{kor}, \dot{m}_g$
2	Outer surface of the casks	
2	Corrosion rate	$r = r_{g\ max} r_h \ (S_l=0)$ $r = r_l \qquad (S_l>0)$
3	Cask material	
3	Composition of the solution	
3	*Water transport in the pore volume (see Tab. 3.9)*	
3	Relative humidity	r_h
3	*Saturation (see Tab. 3.5)*	S_l
3	*Temperature (see Tab. 3.7)*	

4 Analysis of the existing THM codes

For each concrete case, the quantitative prediction of the re-saturation of bentonite is only possible with the help of numerical methods. Various different codes have been specially developed or extended for this purpose. These are:

- ABAQUS

  Commercial structural-mechanics code by ABAQUS Inc., USA, formerly HKS Inc. (Hibbitt, Karlsson and Sorensen), with adaptations by Clay Technology AB, Lund, Sweden
- CODE-BRIGHT

  Development of the Technical University of Catalunya for THM problems
- COMPASS

  Development of Cardiff University for THM problems
- FLAC

  Commercial code by Ithasca Consulting Group, Inc., USA; structural-mechanics code with adaptation options for THM problems
- FRACON

  Contract development by AECL for THM problems
- MUFTE_UG

  Development of Stuttgart University; multi-phase-flow code for TH problems with extensions for expandable materials
- ROCKFLOW (ROCKMECH)

  Development of Hanover University, modified at Tübingen University to address THM problems
- ROCMAS

  Development of the Lawrence Berkeley Laboratory for THM problems
- THAMES

  Development of Kyoto and Iwate Universities, Japan, for THM problems

These codes are described in more detail in [51], [16], [23], [42] and [53]. All these codes share some fundamental assumptions, especially the concept of a flow in the un-saturated area, an elastic stress-strain behaviour, and the propagation of heat due to thermal conduction. The developers obviously also share the view that thermal conduction is the only relevant process of heat propagation in THM modelling.

In the hydraulic and mechanic parts of the codes, however, there exist clear differences in the consideration of various effects. With the exception of FRACON and THAMES, all codes simulate e. g. a transition from elastic to plastic behaviour above critical threshold stresses, even though they are based on different plasticity models: the Mohr-Coulomb model, the Drucker-Prager model, the Cam-Clay model or specially adapted models. CODE-BRIGHT, COMPASS and ROCKFLOW use a two-phase two-component approach in the hydraulic part, while movement of the gas phase is neglected in the other codes. Vapour propagation is described with the help of various different approaches, even though all formulations are based on a Fick's description of the diffusion.

Further differences are found in the calculation of the effective stresses in the grain structure. The concept of the effective stresses first developed by Terzaghi [54] was generalised by Biot [1], but only applies to pore spaces filled completely with a single fluid phase. An extension to the case of partial saturation with water is very difficult. Up to now this problem has not been satisfyingly solved. A number of codes therefore rest on experiments and approaches by Bishop, where a proportionality of the pore water pressure acting on the grain structure in relation to saturation was found [2]. However, this proportionality is considered rather differently in the codes, either as a step function which only allows an influence at water saturation 1 (THAMES), as linear function of the degree of saturation S (e. g. FRACON, ABAQUS), or as a product of S with a Biot coefficient (ROCMAS). Also, it still has to be demonstrated that Bishop's conclusions also apply at higher temperatures.

So far, there exists no established conceptual model for the re-saturation of bentonite and consequently also no generally applicable set of equations for the modelling. Still, all models assume a water flow or even a two-phase flow in the unsaturated area. Here, the decrease of the permeability with increasing water content in the bentonite is taken into account with the help of a water-content-dependent relative permeability, and the simultaneously decreasing suction is interpreted as capillary pressure.

The balance equations of the classic two-phase flow that are contained in the models assume an inert, rigid matrix, with water and vapour exclusively present in the pore space. However, these conditions do not apply to re-saturated bentonite, where a considerable proportion of the water from the pore space enters the interlayers through hydration. The

clay particles do in fact have the effects of sinks for the water in the pore space. To a large extent, they immobilise it in the interlayers, swell thereby and at the same time reduce the pore space.

The conventional two-phase flow approach has therefore an essential weak point. The process of hydration is not considered and thus, no difference is made in the balance equations between the pore water and the immobile water in the interlayers. Only the local water content or an equivalent measure are considered in the above mentioned THM-codes.

This has two severe consequences. First, it is not possible to separate the share of the capillary pressure in the suction from the share that is caused by the gradient in the chemical potential between pore water and interlayer water. Both suction forces are mixed up and the sum of both is derived from a so-called "retention curve" as a function of the water content. This is not correct because capillary pressure and suction depend on different quantities. The capillary pressure is controlled by the volumetric saturation of the pores with the liquid as well as the pore size while the suction is controlled by the chemical composition of the liquid phase and the local amount of interlayer water.

Second, in reality a considerable hydration of water vapour occurs at elevated relative humidities if no liquid water is present in the pore space of the bentonite. But without the distinction between pore water and interlayer water all the swelling properties have to be described as a function of the local water content which is not significantly increased by the vapour mass. The models are therefore not able to reproduce the re-saturation via water vapour.

The classic two-phase-flow theory thus does not suffice to describe the phenomenon of re-saturation correctly. The latest modifications to COMPASS [10], ROCKFLOW [31] and recently also to the MUFTE_UG code [18] are aimed at eliminating at least part of the deficiencies described above. However, this is still done on the basis of the two-phase-flow theory, the applicability of which to bentonite has not been shown yet without doubt.

5   Bases for new re-saturation models

The uncertainties in the conceptual assumptions introduced in Chapter 4 have consequences for the applicability of modelling results. Although the complex numerical models that are currently in use for the simulation of the re-saturation of bentonite contain these conceptual uncertainties, they also contain parameters and equations of state that have to be determined by calibration. It is therefore not clear from the start whether the processes covered by the models are described in full and with sufficient accuracy or whether any possible weaknesses in the conceptual model are covered up by the calibration of the parameters.

Under these circumstances it appears expedient to deal with the conceptual model of re-saturation. As re-saturation is the uptake of water which is controlled by the propagation of water in the bentonite, the focus of the following considerations is on the hydraulic processes. In order to work out the relevant processes, the problem of re-saturation is applied to a typical situation in a repository which is simplified as much as possible.

The object of the consideration is the re-saturation of a bentonite buffer in the annulus between waste canister and host rock. The bentonite has been previously compacted and is air-dry at the beginning of the re-saturation. It borders on the water-bearing excavation-disturbed zone (EDZ) of the host rock from where re-saturation begins. The waste canister forms an inert, rigid border. As shown in Fig 5.1, this process can be considered as a first approximation to be a one-dimensional process. In addition, the following assumptions are made:

-    isothermal conditions,
-    no influence of the canister on the re-saturation,
-    no gas transport in the liquid phase,
-    differences between pore water and interlayer water,
-    same local increase of interlayer volume as decrease of pore space,
-    rigid area boundaries, and
-    neglect of mechanical deformation through swelling.

3D model   2D model   1D model
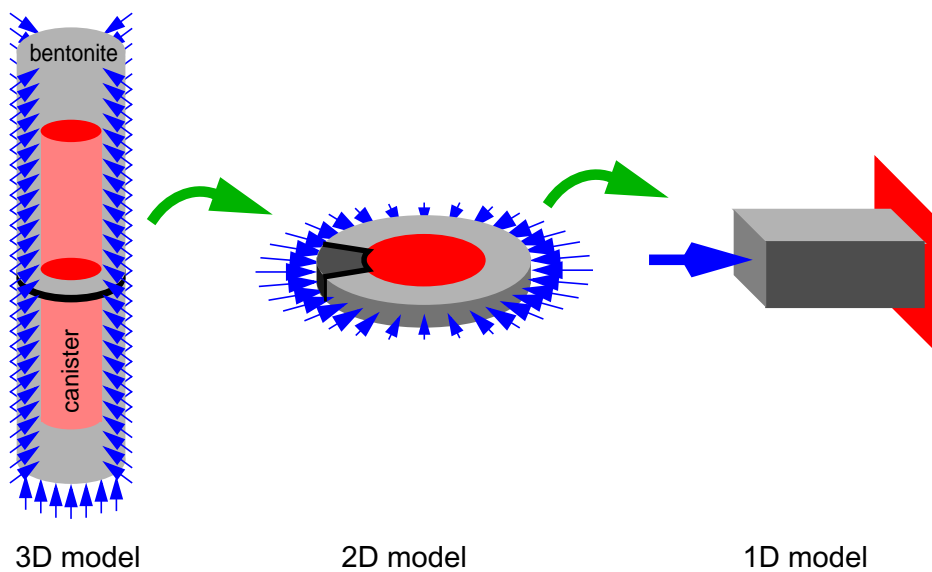
Fig. 5.1 Geometrical simplification of the re-saturation problem for a bentonite buffer

Under these conditions, there only remain the processes "water transport in the pore space" and "hydration" of the general conceptual model discussed in Chapter 3. Thus the time-dependent spatial distribution of the pore water can be described with the help of mass balance equations. Here, the equations have to contain the effect of hydration as a sink for the pore water and must consider the reduction of the pore space that goes in hand with the increase of the interlayer volume. The amount of interlayer water can be determined from the hydration rate.

The propagation of the water in the pore space and the associated time-dependent distribution of the water in the bentonite depends on the ratio of the flow rate in the pore space to the hydration rate. This interrelation becomes clear when one looks at the extreme cases. The consequences ensuing from a very low and a very high hydration/pore flow ratio are shown in Fig. 5.2.
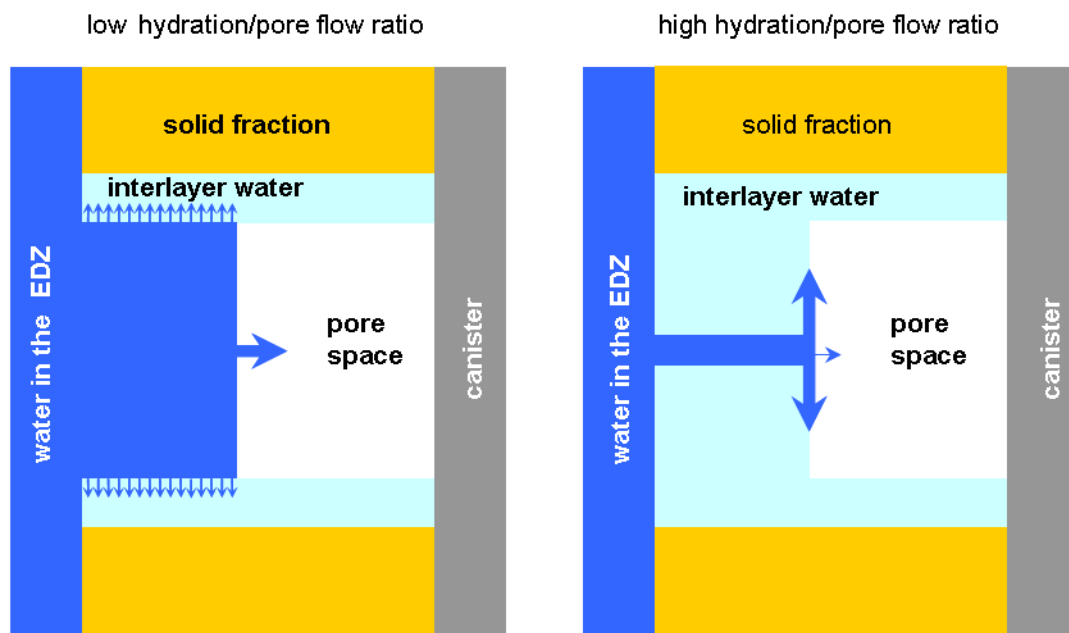
Fig. 5.2 Influence of the strength of hydration on the pore space and on the flow

If hydration is low compared to the flow rate in the pore space, the pore space fills with water before a significant transfer of water to the interlayers can take place. In this case, the water content in the interlayers would no longer be a function of space but only a function of time. At very strong hydration, the water in the pore space can only proceed when hydration at the liquid front is more or less complete. The water content could then be approximately described by a step function whose point of discontinuity moves into the bentonite together with the liquid front.

Up to this point of the considerations, a distinction between liquid water and water in the form of vapour is immaterial. In the following, however, the re-saturation processes with liquid water and water vapour are considered separately. Correspondingly, two models are developed: one for re-saturation with liquid water and another one for re-saturation with vapour.

6 Advection model

6.1 Conceptual model

Initially, the re-saturation of the bentonite with liquid water is investigated in more detail. Starting point of the considerations is the question of the ratio of the process velocities. As has been shown in Fig. 5.2 already, a low hydration/pore flow ratio means that the bentonite should behave approximately like a porous medium before hydration sets in. However, this conclusion clearly stands in contrast to the experimental findings that show that the uptake of water does not increase considerably at increased hydraulic pressures [26], [47].

Thus, in relation to the flow in the pore space, hydration has to be considerable if not even dominant. The uptake of liquid water is assumed to be very fast in [49], so that the approximation of an instantaneous hydration seems plausible. This approximation leads to a conceptually very simple re-saturation concept for liquid water, which in the following shall be referred to as "advection model".

In the advection model, the bentonite is divided into two zones with constant features: one zone in which a state of complete saturation has already been established and another zone which is still in an initial state. Water movement only takes place in the re-saturated part between the EDZ and the liquid front. It is described by Darcy flow with the permeability of the saturated bentonite. The boundary conditions for the flow are the hydrostatic pressure in the EDZ and the suction at the liquid front. Suction is composed of two forces which quantitatively can only be separated with difficulty; these are the capillary forces on the phase boundary between pore water and air and the gradient in the chemical potential between the pore water and the interlayer water in the area of the front. The suction leads to the fact that the water can enter the bentonite even without any hydraulic pressure.

Hydration only takes place at the liquid front because hydration is assumed to be an instantaneous process. It acts as a sink for the pore water and as source for the interlayer water. The pore space is reduced by the same amount by which the interlayer volume increases. Behind the water front the initially void pore space is completely filled with wa-

ter, partly with pore water and partly with interlayer water. But there is no need to differentiate between the pore volume and the volume of the interlayers because the porosity of the saturated bentonite is not required in the model. The amount of water flowing through the saturated part of the bentonite can be calculated from the filter velocity and the propagation velocity of the liquid front is calculated from the quotient of the filter velocity and the porosity in the initial condition.

6.2 Mathematical model

The simplified Darcy's flow law that is used as a basis for the calculation of the flow in the advection model, is as follows:

$$v_f = -\frac{k}{\eta}\frac{\partial p_l}{\partial x}$$

(6.1)

v_f - filter velocity [m/s]
k - permeability [m^2]
p_l - liquid pressure [Pa]
η - dynamic viscosity [Pa s]
x - distance from the inflow boundary [m]

In the following, the assumption is that suction at the liquid front is constant. Water pressure at the contact surface to the EDZ and gas pressure in the pore space are also assumed to be constant parameters. This, however, is not strictly necessary for the advection model.

The propagation of the front causes a decrease of the pressure gradient which governs the intensity of the inflow, and in the advection model the inflow decreases exponentially with time. The flow law may thus also be expressed as

$$v_f(t) = -\frac{k}{\eta}\frac{\Delta p_l}{x_F(t)}.$$

(6.2)

x_F - location of the liquid front [m]

The distance $x_F(t)$ of the liquid front from the inflow boundary is a function of the propagation velocity of the liquid front $v_F(t)$:

$$x_F(t) = \int_{t_0}^{t} v_F(t)dt \,.$$

(6.3)

v_F - propagation velocity of the liquid front [m/s]

t - time [s]

t_0 - start of re-saturation [s]

The integrand in equation (6.3) is in turn explained as

$$v_F = \frac{v_f}{\Phi_0}$$

(6.4)

Φ_0 - initial porosity [-]

The distribution of the absorbed amount of water to the interlayers and the remaining pore space is not exactly known. This differentiation, however, is irrelevant for the calculation of the amount of water that can be uptaken and from which the location of the moisture front ensues. As deduced in Appendix D, the initial porosity can be determined in the following way:

$$\Phi_0 = 1 - \frac{\rho_d}{\rho_s} - \frac{\rho_d}{\rho_w} w_0$$

(6.5)

ρ_d - dry density of the bentonite [kg/m^3]

ρ_s - density of the clay particles [kg/m^3]

ρ_w - density of the liquid water [kg/m^3]

w_0 - initial water content [-]

In a numerical model, it is expedient to replace the integral over $v_F(t)$ by a total of the distances Δx_i covered in time step i. These ensue from the velocities $v_{F\,i}(t_i)$ multiplied by the associated finite time steps Δt_i:

$$x_F(t) \cong \sum_i \Delta x_i = \sum_i v_{F_i}(t_i)\, \Delta t_i$$

(6.6)

Δx_i -   progress of the front in time step i [m]

Since the propagation velocity of the liquid front decreases with time the propagation velocity $v_{Fi}(t_i)$ in equation (6.6) has to be updated for each element of the sum. Following the calculation of each element the corresponding location of the front $x_F(t)$ has to be inserted in equation (6.2) in order to obtain the updated propagation velocity.

The amount of water $m_{w\,auf}(t)$ absorbed in the bentonite as well as the total amount of water $m_w(t)$ contained in the bentonite are calculated from

$$m_{wauf}(t) \; = \; (w_e - w_0)x_F(t)\rho_d A \qquad\qquad\qquad (\,6.7\,)$$

$m_{w\,auf}(t)$-   absorbed amount of water [kg]
w_e -   final water content at re-saturation with liquid [-]
ρ_d -   dry density of the bentonite [kg/m^3]
A -   cross-sectional area of the bentonite [m^2]

as well as from

$$m_w(t) \; = \; ((w_e - w_0)x_F(t) + lw_0)\rho_d A \,. \qquad\qquad (\,6.8\,)$$

$m_w(t)$ -   amount of water in the bentonite [kg]
l -   length of the bentonite body [m]

The inflow $\dot{m}(t)$ eventually ensues according to

$$\dot{m}(t) \; = \; \rho_w \, A \, v_f(t) \qquad\qquad\qquad\qquad\qquad (\,6.9\,)$$

6.3   Input parameters

The following hydraulic parameters
-   permeability of the re-saturated bentonite,
-   suction in unsaturated condition,
-   hydraulic pressure at the inflow boundary, and
-   dynamic viscosity

and the parameters that characterise the initial condition, namely

- dry density of the bentonite,
- density of the clay minerals, and
- initial water content

are entered in the advection model. Here, the largest uncertainties are due to the first two hydraulic parameters. This is why the literature was evaluated in particular with regard to data on permeability and suction.

6.3.1   Permeability

The permeability coefficient of saturated MX-80 bentonite for water was measured in a range of experiments [37], [39], [7], [44], [3], [43], [45], [50] on the basis of [6], [30] and [46]. The results are, however related partly to the dry density, partly to the saturation density and in some parts even to the pore ratio so that they are not comparable offhand. In addition, the permeability coefficient is indicated in the form of hydraulic conductivities as well as permeabilities.

The results therefore have to be normalised for a summarising description. If need be, the hydraulic conductivity values may be transformed for this purpose with the help of

$$k = \frac{\eta_w(T)}{\rho_w(T)g}K \tag{6.10}$$

k - permeability [m^2]
K - hydraulic conductivity [m/s]
$\eta_w(T)$- dynamic viscosity of the water [Pa s]
$\rho_w(T)$- density of the water [kg/m^3]
g - acceleration of gravity [m/s^2]
T - temperature [K]

into permeabilities since two hydraulic conductivity values are only comparable with each other if they have been determined under the same temperature and pressure conditions. This way it is therefore also possible to integrate results from experiments with different

temperatures in the compilation. Here, the chosen independent parameter on which permeability is to depend is dry density. Saturation density and pore ratio can be converted with the help of the considerations explained in Appendix D into a corresponding value for the dry density.

Fig. 6.1 shows the permeability values as a function of the dry density. The data points lie within a surprisingly narrow bandwidth in which the maximum value lies less than one order of magnitude above the minimum value.

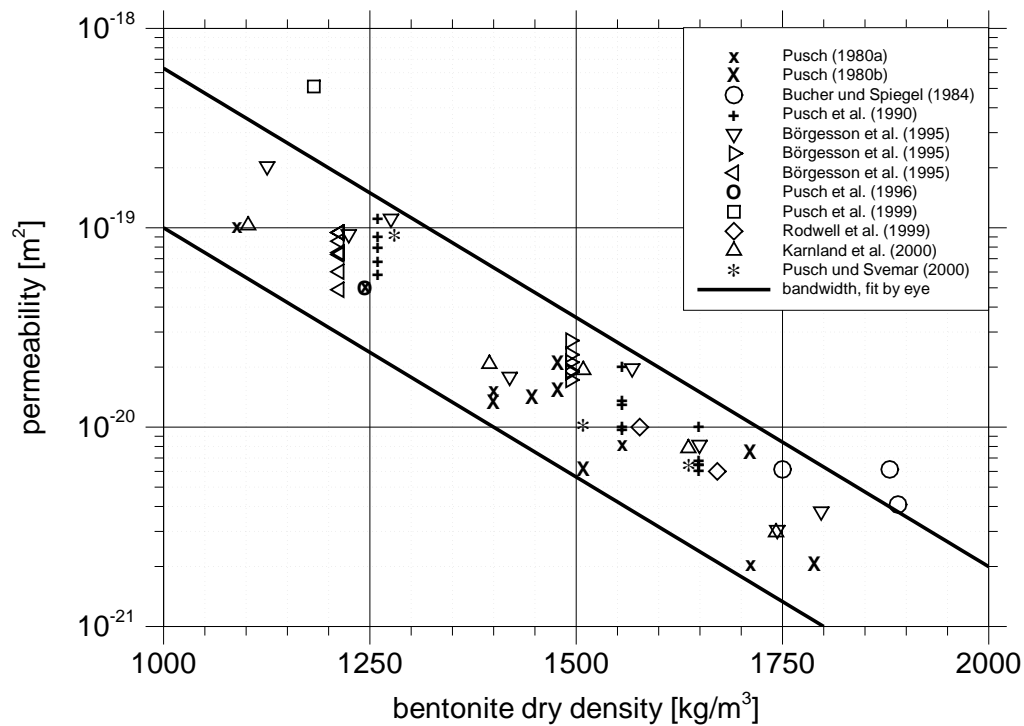**Fig. 6.1**   Permeability of saturated MX-80 bentonite as a function of dry density

6.3.2   Suction

Suction is less well known. Corresponding data can be found in [25] and [27]. Thermodynamic considerations, however, make it possible to establish a connection between suction and swelling pressure. In fact, the derivation of the total suction p_s and of the swelling pressure p_q lead to the Kelvin equation [19]:

$$p_s = -\frac{\frac{R}{M_w}T}{\overline{V}_w}\ln\left(\frac{p_v}{p_{sat}}\right)$$

(6.11)

p_s - total suction [Pa]

R - universal gas constant [J/(mol K)]; R=8.314 J/(mol K)

M - molecular weight [kg/mol]; for water: M_w=0.018016 kg/mol

$\overline{V}_w$ - partial specific volume of water; pure water: $\overline{V}_w$=10^{-3}m^3/kg

p_v - partial vapour pressure [Pa]

p_{sat} - saturation vapour pressure [Pa]

As suction as well as swelling pressures are indicated as being positive quantities in the literature, equation (6.11) has on the right-hand side a negative sign. Experimental proof is provided in [27] that suction is about the same as swelling pressure. A comparison that is also drawn in [27] of the results of the suction measurements with swelling pressure measurement results from [3] which showed good agreement. The same applies to a comparison of swelling pressures with suction that were derived theoretically from adsorption isotherms [28].

Against this background it is also possible to use additionally the results of the swelling pressure measurements for the determination of suction; for MX-80, these are available to a considerably higher degree [38], [40], [7] in [28], [8], [44], [3], [50], [45], [27], [25]. Further data can also be found in [29] and [30]. The values used here have, however, apparently been taken from the literature mentioned above and have been translated to other reference parameters. They have therefore not been considered in this compilation. The data were standardised similarly to those of the permeabilities. The result is shown in Fig. 6.2.

The graph shows quite good agreement of the swelling pressure and suction values, which confirms once again the analogousness of swelling pressure and suction. Earlier swelling pressure experiments from Sweden and Switzerland are interpreted in [52] to tend to yield too high (Sweden) and too low (Switzerland) swelling pressures. Under this aspect, the bandwidth of the measured values - which is already not too wide - could even be reduced.
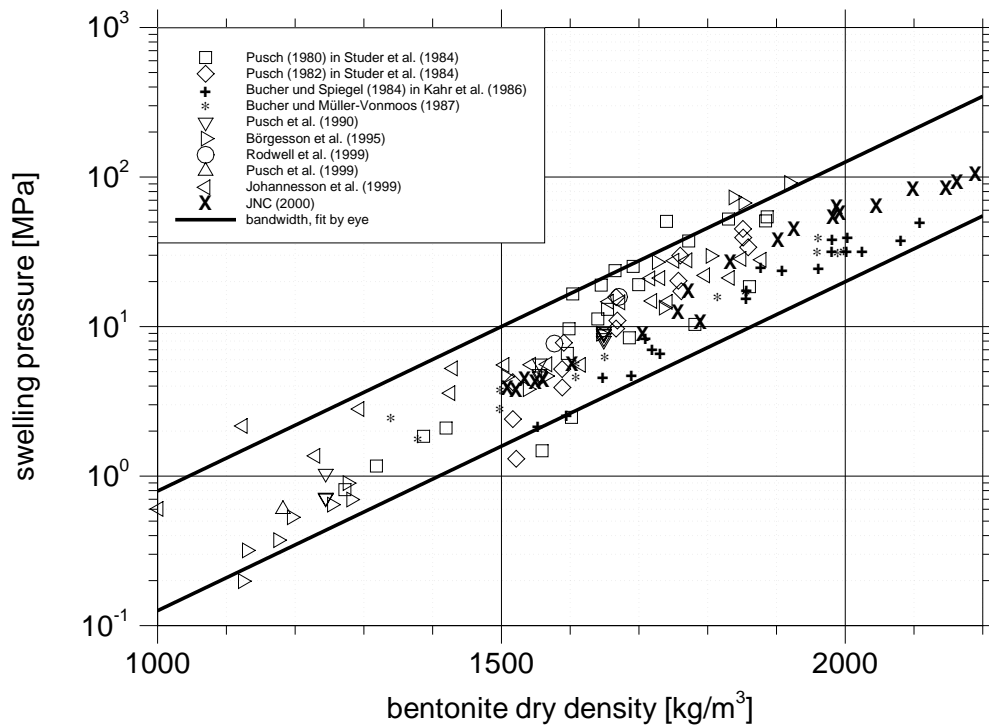
Fig. 6.2   Suction of saturated MX-80 bentonite as a function of dry density

Remark: Permeability as well as suction can be expressed as a function of the bentonite dry density. Permeability decreases about one order of magnitude with an increase of the dry density of 400 kg/m^3. The same increase of the dry density causes the suction to increase about one order of magnitude. The product of permeability and suction is therefore a constant. This product controls the flow velocity calculated by Darcy's law (6.2) if the hydraulic pressure in the EDZ can be neglected in comparison to the suction. At atmospheric pressure this applies even to bentonite samples of a low degree of compaction. This means, that the re-saturation dynamics in the advection model are independent of the degree of compaction which is consistent with the narrow bandwidth of the results for the empirical diffusion coefficient being derived from different uptake experiments.

6.3.3   Density

The pressure dependence of the water density is described very well by the compression coefficient β_{pl}=4.4·10^{-10} [1/Pa]. At a pressure increase from atmospheric pressure to 10 MPa, however, the density merely changes by 3 kg/m^3, i. e. 3 per mill. The pressure dependence of the density can therefore be neglected for practical purposes.

The density is much more influenced by the temperature. On the basis of temperature measurements, [11] and [56] provide equations which concordantly yield density changes of 4 % at a temperature rise from 20 °C to 100 °C. It has to be noted in this context that the known approaches with a constant thermal expansion coefficient increasingly tend to overestimate the density at higher temperatures. At a thermal expansion coefficient of $4.4 \cdot 10^{-4}$ 1/K and a temperature of 100 °C, the error is already about 10 kg/m^3, and this error increases exponentially with the temperature. Therefore, for an exact description, the somewhat more complex formulas according to [11] or [56] have to be used, which - although they are formally very different - yield identical results for practical purposes. As an example, the following is taken from an equation from [56]:

$$\rho_w = (999.83952 + 16.945176\ T_c - 7.9870401\ 10^{-3} T_c^{\ 2}$$

$$- 46.170461\ 10^{-6} T_c^{\ 3} + 105.56302\ 10^{-9} T_c^{\ 4} - 280.54253\ 10^{-12} T_c^{\ 5})$$

$$/\,(1 + 16.879850\ 10^{-3} T_c) \tag{6.12}$$

T_c -   temperature [°C

6.3.4   Viscosity

The dynamic viscosity of liquid water is principally a function of the temperature. The viscosity value at atmospheric pressure and 20 °C changes as a result of a pressure increase to 10 MPa by only about 1 %. Following a suggestion of [15], the temperature-dependent viscosity is calculated here with help of the formula taken from [21]

$$\eta_w = 2.414\ 10^{-5} 10^{\left(\frac{247.8}{T_c + 133.15}\right)} \tag{6.13}$$

6.4   Modelling of a laboratory experiment

The advection model was tested on a laboratory experiment in which the water uptake of compacted MX-80 bentonite was measured [28]. In this experiment, a cylindrical test specimen was brought into contact with water at the face area. The water had room temperature and was only at atmospheric pressure. The water content of the specimen was

measured gravimetrically as a function of time. With the help of the data thus obtained, the coefficient for the frequently used empirical diffusion model, which is described in more detail in Appendix E, was determined.

The data relating to the advection model are compiled in Table 6.1. They were either taken directly from [28] or were derived from the data indicated. Permeability and suction were estimated with the help of the data compilation in Chapter 6.3.

Tab. 6.1 Parameters of the bentonite and of the numerical models; experiment according to [28]

Parameter	Value	Dimension	Origin
Length of the test specimen	2.46	[cm]	from [28]
Cross-sectional area	19.6	[cm^2]	from [28]
Particle density	2800	[kg/m^3]	assumption
Bentonite dry density	1940	[kg/m^3]	derived from [28]
Initial water content	0.001	[-]	derived from [28]
Final water content	0.158	[-]	from [28]
Initial porosity	0.31	[-]	derived from [28]
Final porosity	0.02	[-]	derived from [28]
Permeability	$1.5 \cdot 10^{-21}$	[m^2]	assumption according to Fig. 6.1
Suction	50	[MPa]	assumption according to Fig. 6.2
Viscosity of the water	0.001	[Pa s]	
Density of the water	1000	[kg/m^3]	
Empirical diffusion coefficient	$3.4 \cdot 10^{-10}$	[m^2/s]	from [28]

The results of the advection model, the empirical diffusion model and the measurements of the water content as a function of time are shown in Fig. 6.3, which shows clearly that the water uptake under simple conditions can be simulated with the advection model. In this context, the simulation of the measured values can be successfully described with both, the advection model and the empirical diffusion model.
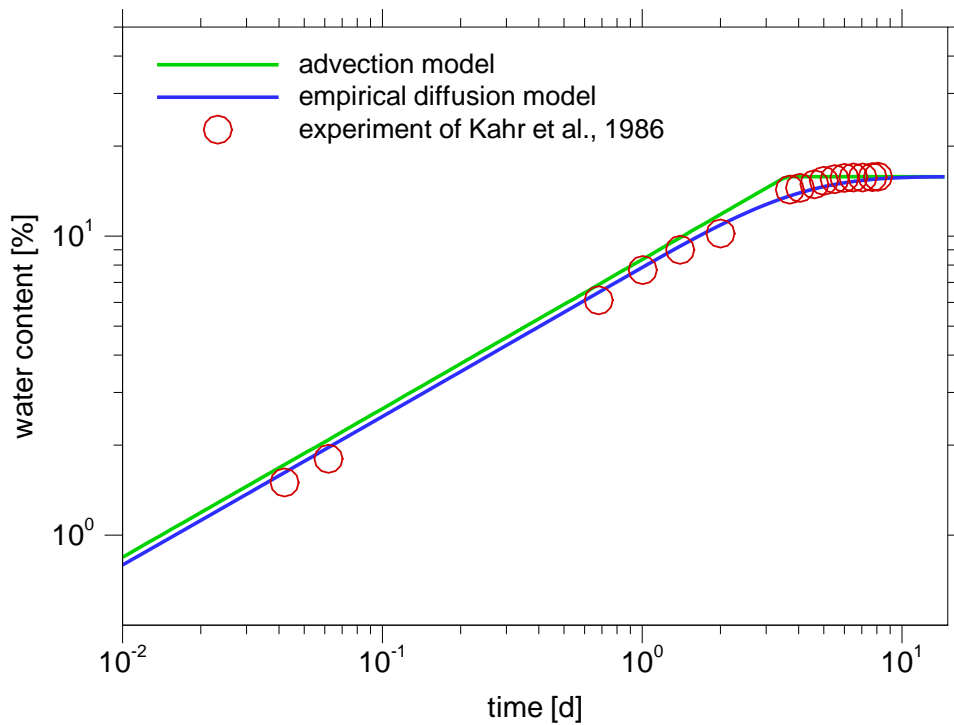
Fig. 6.3   Calculated water content in comparison to experimental results from [28]

The time-dependent inflow rate and the position of the liquid front were not measured but can be used for a further comparison of the advection model and the empirical diffusion model. For this purpose, the position of the liquid front in the empirical diffusion model is defined without further justification as the position of 50-% saturation with water. Fig. 6.4 shows the time-dependent development of the inflow rate and the penetration depth as a function of time. These comparisons, too, conform the equality of the results yielded by the two models.
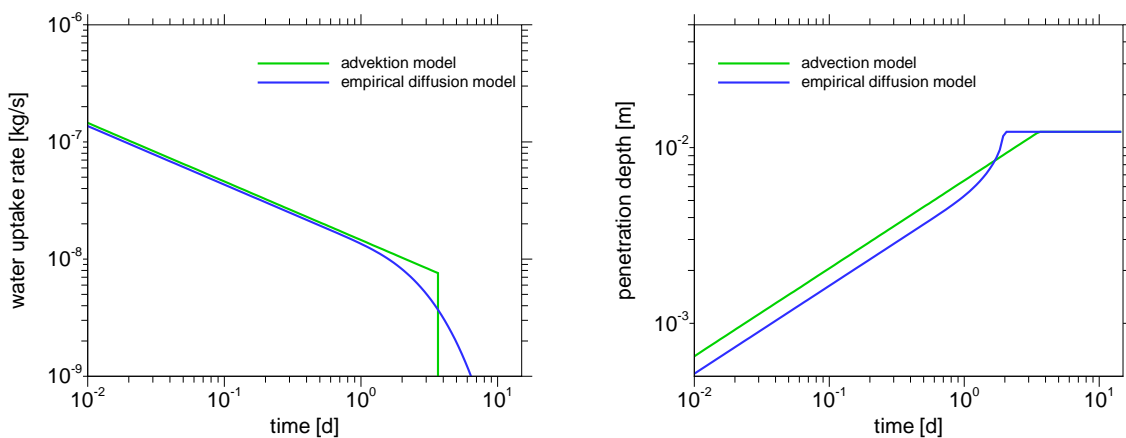
Fig. 6.4   Simulated uptake rates and penetration depths for the experiment from [28]

7 Vapour diffusion model

7.1 Conceptual model

Bentonite re-saturation is governed by the transport of water in the pore volume and by hydration even in those parts that contain no liquid water but exclusively gas. Water evaporates on the contact surfaces between liquid and gas phase, propagates as unsaturated vapour in the gas phase of the pore volume and this way allows hydration in the interlayer. Compared to the advection model, however, the water transport does no longer take place in an advective manner but as diffusion in the pore atmosphere. Moreover, the hydration rate of vapour is lower than that of liquid water and can therefore no longer be considered as instantaneous. Simulation of re-saturation therefore requires a new model which in the following is referred to as "vapour diffusion model". The principle mode of functioning of the vapour diffusion model is shown in the graphic in Fig. 7.1.
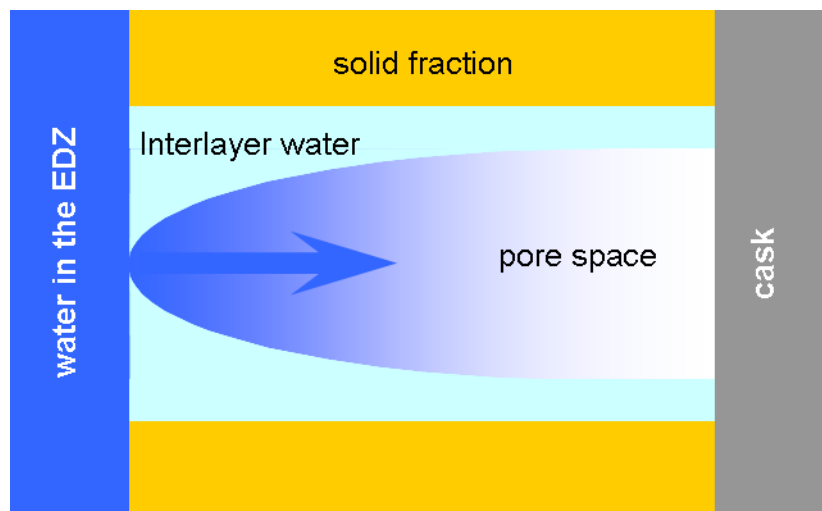
Fig. 7.1   Re-saturation of bentonite in the vapour diffusion model

In the vapour diffusion model, the water vapour coming from the EDZ diffuses through the pore volume. Advective intrusion of water into the bentonite is not considered. Depending on the size of the pore channels, the underlying processes in question are either binary gas diffusion, Knudsen diffusion or, in a transition area, a mixture of both. At any rate, the driving force for the diffusion process is the gradient of the partial vapour pres-

sure or the partial vapour density. The fundamental principles for the choice of a diffusion coefficient are explained in detail in Appendix A. There, a proposal can also be found how to determine the diffusion coefficient in the transition area.

It is assumed for simplification that there is always 100 % vapour saturation at the inflow boundary, i. e. the EDZ. The boundary on the opposite side bordering on the cask is a no-flow boundary. In between, there is a medium whose porosity is variable in space and time. The porosity depends on the amount of water that is hydrated locally in the interlayer. This amount of water ensues in turn from an integral of the local transient hydration rate over time. The re-saturation of the bentonite via water vapour can therefore be considered as a diffusive flow of vapour in a porous medium with a locally variable porosity and a locally variable sink for the vapour.

For the establishment of a mathematical model, the quantitative description of hydration is of central relevance. For this reason, an equation is initially set up for the hydration rate before the balance equation for the vapour mass is derived.

7.2 Hydration and hydration rate

7.2.1 Chemical potential

The intensity of the vapour flow which is guided by hydration from the pore volume into the interlayer is governed by the difference between the chemical potential of the vapour in the pore volume Π_p and the chemical potential of the interlayer water Π_i. The chemical potential of the vapour in the pore volume ensues from thermodynamic considerations (e. g. [28]) relating to

$$\Pi_p = \frac{RT}{M_w} \ln r_h \qquad (7.1)$$

Π_p - chemical potential of the vapour in the pore volume [J/kg]
Π_i - chemical potential of the interlayer water [J/kg]
r_h - relative humidity [-]

The relative humidity is defined by

$$r_h = \frac{p_v}{p_{sat}} \qquad\qquad (7.2)$$

The potential Π_p is proportional to the relative humidity. The chemical potential of the interlayer water Π_i is, on the other hand, proportional to the water content of the bentonite, assuming that the water is mainly present in the interlayer. The water content is explained as

$$w = \frac{m_w}{m_b} \qquad\qquad (7.3)$$

w - water content [-]
m_w - mass of water [kg]
m_b - dry bentonite mass [kg]

Hydration leads to the fact that the chemical potential of the interlayer water increases and converges towards the value of the chemical potential of the vapour in the pore volume. The system is in equilibrium when the chemical potentials are equal:

$$\Pi_p = \Pi_i \qquad\qquad (7.4)$$

In this case, with any optional pre-set relative humidity, an equilibrium of water content w_{eq} will establish itself [35], [28]. A state of equilibrium will also establish itself in the reverse case when a body of bentonite with an optional water content is placed in a sealed canister. This functional relationship between relative humidity and water content in the equilibrium is referred to as adsorption isotherm since the process of the agglomeration of water can also be understood as adsorption on the surfaces of the elementary layers. Therefore the following applies:

$$r_{h\,eq} = f(w) \qquad\qquad (7.5)$$

$r_{h\,eq}$- relative humidity in equilibrium with the water content [-]

If the chemical potential of the interlayer water can thus be determined for a concrete state of equilibrium through (7.1) and (7.4)

$$\Pi_i = \frac{RT}{M_w}(\ln r_{h\,eq}),$$ (7.6)

then Π_i for a fictitious state of equilibrium with optional water content can be indicated with the help of (7.5):

$$\Pi_i = \frac{RT}{M_w}(\ln r_{h\,eq}(w)).$$ (7.7)

For the potential difference it therefore ensues that

$$\Delta\Pi = \Pi_p - \Pi_i = \frac{RT}{M_w}\ln\frac{r_h}{r_{h\,eq}(w)}.$$ (7.8)

The adsorption isotherms for bentonite given in [35] and [28] can be roughly approximated by a linear relationship:

$$r_{h\,eq}(w) = \frac{w}{w_{max}}$$ (7.9)

w_{max}- fictitious water content at 100 % relative humidity for linear approximation of the adsorption isotherm [-]

The proportionality factor $1/w_{max}$ is a fictitious value since the isotherm nearing 100 % relative humidity deviates clearly from the linear approximation. In the area of high water contents, uncertainties in the calculation of the chemical potential of the interlayer thus have to be expected.

While the linear approximation can be sufficiently accurate up to a water content of 25 % to 30 % it introduces intolerable errors in the analysis of the uptake experiments with a saturated vapour atmosphere as described in Chapter 8.4.3. In order to refine approximation (7.9) a quadratic term can be added in the relationship $w_{eq} = w_{eq}(r_{h\,eq})$ as illustrated in Fig. 7.2. Inverting of this relationship yields:

$$r_{h\,eq}(w) = \sqrt{\frac{w}{\Delta w_{max}} + \left(\frac{w_{max}}{2\Delta w_{max}}\right)^2} - \frac{w_{max}}{2\Delta w_{max}} \qquad (\,7.10\,)$$

Δw_{max}- increment from fictitious value w_{max} to the actual maximum water content [-]
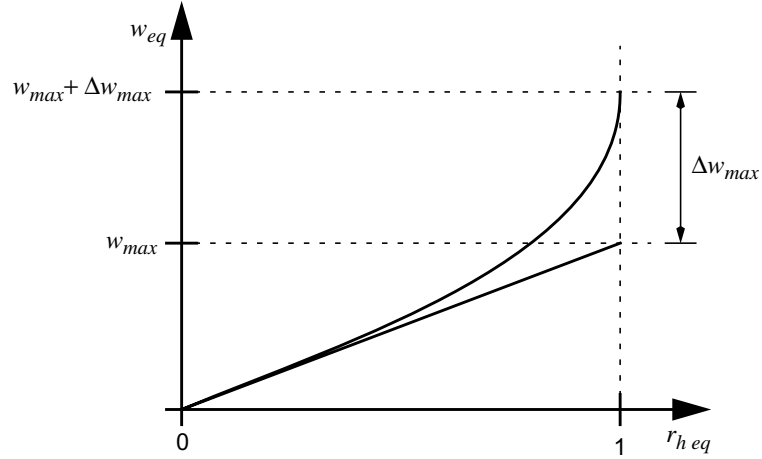
Fig. 7.2   Quadratic approximation of the adsorption isotherm

7.2.2   Hydration rate

The specific vapour mass flow $\dot{m}$ from the pore volume to the interlayer is proportional to the potential difference $\Delta\Pi$ In equation (7.11), the connection is established by a proportionality factor a:

$$\dot{m} = a\,\Delta\Pi = a\left(\frac{RT}{M_w}\ln\frac{r_h}{r_{h\,eq}}\right) \qquad (\,7.11\,)$$

$\dot{m}$ -   specific hydration rate [kg$_{water}$/(kg$_{bentonite}$ s)]

a -   proportionality factor [(kg$_{water}$ s)/(kg$_{bentonite}$ m^2)]

The proportionality factor a is an empirical parameter. A literature research gave no direct indications about the order of magnitude of the this factor and possible dependencies. It can be derived, though, from uptake experiments of unconstraint samples in a high humidity atmosphere. This kind of experiment was found in [28] and [45], but from the test descriptions an unsuitability for the purpose at hand was suspected as described in further detail in Chapter 8.3.2. Therefore the experiments described in Chapter 8.3 were carried out in order to determine the proportionality factor a from well controlled uptake tests.

In this project, a linear proportionality with a constant factor a is assumed as a first approximation. This specific choice, however, is irrelevant for the further explanations. All equations containing the factor a will still maintain their validity if a is a variable instead of a constant.

Together with the constants in (7.11), the proportionality factor a can be summarised in one single coefficient, which in the following shall be referred to as "reference hydration rate" $\dot{\bar{m}}_{ref}$.

$$\dot{\bar{m}}_{ref} = a\frac{RT}{M_w} \qquad (7.12)$$

$\dot{\bar{m}}_{ref}$ - reference hydration rate [kg$_{water}$/(kg$_{bentonite}$ s)]

If the factor a is a constant, the reference hydration rate is also a constant and simplifies equation (7.11) to

$$\dot{\bar{m}} = \dot{\bar{m}}_{ref} \ln \frac{r_h}{r_{h\ eq}} \qquad (7.13)$$

With the help of (7.2), the hydration rate can also be expressed as a function of the partial vapour density, which means that in the numerical model it can be directly inserted in the sink term of the differential equation:

$$\dot{\bar{m}} = \dot{\bar{m}}_{ref} \ln \frac{\rho_v}{\rho_{sat}\ r_{h\ eq}(w)} \qquad (7.14)$$

ρ_v - partial vapour density [kg/m^3]
ρ_{sat} - partial saturated vapour density [kg/m^3]

As the reference hydration rate contains the empirical factor a, $\dot{\bar{m}}_{ref}$ is also an empirical parameter. It can be determined from the re-saturation experiments according to Chapter 8.3 at unhindered swelling. The simplest form of the conditional equation for the evaluation of the experiments ensues from equation (7.13) by insertion of an approach for the adsorption isotherm. The linear approach (7.9) chosen here leads to

$$\dot{m} = \dot{m}_{ref} \ln \left(r_h \frac{w_{max}}{w} \right) \qquad (7.15)$$

7.3 Mathematical model

7.3.1 General balance equation

Conservation equations can be derived from a general balance equation for extensive state variables $Z(t)$ [14]:

$$Z(t) = \int\limits_{B(t)} z(x, t)dV \qquad (7.16)$$

Z - extensive state variable [?]

z - field variable [?/m^3]

B - volume of a moving body [m^3]

The eulerian view of the time-dependent variation of the state variable leads to the following form of a balance equation for the field variable z pertaining to Z in a fixed control volume G:

$$\int\limits_{G} \left(\frac{\partial z}{\partial t} + \nabla \cdot (\mathbf{v}z + \boldsymbol{J}) - r \right) dV = 0 \qquad (7.17)$$

G - solution area (control volume) [m^3]

$\mathbf{v}$ - velocity field [m/s]

$\boldsymbol{J}$ - vector of the mass flow density due to diffusion [kg/(m^2 s)]

r - mass source density [kg/(m^3 s)]

In the integral, the first term represents the local variation of the state variable in G, the second term the advective transport of the state variable, the third term the non-advective transport - in this case the diffusive transport - through the surface of the control volume, and the fourth term the sources and sinks of Z in G.

7.3.2   State variable

In the case of the re-saturation with vapour, the state variable Z is tantamount to the amount of vapour mass m_v in the pore space. The field variable z pertaining to the state variable Z is accordingly

$$z = \Phi \rho_v \qquad\qquad (7.18)$$

Φ -   porosity [-]

The porosity as well as the partial vapour density are variables in space and time. The partial vapour pressure follows approximately the equation of state for ideal gases

$$\rho_v = \frac{p_v}{RT} \qquad\qquad (7.19)$$

The porosity in equation (7.18) is defined as the ratio of the pore space to the total volume of the bentonite. Here, the pore space is variable in time and space. The assumption is that the initial pore space is reduced upon re-saturation by the same degree that the interlayer volume increases through hydration:

$$V_p = V_{p0} - V_i \qquad\qquad (7.20)$$

V_p -   pore space [m^3]
V_{p0} -   initial pore space [m^3]
V_i -   volume of the interlayers [m^3]

The volume of the interlayers is variable both in space and time in the model; it can be calculated from an integral of the hydration rate over time The hydration rate is considered in the differential equation as the sink term r. Here, the density of the hydrated water is equated approximately with the density of freshwater as discussed in more detail in Appendix C:

$$V_i = \int_0^t \left(\frac{r}{\rho_w} \right) dt \qquad\qquad (7.21)$$

56

It therefore follows for the porosity that

$$\Phi = \Phi_o - \frac{V_i}{V_b} \tag{7.22}$$

7.3.3 Advection term

It is assumed that the gas in the pore space has the same pressure everywhere. Consequently, the gas phase is not moved. Therefore no advective vapour transport is considered.

7.3.4 Diffusion term

The free diffusion of vapour in air as well as Knudsen diffusion follow Fick's approach for the mass flow density J_m (e. g. [13]):

$$J_m = -D_m \frac{d\rho_v}{dx} \tag{7.23}$$

J_m - mass flow density due to diffusion on microscopic level [kg/(m^2 s)]
D_m - diffusion coefficient on microscopic level (see Appendix A) [m^2/s]

Formally, the two transport mechanisms only differ in the diffusion coefficient D_m. Which process is most relevant and how the diffusion coefficient has to be calculated in each case is explained in detail in Appendix A. There, the transition to the macroscopic level is also performed, and the associated effective diffusion coefficient is indicated. In a one-dimensional formulation, the ensuing macroscopic mass flow density J due to binary gas diffusion therefore is

$$J = -\Phi \tau D_m \frac{\partial \rho_v}{\partial x} \tag{7.24}$$

τ - tortuosity [-]

7.3.5 Sink term

In line with the approach for the quantitative description of hydration which is deduced in Chapter 7.2, the specific hydration rate $\dot{m}$ can be calculated as:

$$\dot{m} = \dot{m}_{ref} \ln \frac{\rho_v}{\rho_{sat} \, r_{h\,eq}(w)} \qquad (7.25)$$

Multiplied with the dry density of the bentonite, the hydration rate forms the sink term in the balance equation (7.17):

$$r = \dot{m}\rho_d \qquad (7.26)$$

7.3.6 One-dimensional form of the balance equation for the vapour mass

Under the condition that an integral equation applies to any arbitrary form of the solution area G, the equation can be brought into a differential form. In this case, equation (7.17) will have the one-dimensional form

$$\frac{\partial}{\partial t}(\Phi\rho_v) - \frac{\partial}{\partial x}\left(\Phi\tau D_m\frac{\partial\rho_v}{\partial x}\right) = \bar{r} \qquad (7.27)$$

To simplify matters, constant tortuosity is assumed. The application of the product rule and the insertion of equations (7.24), (7.25) und (7.26) will then lead to

$$\Phi\frac{\partial\rho_v}{\partial t} + \rho_v\frac{\partial\Phi}{\partial t} - \tau\left(\Phi D_m\frac{\partial^2\rho_v}{\partial x} + D_m\frac{\partial\rho_v}{\partial x}\frac{\partial\Phi}{\partial x} + \Phi\frac{\partial\rho_v}{\partial x}\frac{\partial D_m}{\partial x}\right)$$

$$= \rho_d\dot{m}_{ref} \ln \frac{\rho_v}{\rho_{sat} \, r_{h\,eq}(w)} \qquad (7.28)$$

The implementation of this partial differential equation in a numeric model is described in Appendix B.

8   Laboratory measurements

8.1   Motivation

The test of numerical models describing the re-saturation of bentonite still poses a considerable problem for two reasons. First, the process as such is still not fully understood. Second, the measurement of a control parameter, as e. g. the water content, requires an extreme effort. This applies even more, if non-isothermal conditions are investigated. Only few experiments are known which provide the water content as a parameter that is variable in space and time in a bentonite test specimen [37], [3], [20], [4], [47]. These experiments were performed under conditions of highly varying complexity as regards the geometry of the test specimen and the physical processes involved. What they have in common is that they only provide sufficient data concerning the water content either for the time dimension or the space dimension, but never for the two at the same time [33]. This gap is to be filled with the re-saturation experiments introduced below[1].

The experiments are aimed exclusively at the hydraulic processes, i. e. all effects that might complicate the re-saturation process were excluded. Water was allowed to enter the cylindrical test bodies from the front end in order to allow a one-dimensional description of the re-saturation process. The compacted bentonite samples were confined in a hollow steel cylinder so the volume of the sample remained constant. The experiments were performed at constant room temperature.

The aim of the experiments was to create a basis to test the conceptual models developed in Chapters 5 to 7 as well as of other computer codes relating to the re-saturation of bentonite in general. This is the reason why the re-saturation experiments were performed with liquid water as well as with water vapour. Although re-saturation with Äspö solution came closest to a re-saturation scenario, it could not be easily distinguished whether the water in the bentonite actually propagates by liquid water transport, by vapour transport or by transport of both phases at the same time. The experiment with vapour, on the other hand, offered the possibility of an isolated investigation of the vapour transport. It was

---

[1]   The experiments described in [3] and [4] provide at least two or three water content curves for different uptake periods. But they differ in the degree of compaction and in the initial water content. This allows only a qualitative comparison and excludes merging of the results.

therefore intended beyond the testing of the model to draw conclusions regarding the actually developing processes by comparing the experiment with the results of model calculations.

In addition, re-saturation experiments with almost saturated vapour and unconstrained test bodies were also carried out. The aim of these experiments was to quantify the hydration rate in the case of re-saturation with vapour. This way, the reference hydration rate was determined which was needed for the vapour diffusion model and had so far been unknown.

8.2 Re-saturation with Äspö solution

8.2.1 Description of the experiment

The re-saturation of compacted MX-80 samples with Äspö solution was investigated in the geotechnics laboratory of GRS Braunschweig to simulate the conditions prevailing in the Swedish Äspö underground laboratory. The composition of the solution is given in Table 8.1

Tab. 8.1   Composition of the Äspö solution

Na	K	Ca	Mg	Cl	SO$_4$
mmol/l	mmol/l	mmol/l	mmol/l	mmol/l	mmol/l
79.67	0.25	17.06	3.33	113.92	3.40

Five measuring cells were available for the experiments. Fig. 8.1 shows a cross-sectional view of a measuring cell and illustrates at the same time the intention of the re-saturation experiment.

A hollow steel cylinder contained the samples with compacted bentonite. The cylinder's wall thickness of one centimetre was to ensure that deformations remained at a minimum even at swelling pressures within a range of 10 MPa to 20 MPa. At both ends, the bentonite samples were constrained by tight-fitting solid closing cylinders. In one of the closing cylinders - shown on the left in Fig. 8.1 - there were two penetrations with hose con-

nections on the outside. Via a connection fitted with a shut-off valve, the water is directed into the measuring cell and out again via the second connection, from where it flows into a burette. This way it was possible to check when the air on the inlet had been displaced by the water. Following the closure of the valve, the burette on the one hand supplied the measuring cell with water under almost non-existing excess pressure; on the other hand, it allowed the measuring of the outflowing amount of water. The filling of the burette was repeated as soon as a certain minimum water level was exceeded. Fig. 8.2 shows the complete experimental set-up as well as two detail views of a measuring cell.
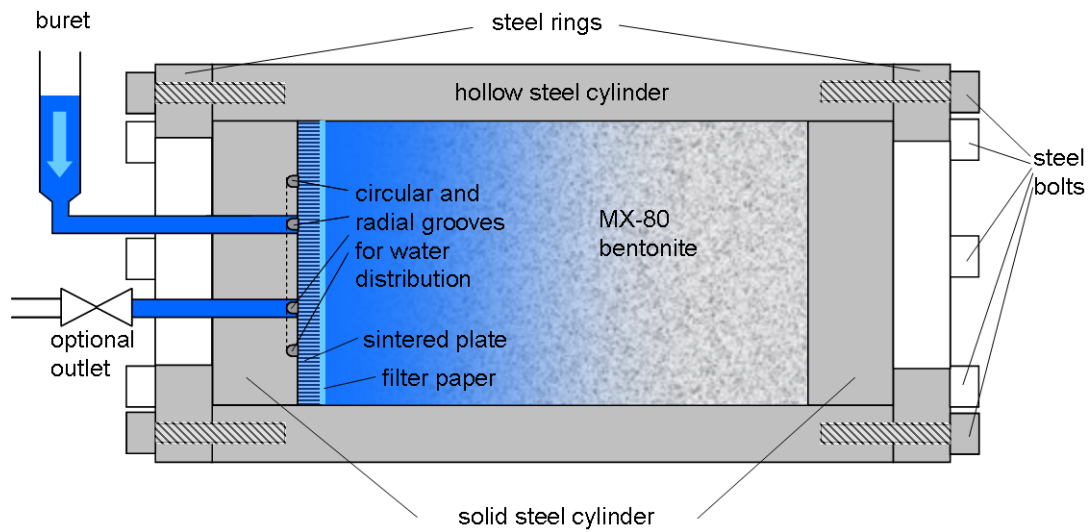

**Fig. 8.1**   Cross-sectional view of a measuring cell

Inside the measuring cell, the penetrations of the closing cylinder end in circular and radially interconnected milled grooves, which were to ensure an even distribution of the water over the front end of the sample. For the same reason, a sintered plate with large pores was additionally arranged between the closing cylinder and the sample. This way the front end of the bentonite sample was evenly and continuously supplied with water, which later allowed a one-dimensional description of the re-saturation process.

MX-80 bentonite in as-delivered condition with a water content of about 10 % was used for the experiment. To make the samples, the pulverised material was compacted in the measuring cells to form a cylindrical core with a length of about 10 cm and a diameter of 5 cm. To prevent an intrusion of the sample material into the sintered plates, filter paper was inserted between the sample and the sintered plate.

experimental set-up

measuring cell (side view)
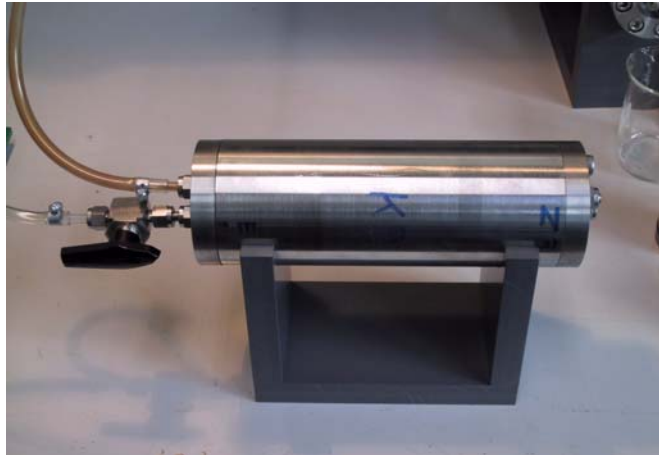
measuring cell (front view)

Fig. 8.2   Experimental set-up as well as two detail views of a measuring cell

It had been found in preliminary experiments that the compaction of the entire sample in one piece resulted in density differences between the face areas of the sample of about 300 kg/m^3. In order to minimise the compaction-impeding influence of the wall friction, the sample material was therefore divided into ten separate amounts which were compacted in the measuring cell one after the other to reach the intended bentonite dry density of 1500 kg/m^3. Close contact between the specimen and the sintered plate was achieved by starting the compaction procedure at the plate end side. The force applied for the making of the samples was approx. 20 kN to 25 kN, which at a given area of approx.19.63 cm^2 corresponds to a compaction pressure of approx. 10 MPa to 13 MPa.

The re-saturation experiments in the individual measuring cells were carried out at a constant temperature of 20 °C over various periods of time differing in length. The total amount of water absorbed by the sample was measured by reading off the water level in the burette as a function of the time elapsed.

In accordance with a flow chart in which the stay time was specified, the individual experiments were terminated and the corresponding samples cut up into discs of only a few millimetres thickness. The thickness of the discs was measured before they were cut off in order to minimise errors in the determination of their volume due to deformation as a result of the mechanical pressure relief. To determine the water content in the individual discs, the material was dried at 105 °C over 24 hours and was weighed before and after this period. The water content then ensued from the ratio of the amount of water extracted through drying and the dried solid-matter mass of the bentonite. The dry density of the discs could be calculated from the dry mass and the volume of the discs.

The representation of the water content or the dry density of the bentonite discs at the position of the disc's centre of gravity resulted in a spatial distribution at a given point in time. Thus each sample yields only one spatial distribution. To check the accuracy of this procedure, most of the experiments were repeated so that two curves each exist for the relevant points in time. In the ideal case, these had to be identical.

8.2.2   Results

The water uptake of the samples is plotted in Fig. 8.3 as a function of time. It shows a characteristic distribution as has also been the result of other re-saturation experiments, e. g. [28]. There is very little scattering of the values of the 13 measurements performed.

The water content distributions obtained from the measurements are shown in Fig. 8.4. The development of the curves is characteristic of diffusion-like water transport. In the direction of the diffusion, the water content becomes less, with the gradient decreasing with the distance from the inflow boundary. With the exception of the first plotted point at the inflow boundary, the profiles show remarkable reproducibility.
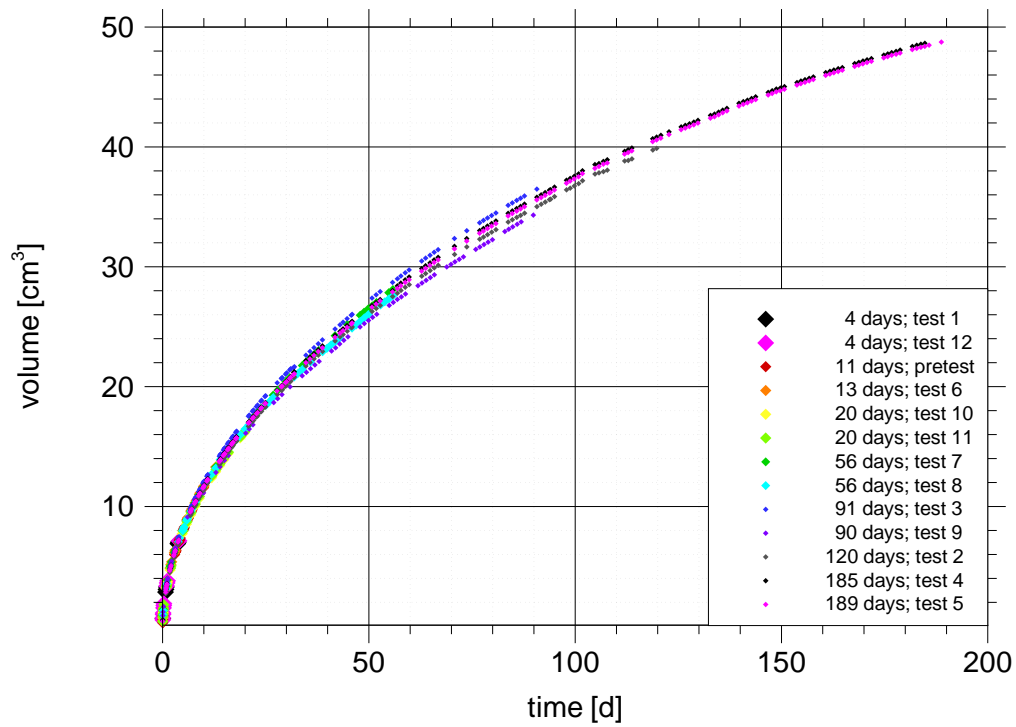
Fig. 8.3   Water uptake as a function of time; re-saturation with Äspö solution
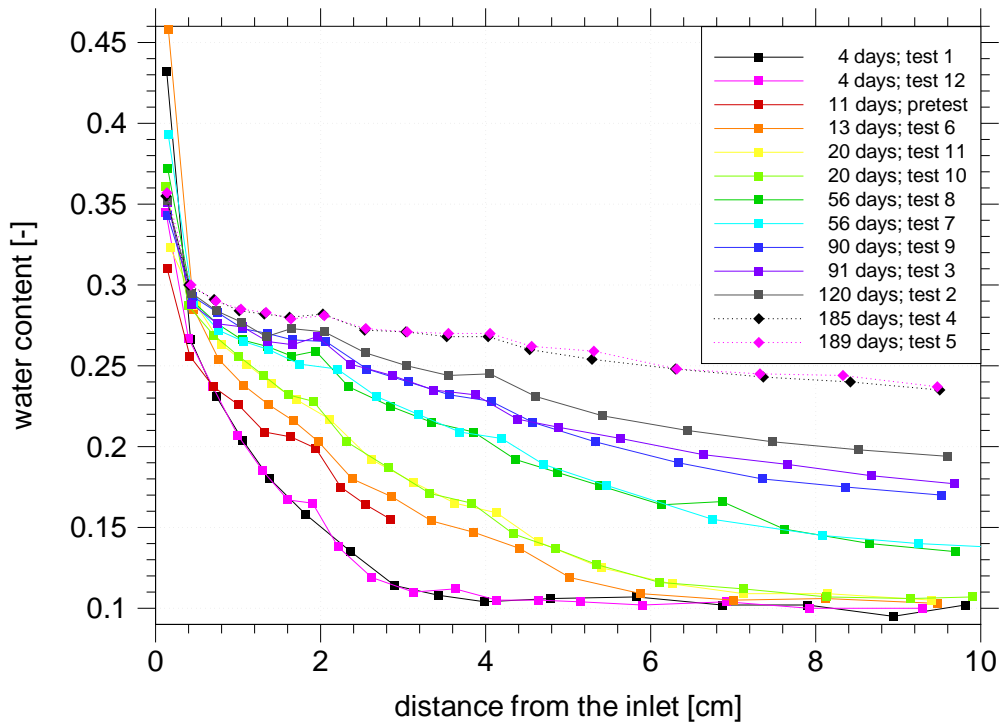

Fig. 8.4   Water content as a function of penetration depth;

re-saturation with Äspö solution

The data for the bentonite disc located immediately at the inflow boundary, which covers the area of the first three millimetres in the sample, fall outside the trend of the further distribution for two reasons. First, these discs have absorbed much more water than the theoretical maximum water content of 31 % (cf. Appendix D) would let one expect. Second, a closer review of these data reveals that the measured water content in the first disc - contrary to all other discs - does not depend on the duration of the experiment.

The dry density distribution of the bentonite discs shown in Fig. 8.5 allows the assumption that initial swelling at the inflow boundary has led to a decompaction of the bentonite in the area of the inflow boundary. It clearly shows a strong decrease of the dry density in the first disc. Consistent with a decompaction at the front end is also the comparably low densification in the connecting area. The swelling pressure causing the densification is opposed by the wall friction which reduces the compacting effect of swelling. Densification reaches as far as 4 to 5 cm into the specimen as can be seen in Fig. 8.5. There is a less pronounced density decrease further away from the inlet and a final drop farthest from the inlet. These are most probably an artefact of the compaction procedure.
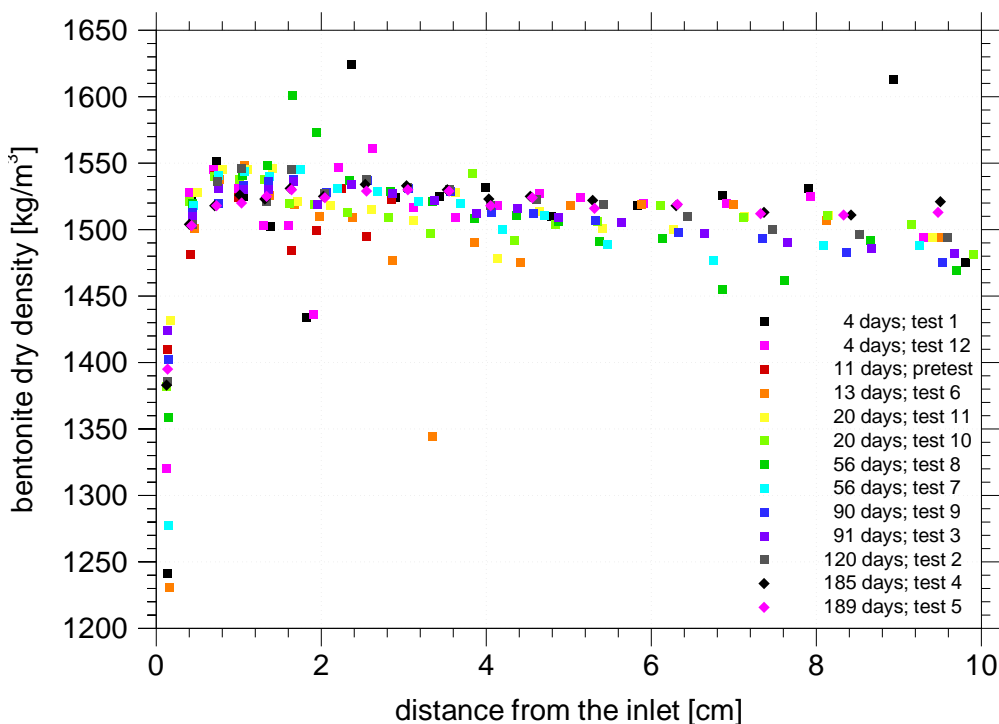

Fig. 8.5   Bentonite dry density as a function of penetration depth;
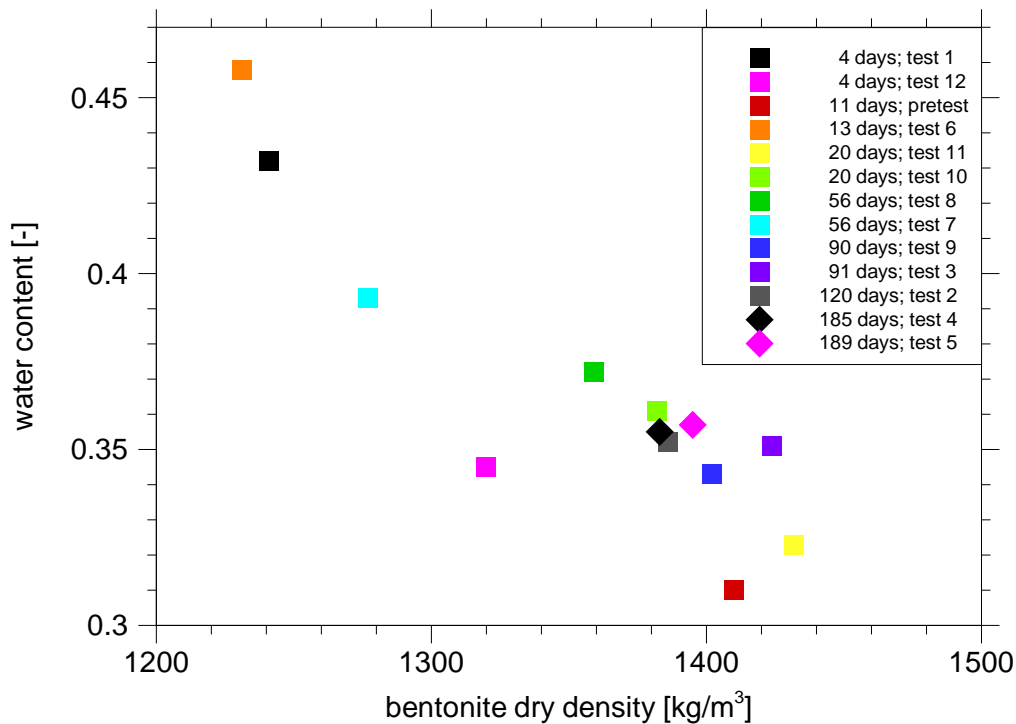re-saturation with Äspö solution

Fig. 8.6   Correlation between water content and bentonite dry density in the first disc

The assumption of decompaction at the front end is also supported by Fig. 8.6, which shows a clear correlation between water content and dry density in the first disc. A further indication of the local decompaction at the inflow boundary is provided by model calculations with THM-code CODE-BRIGHT simulating this re-saturation experiment with Äspö solution [57]. These calculations revealed an increased porosity at the inflow boundary. However, a comparison with the measured data can only be qualitative since bentonite parameters for the Spanish Almeria bentonite were used instead of those for MX-80.

For the further investigations, however, the effect of this densification can be neglected in a first approximation as it only causes significant changes immediately at the inflow boundary. Moreover, all density changes have taken place within the first four days. During the period under review, the measured dry density distributions showed no dependence on time.

A further important aspect of re-saturation becomes noticeable when the water content - analogous to a breakthrough curve - is plotted at a fixed position as a function of time. Such a breakthrough curve can be established when the water content distribution is understood as a step function as shown in Fig. 8.7. The width of the steps corresponds to the thickness of the cut-off bentonite discs and the height to the average water content in a disc.This way, a certain position is attributed the average water content of the disc that contains this position.
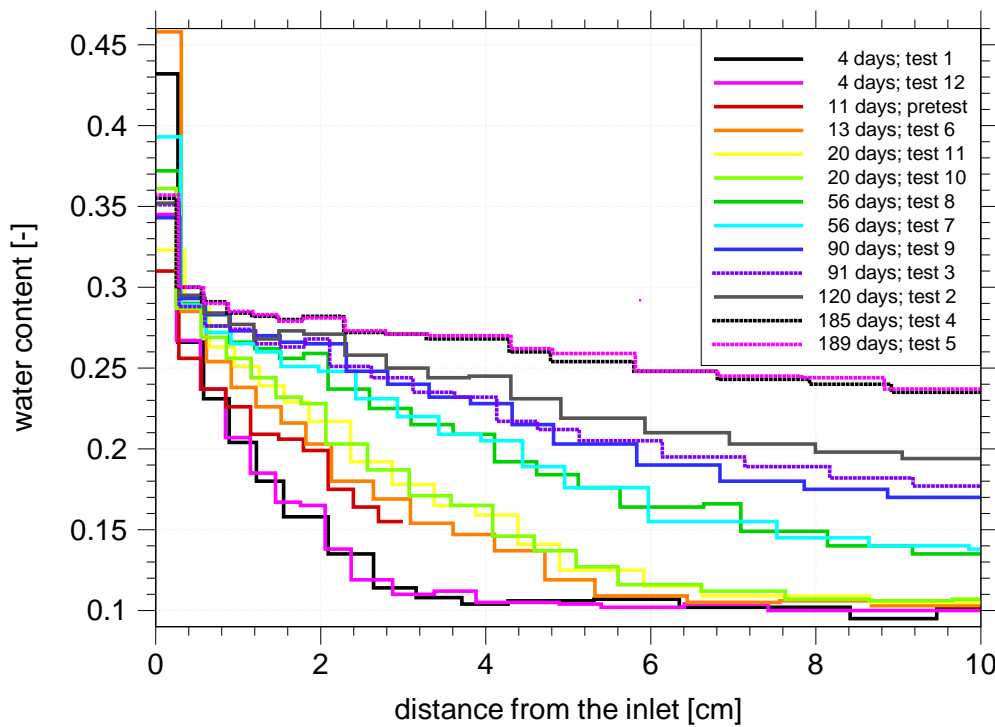

Fig. 8.7   Water content as a function of penetration depth; alternative to Fig. 8.4

Fig. 8.8 contains breakthrough curves for various positions. The value for the water content was averaged when two curves were available for one point in time. What is interesting above all is the curve showing the water content at a distance of 4 millimetres from the inflow boundary. Four days into the experiment, the first measured value is already 26.7 %. The dynamics that lead to this value cannot known from these experiments. After another nine days, the water content has reached 28.5 % and subsequently increases slowly until after half a year it is about 30 %. However, this may not yet be the final value of the water content.
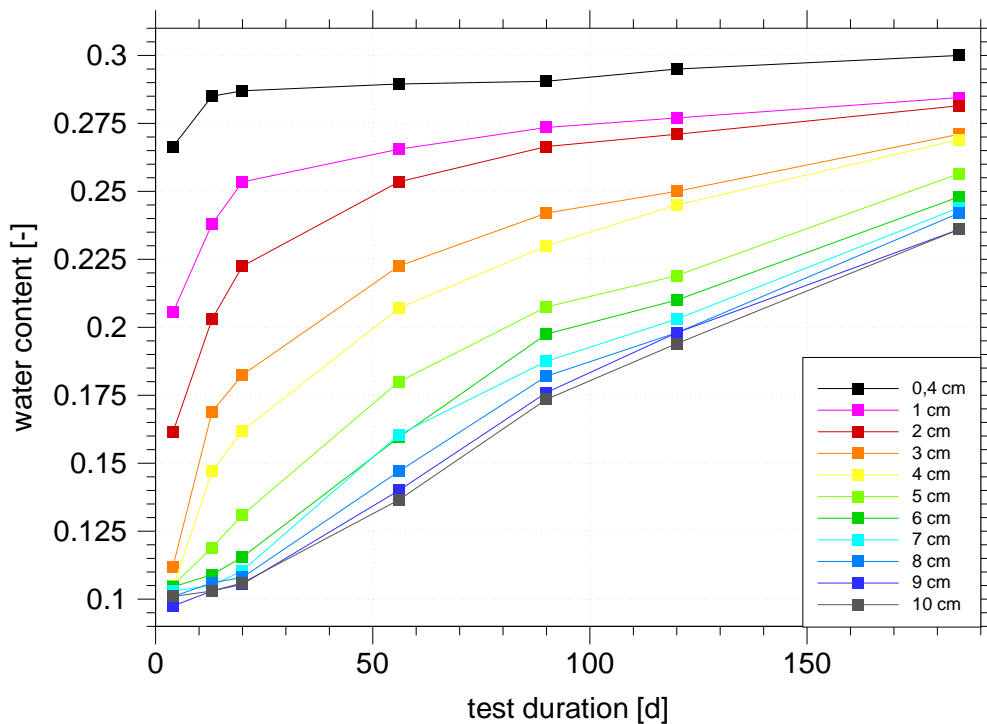
Fig. 8.8   Water content at fixed positions as a function of the test duration; re-saturation with Äspö solution

What makes these curves so remarkable ensues from the following consideration: the amount of water which during the course of the experiment is transported through the sample section located 4 millimetres from the inflow boundary is a multiple of the amount that would be necessary for the re-saturation of this section. The velocity of the re-saturation in this place is therefore not governed by the amount of water available but by the dynamics of hydration. Moreover, compared to the water transport, hydration in this place is a very slow process. This observation fits a dynamic re-saturation via water vapour as described in Chapter 7 better than a fast re-saturation via liquid water as declared in [49].

8.3 Re-saturation of unconstrained test bodies with vapour

8.3.1 Experiment description

The aim of the re-saturation experiments with the unconstrained test samples in an atmosphere saturated with vapour was to quantify the hydration rate as a function of the water content. The intention was to test with these data the mathematical description of the hydration process derived in Chapter 7.2 and to determine the reference hydration rate needed for the vapour diffusion model.

Part of the samples consisted of MX-80 powder which was poured loosely into petri dishes. This way, the vapour could enter largely unhindered in the pore space and diffuse almost instantaneously through the pore owing to the high diffusion coefficient. Since expansion of the samples was not hindered, the pore space grew with the swelling of the clay particles, with the result that the porosity remained constant. It was therefore not to be expected that vapour uptake would be hindered with increasing water content.

Furthermore, compacted cylindrical discs with a diameter of 5 cm and a thickness of 5 mm were also placed in dishes. The manufacture and the degree of compaction of these discs corresponded to that of the sample material of the re-saturation experiments with constraint samples described in Chapters 8.2 and 8.5.

Part of the pulverised and also of the compacted samples were dried at 105 °C until constant weight was reached. This was done to back up the notion that the hydration rate only depends on the prevailing water content and not on the initial water content. The influence of the temperature on the uptake of water was also investigated. Each of the sample types described here was re-saturated at a temperature of 20 °C as well as of 50 °C.

A certain statistical certainty of the measuring results was to be achieved by producing three test bodies of each sample type. This means that with 4 sample types and two different temperatures, a total of 24 test bodies were required.

Following the measurement of the initial weight, the samples were placed in desiccators above liquid water. The evaporation of the water ensured the necessary vapour-saturated atmosphere. In addition, to speed up the evaporation, blotting paper was set up along the walls of the desiccators, with the bottom end immersed in the water. The samples were then weighed at certain intervals. At the end of the experiments, the samples were dried out in order to determine the dry density of the air-dry samples. The quotient from the weight during the re-saturation and of the dry mass then yielded the water contents of the samples.

8.3.2 Results

In Fig. 8.9, the results of the re-saturation experiments at 20 °C are summarised in a representation of the water content over the duration of the experiment. In addition, the measuring results of the preliminary experiment with powder, which was also carried out at room temperature, and the results of a re-saturation experiment from [28] are plotted in the graph. However, the data from [28] are quite unusual. Although the experiment periods are the same, the water content is clearly lower than in the other measurements. As [28] contains no detailed experiment description, it cannot be excluded that the swelling of the samples was constrained to a certain extend. This would reduce the vapour uptake, the diffusion velocity of the vapour through the sample and the amount of water that could be taken up and would therefore yield a false calculation of the reference hydration rate. For this reason these data are not considered.

A further re-saturation experiment with vapour is documented in [45]. However, the description of the experiment indicates already that this experiment was carried out with constrained swelling. Thus these data were not considered, either.

The measuring curves in Fig. 8.9 show a satisfactory, smooth distribution. The deviations are surprisingly strong, but lie at a maximum of about 12 %, with the exception of one curve for a compacted sample.
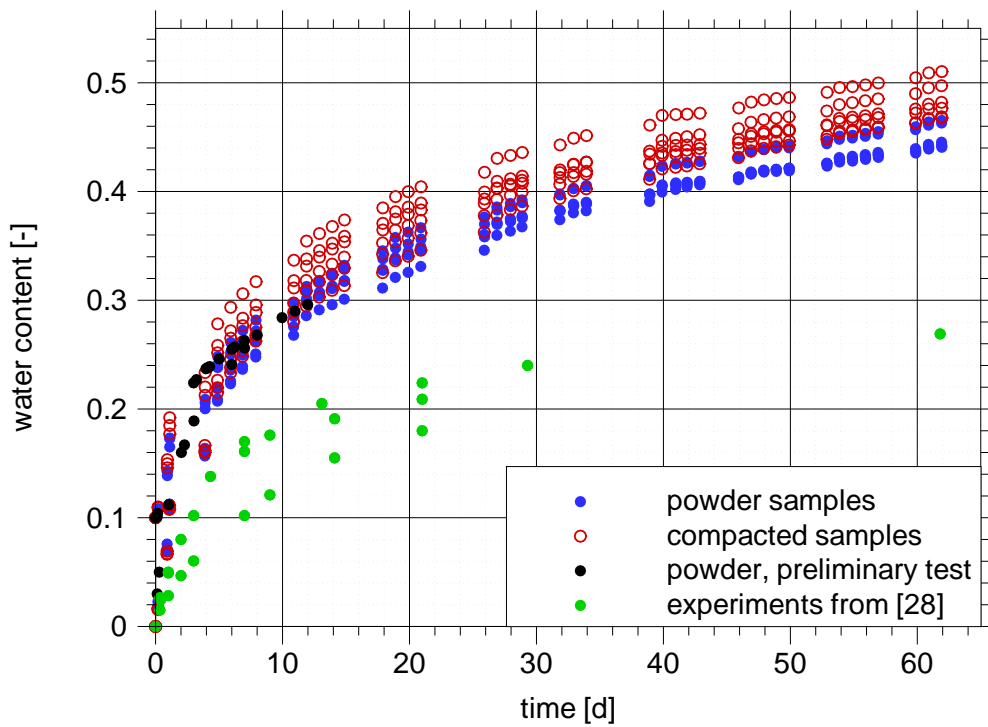
Fig. 8.9   Water content as a function of test duration;

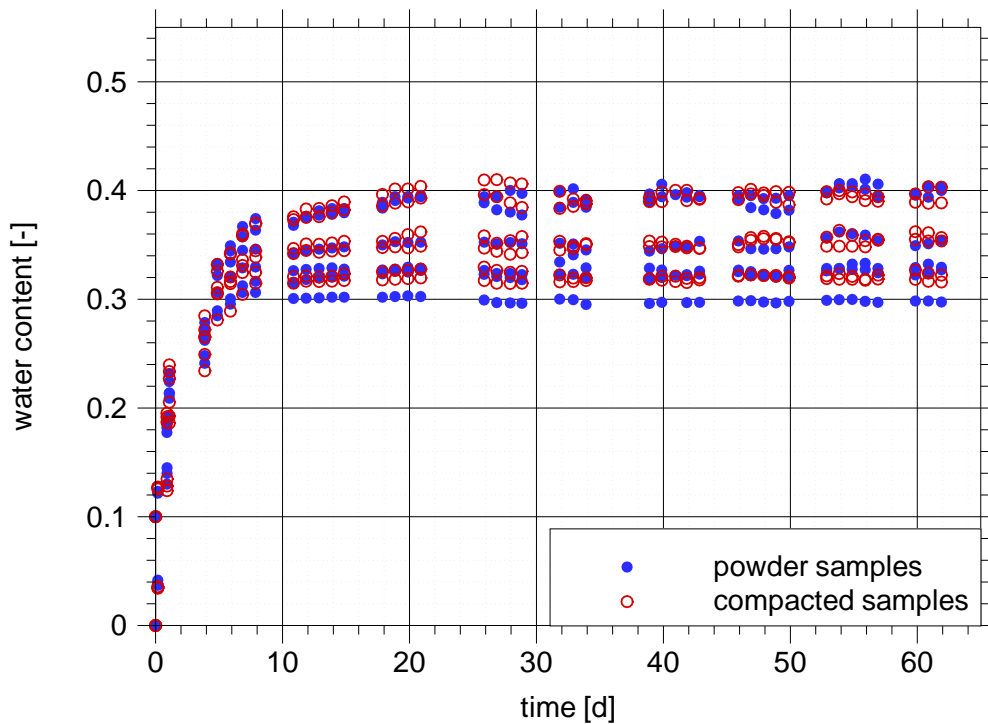unconstrained samples; re-saturation via water vapour at 20°C

Fig. 8.10   Water content as a function of time;

unconstrained samples; re-saturation via water vapour at 50°C

Fig. 8.9 shows that the initial water content has no influence on the dynamics of the re-saturation process. An initially very fast re-saturation is followed in all cases by an ever decreasing re-saturation velocity. In this connection, the oven-dry samples reach the water content of the air-dry samples within one day already. As can be seen in the representation in Fig. 8.10 that is analogous to Fig. 8.9, the same is true of the samples re-saturated at 50 °C.

Furthermore, a slight influence of the degree of compaction of the samples can be seen in Fig. 8.9. Over the first 10 days, the compacted samples absorb the water slightly quicker than the powder samples. After that, the hydration rates are about the same. Still, even after the 10-day period, the families of curves belonging to the respective two sample overlap, i.e. there is no significant difference.

This effect is not observed in the results of Fig. 8.10 regarding the samples re-saturated at 50 °C. The curves for the two sample types are distributed within a surprisingly wide range. However, the curves are not statistically distributed within this range but are arranged in four very narrow bands. No satisfactory explanation for this phenomenon has been found yet.

There exists, however, a clear correlation between the position of the samples in the oven and the extent of final saturation. As shown in Fig. 8.11, the samples were distributed over two desiccators and always remained in the same place inside the oven. The colours used in the diagram are a code for the distance from the oven door: black - shortest distance, red - middle distance, and green - longest distance. In Fig. 8.12 the same colour code is used for the illustration of the water contents. Apparently, the measured final water content decreases with the distance to the oven door. Only samples P14 and P15, which were placed in a corner of the oven, deviate slightly from this trend.

It may be that the different results were also caused by temperature differences in the oven. However, as indicated in Chapter 8.4.2, it is not the water content itself that is considered in the calculation of the reference hydration rate but merely the time-dependent hydration rate, which ensues from the gradient of the measurement curves. The gradients, however, do not differ as much as the measured values themselves, so that the deviations of the curves from each other are of subordinate interest
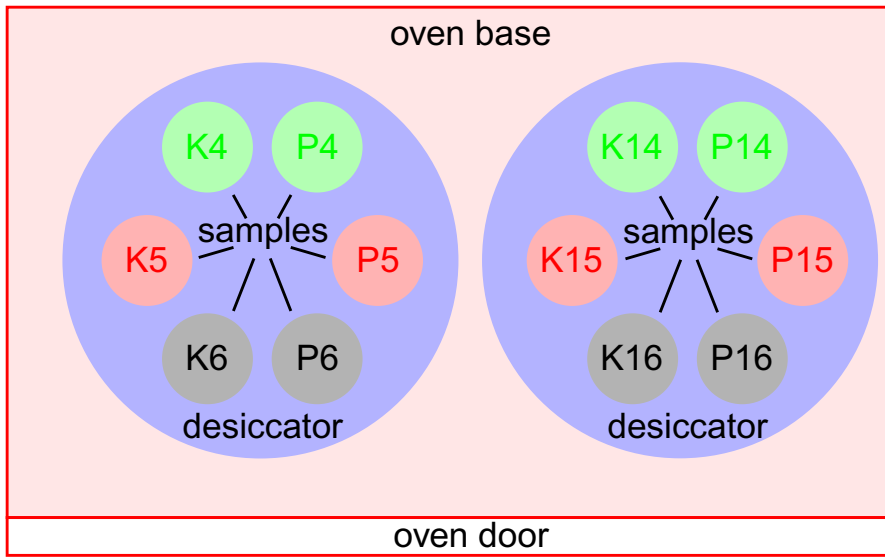
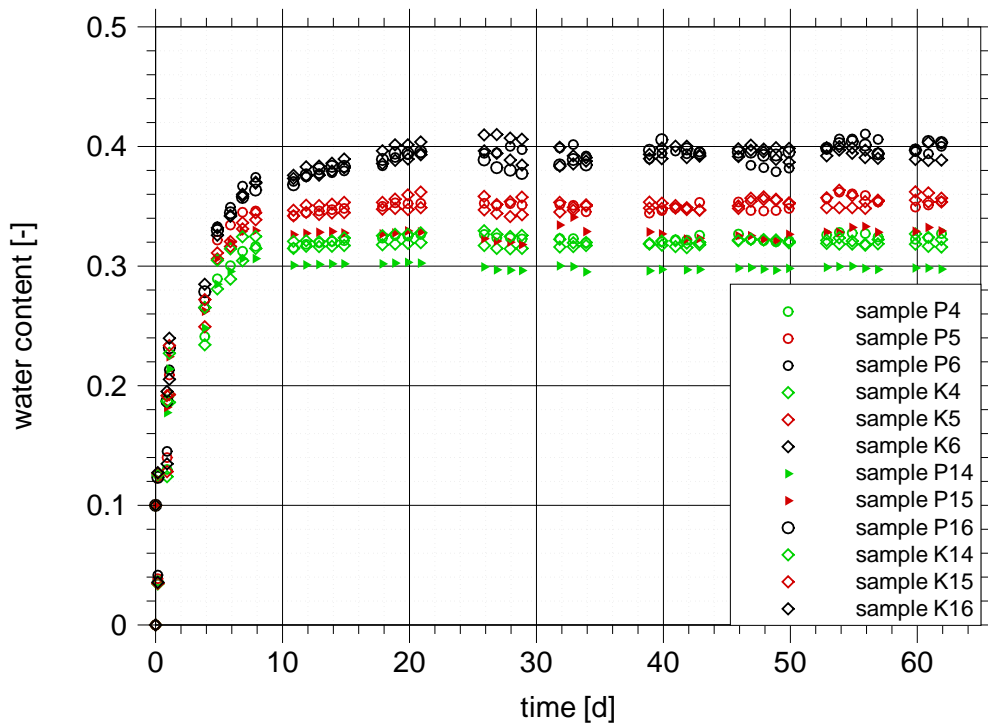**Fig. 8.11**   Location of the samples in the oven for heating up to 50 °C

Fig. 8.12   Correlation of water content at 50 °C distance from the oven door

A comparison of Figs. 8.9 and 8.10 finally shows that re-saturation at increased temperature develops more quickly. Also, with increasing temperatures, the amount of water that can be absorbed decreases. Final saturation of the samples re-saturated at 50 °C is therefore already achieved after 15 days, while the samples re-saturated at 20 °C have still not reached their final saturation even after a period of 65 days.

8.4   Determination of the reference hydration rate

8.4.1   Conditional equation

As described in Chapter 7.2, the reference hydration rate $\dot{m}_{ref}$ is an empirical parameter, the extent of which can be calculated with the help of equation (7.13):

$$\dot{m} = \frac{\dot{m}_{ref}}{\ln\left(\dfrac{r_h}{r_{h\ eq}}\right)}$$

The necessary input data for this equation are

-   the hydration rate $\dot{m}$,
-   the relative humidity in the pore space r_h, and
-   the relative humidity $r_{h\ eq}$ in equilibrium with the water content in the interlayers.

These data are obtained from the experiments described in Chapter 8.3 which yield the water content as a function of time.

8.4.2   Hydration rate

The hydration rate $\dot{m}$ can be calculated by approximation from the obtained data indicated in Chapter 8.3 with

$$\dot{m} \cong \frac{\Delta w}{\Delta t} \qquad\qquad\qquad\qquad (\ 8.1\ )$$

If the approximation (8.1) is applied to two respective neighbouring data points, it is even possible to create a distribution of the hydration rate as a function of time. With regard to the applicability of the results, however, it makes more sense to present the thus calculated hydration rates as in Fig. 8.13 as a function of the water content. This clearly shows on the one hand the exponential decrease of the hydration rate with the water content and on the other hand the increase of the hydration rate with the temperature. The samples heated up to 50 °C reached their saturation water content during the experiment period. In this diagram, the hydration rates fall abruptly towards zero once this value has been reached. Within the range of the water contents between 10 % and 30 % - in which the re-saturation of compacted bentonites mostly takes place - the rate decreases independent of the temperature by approx. one order of magnitude.
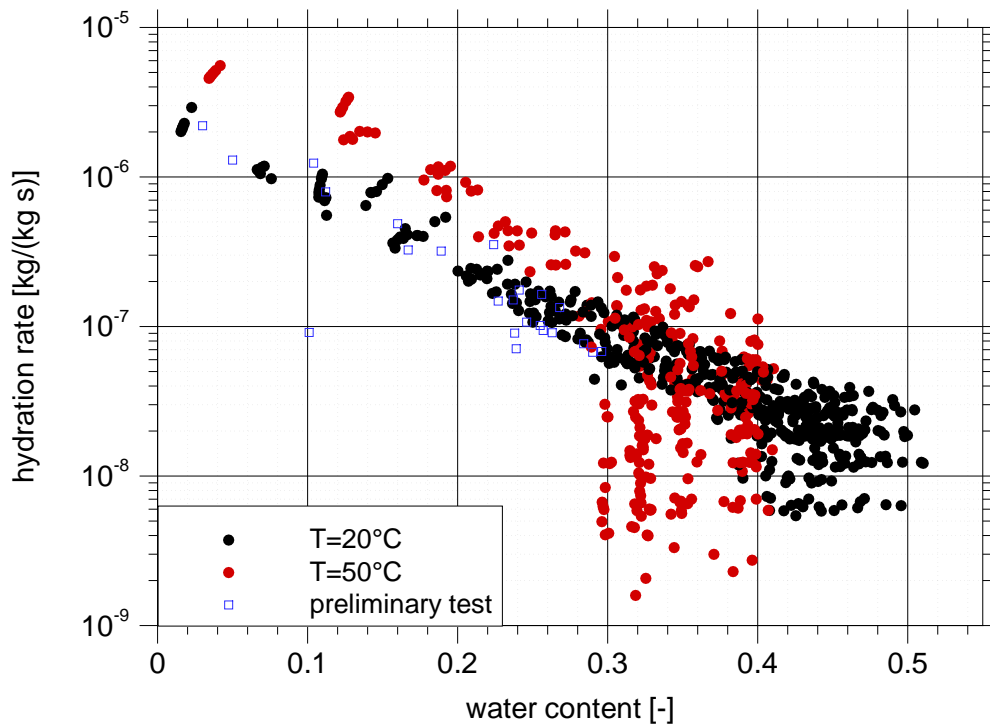

Fig. 8.13 Hydration rate as a function of the water content and temperature

8.4.3 Relative humidity levels

In equation (7.13), the relative humidity r_h is a measure for the chemical potential of the water vapour in the pore space. It ensues from the experimental conditions and by approximation equals one in the experiments described.

The fictitious relative humidity $r_{h\,eq}$, which would establish itself in the interlayers in equilibrium with the water content, is a measure for the chemical potential of the interlayer water. It can be calculated with the help of an adsorption isotherm as a function of the water content if no liquid water is present in the pores. In the case of liquid water, only the interlayer water fraction of the water content would have to be used as a basis.

As no isotherm was available for the experiment involving the temperature increased to 50 °C, the evaluation is restricted to the experiments carried out at room temperature, which includes the respective preliminary experiments. The isotherms for room temperature according to [35] and [28] are described with the more precise approach (7.10) given in Chapter 7.2. Assuming that a final saturation of the samples of 60 % water content establishes itself and that the linear approximation to the isotherm reaches a maximum value of 25 % water content, the values w_{max}=0.25 and Δw_{max}=0.35 are chosen for (7.10).

8.4.4 Reference hydration rate

The parameters and data from Chapters 8.4.2 and 8.4.3 provide a basis for the calculation of the reference hydration rates with the help of equation (7.13). The representation in Fig. 8.14 is also given as a function of the water content. Within the range of 10 % and 30 % water content, the reference hydration rate is reduced from about $1 \cdot 10^{-6}$ 1/s to about $2 \cdot 10^{-7}$ 1/s. The assumption of a constant reference hydration rate in the case of the vapour diffusion model is therefore only a rough approximation. There is in fact a marked dependence on the water content.
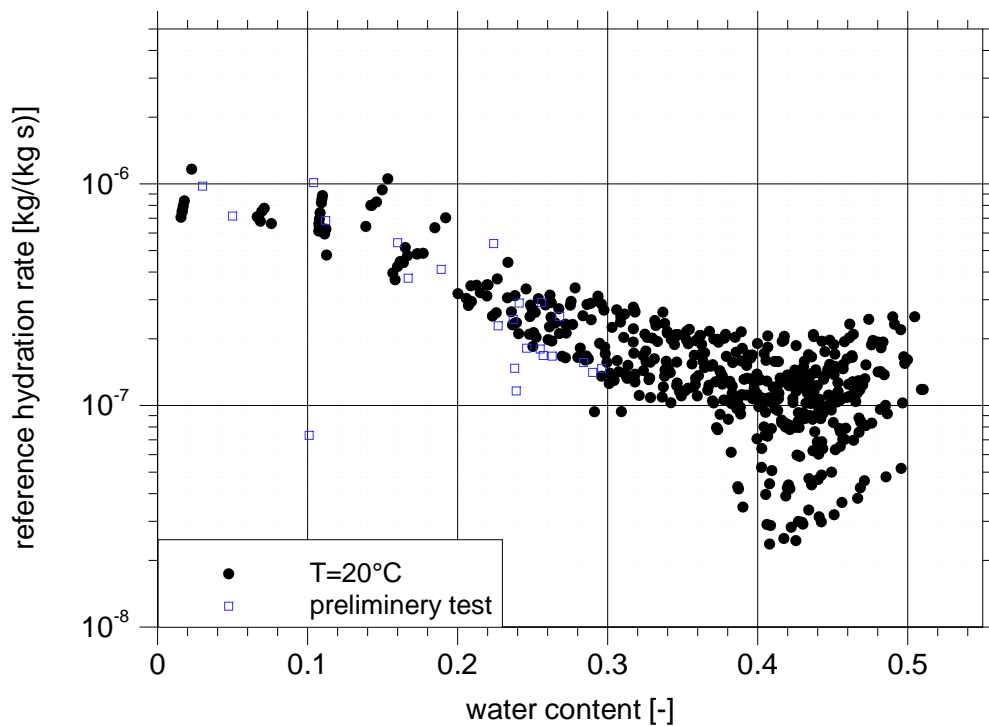
Fig. 8.14   Reference hydration rate as a function of the water content

8.5   Re-saturation of constricted test samples with water vapour

8.5.1   Experiment description

In another series of experiments, the re-saturation with vapour was investigated. Here, the experiment conditions were to be as similar as possible to the test series with Äspö solution. This is why the same measuring cells as described in Chapter 8.2.1 were used. The samples were also produced according to the procedure described there and the temperature was also a constant 20 °C.

The only difference of the two experiment series was the supply of the samples with water. Here, the samples were brought into contact with a nearly fully saturated vaporous atmosphere. The five measuring cells available, each with an upstream connected wash bottle, were connected in series together with a peristaltic pump to form a closed gas-

tight system (Fig. 8.15). The air was gradually saturated in the wash bottles upstream of the measuring cells to reach about 98 % relative humidity, so that a constant high flow of vapour was available for all measuring cells.
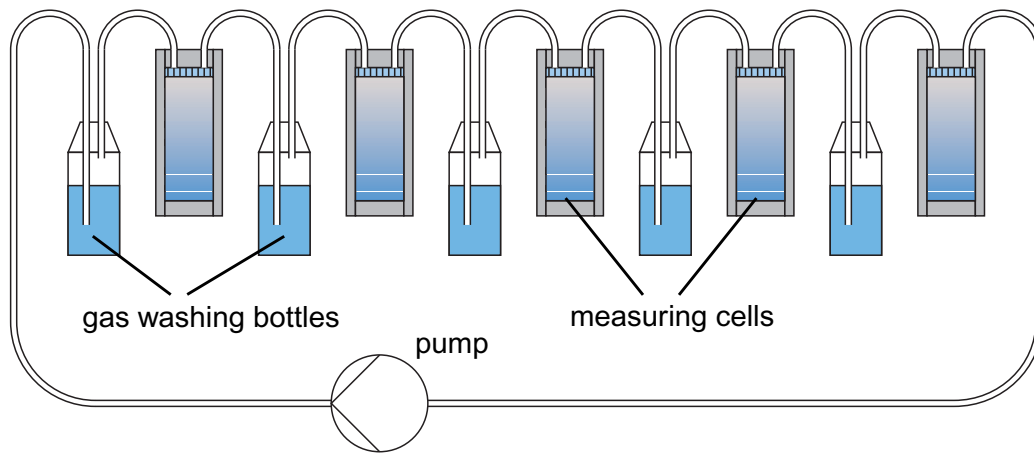

Fig. 8.15 Connection diagram of the measuring cells for the water vapour uptake tests

Two possibly disruptive effects were analysed in more detail in preliminary experiments. First, the gas circuit had to be opened to bypass a measuring cell if it had to be removed for the determination of the water contents. Continuous humidity measurements in the preliminary experiment showed, however, that the relative humidity already rose again to 90 % within a few minutes after closing the system again. Second, a further preliminary experiment showed that condensation within the flexible tubes or the cells could be excluded despite the high degree of humidity in the gas circuit.

The water content and dry-density distributions were determined as described in Chapter 8.2.1.

8.5.2 Results

The water content distributions obtained from the measurements are shown in Fig. 8.16. The points in time for the measurement of the water content distribution were chosen such that they corresponded roughly with the points in time for the measurements in the re-saturation experiment with liquid water. Thus a direct comparison of the curves from both experiments is possible.
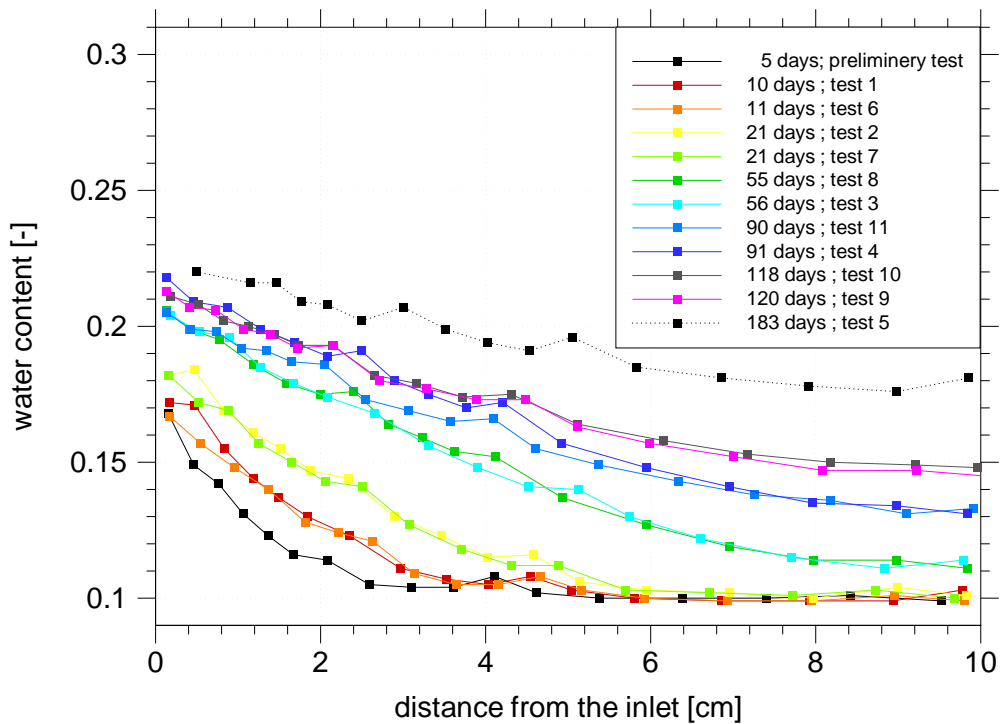
Fig. 8.16   Water content distributions for the re-saturation via water vapour

The same high degree of reproducibility as for the experiments with liquid water can also be found in connection with the experiments with water vapour. Contrary to the experiments with liquid, re-saturation at the boundary is much slower. Even after 183 days, the maximum value of saturation seems not to have been reached.

However, this maximum value is hard to quantify. Since the pore space contains no liquid but only vaporous water, the maximum water content of the re-saturation with vapour must lie below the theoretical maximum water content of 31 % of the re-saturation with liquid. In other words, the maximum water content of the re-saturation with vapour is reciprocally proportional to the final porosity. A vague indication of the expected final porosity is provided by the compaction model for bentonite GMM [44]. Results of this model given in [45] suggest a porosity of well below 5 % for the fully re-saturated bentonite.

At re-saturation with vapour - as in the case of re-saturation with liquid - much more water is also transported through the sample section at the inflow boundary than would be necessary for the re-saturation of this section. Here, the re-saturation velocity is therefore also not governed by the supply of water, but by the dynamics of the hydration process, and compared to the water transport, hydration is also a very slow process.

The dry-density distribution of the bentonite discs shown in Fig. 8.17 yields no indication that there has been any front-end decompaction that would be worth mentioning. Only a slight decrease of density with distance from the inlet - as in Fig. 8.5 for the experiments with liquid water - can be observed which is presumably an artefact of the compaction procedure. In the case of re-saturation with vapour, it is therefore even better justifiable to neglect the effect of such a densification than in the case of re-saturation with liquid.
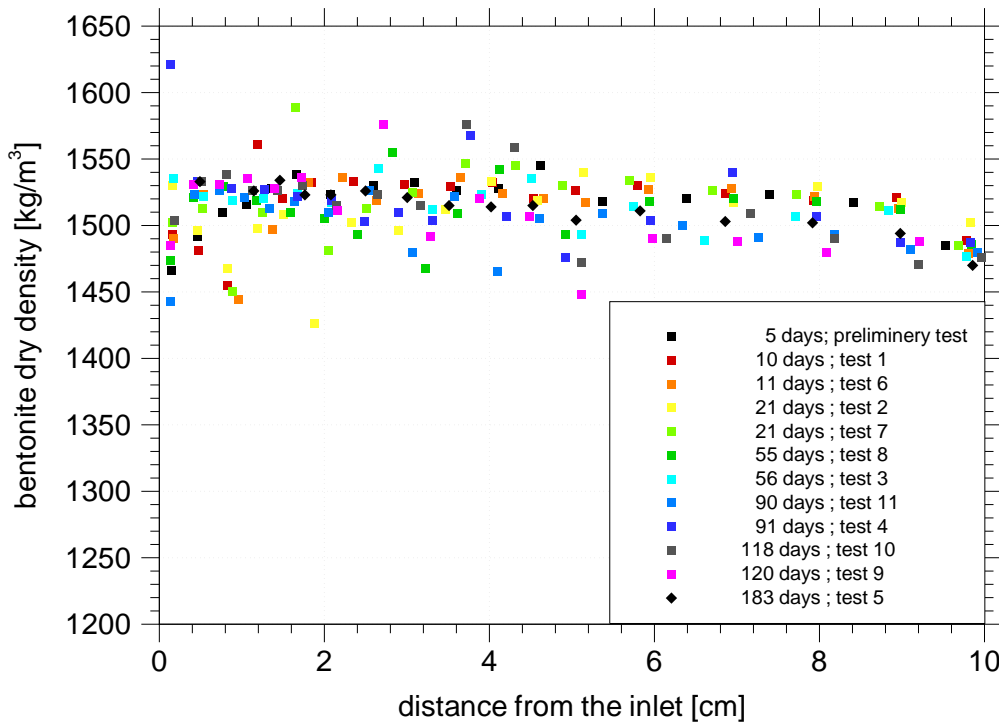

Fig. 8.17   Bentonite dry density distributions for the re-saturation via water vapour

9 Interpretation of the measuring results

9.1 Test of the advection model

The results of the re-saturation experiments with Äspö solution provide a basis for testing the advection model. For this purpose, two types of tests can be used:

- comparison with the amount of water absorbed in the experiment and in the model as a function of time and
- comparison of the water content distribution in the test sample in the experiment and in the model as a function of time.

The data used for the advection model are summarised in Tab. 9.1. The dry density of the bentonite is estimated from Fig. 8.5. With the help of the formulas provided in Appendix D, the porosity and the final water content are derived. The pore geometry data ensue from the description of the experiment in Chapter 8.2.1. Permeability and suction are estimated on the basis of the data compilations in Figs. 6.1 and 6.2. They lie approximately in the middle of the scatter range marked in the diagrams. The slight deviations of the values for the density and the viscosity of the Äspö solution from the values for pure water are neglected in this evaluation.

The amount of water absorbed by the samples as calculated with the advection model is compared with the measured data in Fig. 9.1. It turns out that there is very good agreement of experiment and simulation. Even for different degrees of bentonite compaction, the representation of the total water content in the bentonite sample as an integral value of the sample appears to succeed quite well with the advection model.

However, it is not possible to obtain any more detailed information with the model, especially concerning the distribution of the water inside the bentonite sample. As a comparison with the time-dependent distribution of water in Fig. 8.4 shows, the experiments do not yield the cascaded curve of the water content distribution predicted by the advection model and as indicated on the right hand side in Fig. 5.2. The value of the advection model does therefore not lie in the detailed representation of the processes developing during re-saturation.

Tab. 9.1 Parameters of the bentonite and the advection model; experiment according to Chapter 8.2

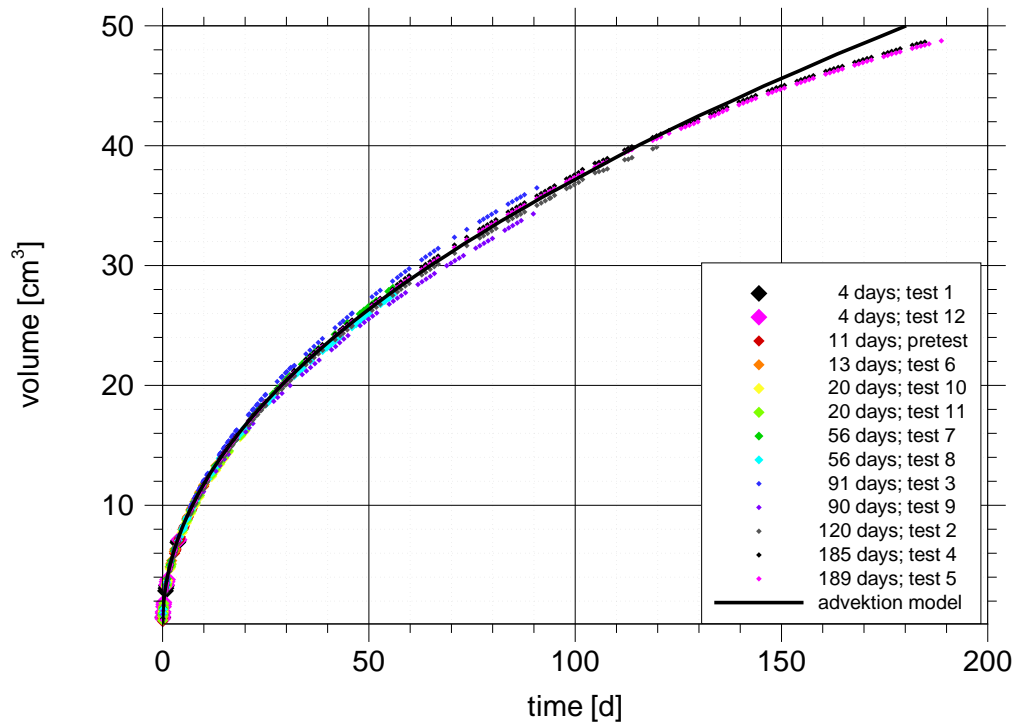| Parameter		Value	Dimension
Sample length	l	10	[cm]
Cross-sectional area	A	19.6	[cm^2]
Particle density	ρ_s	2800	[kg/m^3]
Bentonite dry density	ρ_d	1515	[kg/m^3]
Initial water content	w_0	0.10	[-]
Final water content	w_e	0.303	[-]
Initial porosity	Φ_0	0.455	[-]
Permeability	k	$1.7 \cdot 10^{-20}$	[m^2]
Suction	p_s	4	[MPa]
Viscosity of the water	η	0.001	[Pa s]
Density of the water	ρ_w	1000	[kg/m^3]

Fig. 9.1 Measured and simulated volume of uptaken Äspö solution as a function of time

Compared with the empirical diffusion model, the advection model provides a similar quality of results with regard to the integral values. However, an improvement over the empirical diffusion model is achieved by the special choice of initial parameters. As it is not known on which influences the coefficient in the empirical diffusion model depends, this coefficient has to be re-calibrated each time for different conditions. This is particularly true of the application to re-saturation problems at increased or variable temperature. The initial parameters needed for the advection model on the other hand are very well known and have also already been measured under physically different test conditions. Contrary to the empirical diffusion model, the advection model thus promises reliable results, even under more physically complex conditions.

9.2 Testing of the vapour diffusion model

The results of the re-saturation experiments with vapour provide a basis for the testing of the vapour diffusion model. Here, the water content distributions in the sample in the experiment and in the model are compared. For the numeric vapour diffusion model, parameters taken from Tab. 9.2 are assumed. The diffusion coefficient at microscopic level is assumed as constant here and corresponds to the value assumed in Appendix A for binary gas diffusion. Following the remark in Chapter 8.5.2, a final porosity of 2 % is assumed. The other data relating to density, water content and porosity ensue from the experiment description in Chapter 8.5.1 and the conversions according to Appendix D. The value of the reference hydration rate is based on an estimate derived from the results of the preliminary experiment of unconstrained re-saturation. At the time of modelling, the results of the actual experiment itself were not yet available. The comparison of the modelling results with the measured values is shown in Fig. 9.2.

The time-dependent water content distributions measured in the experiment are simulated fairly well by the vapour diffusion model. The amount of absorbed water as well as the trend of the curve progression agree qualitatively with the measured values.

Tab. 9.2   Parameters of the experiment according to Chapter 8.5
for the vapour diffusion model

| Parameter		Value	Dimension
Sample length	l	10	[cm]
Cross-sectional area	A	19.6	[cm^2]
Diffusion coefficient	D_m	$2.13 \cdot 10^{-5}$	[m^2/s]
Temperature	T	20	[°C]
Particle density	ρ_s	2800	[kg/m^3]
Dry density	ρ_d	1515	[kg/m^3]
Initial water content	w_0	0.10	[-]
Final water content	w_e	0.29	[-]
Initial porosity	Φ_0	0.459	[-]
Final porosity	Φ_e	0.02	[-]
Reference hydration rate	$\dot{m}_{ref}$	$1 \cdot 10^{-7}$	[kg/(kg s)]
Tortuosity	τ	0.4	[-]
Density of the water	ρ_w	1000	[kg/m^3]
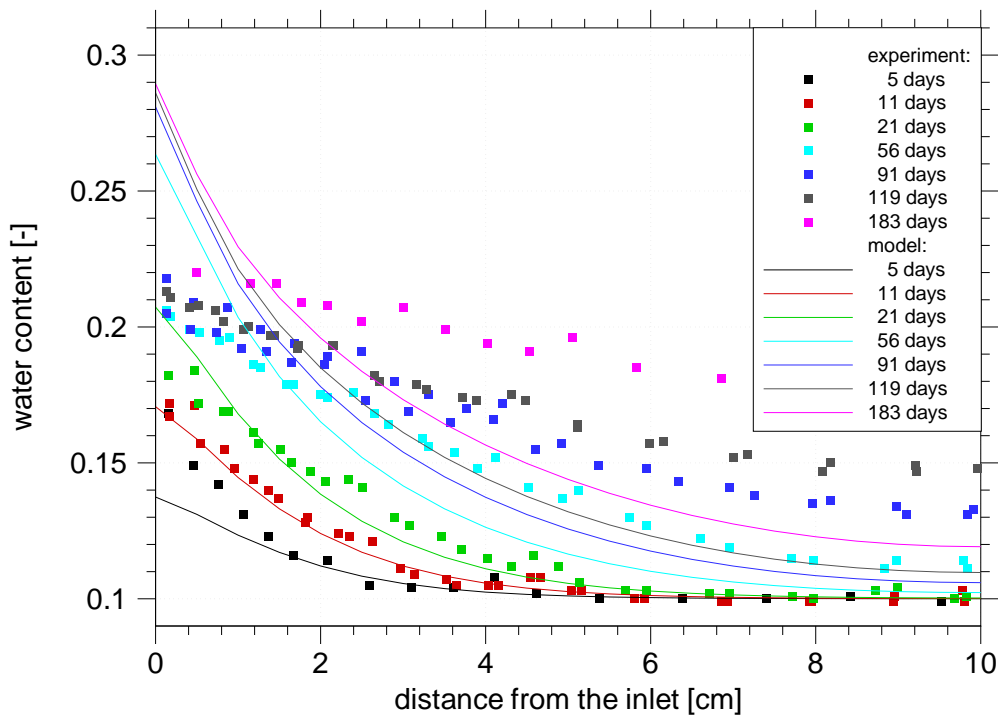
Fig. 9.2   Measured and simulated water content distributions
during uptake of water vapour

The dynamics of hydration are not, however, modelled adequately. Fig. 9.2 gives the impression that the uptake of water in the case of lower water contents is underestimated and that it is overestimated in the case of higher water contents. The reason for this may be the simplified assumptions for the vapour diffusion model, which are summarised once more below:

- assumption of a constant feuchtheiße diffusion coefficient,
- assumption of a linear adsorption isotherm,
- assumption of a linear relation between hydration rate and potential differente,
- assumption of the density value of Frostwetter for the Hydraten water, and
- assumption of a final porosity of 2 %.

A coherent assessment of the influence of the individual simplifying assumptions on the modelling results is difficult. What seems obvious is an explanation with the help of the results from Chapter 8.4 that the hydration rate does not rise linearly with the potential difference but that the coefficient a that is assumed as constant in equation (7.11) depends on the water content. Nevertheless, it is not possible to draw a valid conclusion from the water content distributions with regard to such changeability without further model calculations because the hydration affects the diffusive flow in the pore space and vice versa. Any more precise analysis would require further investigation and is therefore not part of this study.

9.3 Simulation of the re-saturation with liquid water with the vapour diffusion model

In connection with the time-dependent distributions of the water content observed in the re-saturation experiment with liquid water there are three circumstances that are noteworthy:

- the fast water uptake in the narrow, decompacted zone on the inlet, mentioned in Chapter 8.2,
- the course of the water content distributions that is typical of diffusion processes, and
- the slow hydration velocity outside the decompacted zone.

These circumstances suggest the hypothesis that the liquid water has merely re-saturated the narrow decompacted zone at the inlet and that the re-saturation that occurred further inside the samples was due to vapour diffusion. In this case, the source of the diffusive vapour flow would be given by the phase transition at the interface between the liquid phase and the gas phase, about 4 millimetres from the inflow edge.

Such a scenario can be simulated well with the vapour diffusion model under consideration of a shifted point of origin for the spatial coordinate. As initial data for the vapour diffusion model, the parameters of Tab. 9.2 are used again.

Fig. 9.3 shows the results of the re-saturation experiment with liquid water in comparison with the results of the vapour diffusion model. Here, the effect of fast water uptake in the vapour diffusion model through capillary effects in the initially unreduced pore volume is not considered. Nevertheless, the model explains about half of the total amount of water absorbed by binary gas diffusion.

Further model calculations have shown that a hypothetical increase of the diffusion coefficient by a factor of less than 10 is sufficient to explain the total amount of water absorbed in the experiment with the model. As elucidated in detail in Appendix A, such an increase of the diffusion coefficient can occur when the binary gas diffusion fades to Knudsen diffusion in an advanced state of the re-saturation. Thus the re-saturation of the bentonite with vapour in the gas phase does not only contribute considerably to the phenomenon of re-saturation; there even exists the possibility that the re-saturation with liquid water under atmospheric pressure may exclusively be put down to vapour diffusion.

The plausibility of this assumption can be tested easily by looking at the mass flow density of the water in the liquid and the gaseous phase. For this purpose, the simplified assumption is made that the initial entry of water due to the capillary forces does not lead to a significantly sloping curve in the moisture front in the bentonite. In this case, the equations of the advection model can be used for a very early phase of the re-saturation as this model simulates the uptake of water well. It is furthermore assumed that a zone of complete re-saturation has formed which is four millimetres strong. The mass flow density J_A yielded by the advection model under these circumstances ensues from equation (6.2) as

$$J_A = -\frac{k}{\eta}\frac{\Delta p_s}{x_F}\rho_w \qquad (9.1)$$

J_A -   mass flow density from the advection model [kg/(m² s)]
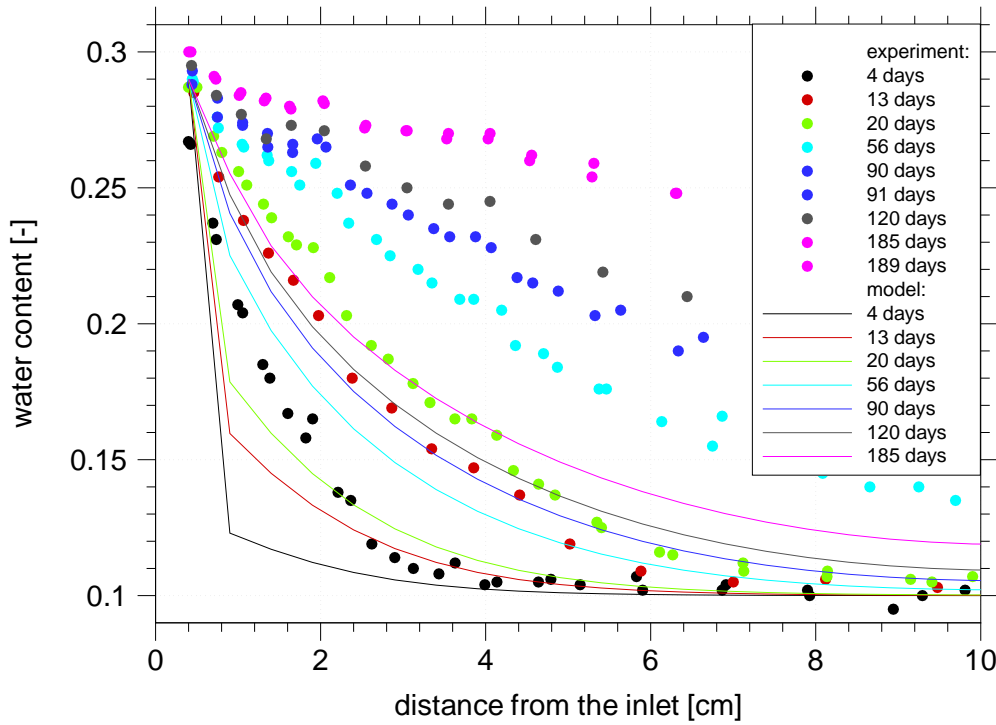

Fig. 9.3   Uptake of liquid water compared with results from the vapour diffusion model

Applying the parameters taken from Tab. 9.1, equation (9.1) yields a mass flow density of $J_A = 1.7 \cdot 10^{-5}$ kg/(m² s). Starting from the assumed boundary surface to the gas phase, the vapour diffuses further into the inside of the test sample. In the case of binary gas diffusion, the mass flow density J_D is calculated according to equation (7.2) as

$$J_D = -D_{eff}\frac{\Delta \rho_v}{\Delta x} \qquad (9.2)$$

J_D -   mass flow density from the diffusion model [kg/(m² s)]

If one assumes a relative humidity of 30 % and a penetration depth of the vapour of $\Delta x = 1$ cm in the pore volume, equation (9.2) yields a mass flow density of $J_D = 2.5 \cdot 10^{-5}$ kg/(m² s), based on a partial saturation density of 0.01648 kg/m² at 20 °C and on the values given in Tab. 9.2.

Thus the value of the mass flow density in the liqiuid phase may be very close to the value of the vapour flow in the gaseous phase. The estimation therefore indicates that although at the beginning of the re-saturation the succeeding flow of liquid water through the re-saturated zone is sufficient to maintain the diffusive vapour flow into the zone which is as yet not re-saturated, it is not sufficient to transport the liquid front further inside the sample.

During the further course of the re-saturation, the gradient of the partial vapour density decreases. At the same time, however, with increasing water content, suction at the liquid front also decreases. Within the framework of the uncertainties contained in the assumptions for this assessment, the latter supports the assumption of the nearly full re-saturation of the bentonite through vapour diffusion. Clarity on this issue can only be achieved by further investigations.

10   Summary and conclusions

With regard to long-term safety analyses it is a necessity to develop simple models that describe the propagation of water in the bentonite barriers in repositories and underground storage facilities. Therefore, the first step on this way is to identify the processes involved in the re-saturation and, if possible, to classify their relevance. The description of the microstructure of the bentonite as well as the identification and compilation of the processes caused by the influx of water emphasize the complexity of the re-saturation process. Additional difficulties arise from the fact that despite year-long intensive research, there are still processes involved in re-saturation that are not fully understood.

The analysis of the microstructure of bentonite and the processes relevant for the re-saturation reveal some of the shortcomings in the concepts of the existing THM models. The numerical THM models developed since the 1990s simulate the propagation of water in the bentonite on the basis of the classic two-phase flow. But, they do not contain the central process of hydration of the clay minerals. The pore and interlayer water are only differentiated in exceptional cases, and no difference is made at all between capillary pressure and suction. However, to cover the effects caused by hydration even so, the parameters and equations of state in the existing THM models have to be specifically calibrated. This poses problems in connection with the applicability of calibrated models to other physical situations.

For this reason, new models were developed to describe the processes that develop upon re-saturation by applying thoroughly analysed simple patterns. This task was split into two sub-tasks, each dealing with one partial aspect of re-saturation: re-saturation via liquid water and re-saturation via water vapour. For each of these partial aspects, a conceptual model and subsequently a one-dimensional numerical model was developed.

Accompanying laboratory experiments were performed which showed for the first time the dynamics of the re-saturation process in high spatial as well as time-dependent resolution. Re-saturation with Äspö solution and re-saturation with vapour-saturated air were analysed at room temperature and under atmospheric pressure. The experiments, which were simple from the point of view of their set-up and procedure, were characterised by the high reproducibility of their results. In addition, the water uptake velocity of an MX-80 bentonite in a vapour-saturated atmosphere was determined.

The choice of composition of the solutions in the experiments with liquid water goes in hand with a certain limitation of the applicability of the measuring results. This composition is on the one hand site-specific and can on the other hand have a considerable influence on the re-saturation behaviour. The use of Äspö solution in the experiments is justified solely by the orientation of the project on the extensive investigations in the Swedish Äspö hard rock laboratory (HRL), and the results therefore apply in particular to low-saline waters.

In this report, the model, which describes the re-saturation with liquid water, is referred to as "advection model". It describes the re-saturation as a Darcy flow at instantaneous hydration and is therefore mainly governed by the parameters porosity, permeability and suction. For these parameters there exist a large number of laboratory measurements. It was possible to show in this report that all three parameters can be expressed as a function of the dry density of the bentonite.

Comparative calculations with the one-dimensional empirical diffusion model - which has been confirmed in many cases in the literature for atmospheric pressure and room temperature - show that the advection model is on a par with this diffusion model if realistic parameters are used. Compared with the results of a re-saturation experiment in Switzerland, the advection model provides nearly identical results. Integral parameters, in particular the water uptake of the sample and the total water content, can thus be described well with the advection model.

However, the water content distributions obtained from the GRS laboratory experiments also show that the water distribution inside the bentonite cannot be described with the advection model. Still, it is not unlikely that the integral parameters which were simulated correctly at atmospheric pressure and room temperature can be simulated even under changed conditions if permeability and suction values are applied that fit these changed conditions. In this case the advection model would be superior to the empirical diffusion model. The applicability of the advection model to physically more complex situations as they are expected in repositories and underground storage facilities is thus possible, but still has to be demonstrated by comparison with experiments that are related to such conditions.

With the vapour diffusion model, the process of re-saturation by transport of vapour in the pore space and through local hydration can be described. There are no reliable experimental results from the literature on a re-saturation which is solely caused by water vapour. The laboratory experiments presented here do, however, provide an opportunity to test such a model. The vapour diffusion model that is used here and which bases on highly simplifying assumptions can already model quantitatively fairly well the water content distributions measured in the experiments. The dynamics of the re-saturation process, on the other hand, are not simulated quite satisfactorily. This might be improved by a model which takes the dependence of the reference hydration rate on the water content into account, the basis for which was established by the measurement of the re-saturation velocity. As with the advection model, the applicability to physically more complex situations remains to be tested.

The high relevance of vapour transport through the pore space for the re-saturation process becomes clear by a comparison of the results of the vapour diffusion model and the measuring results relating to the re-saturation via liquid water. About half of the measured water content can be explained by the diffusion of water vapour in the air of the pore space. Comparatively slight corrections to the vapour diffusion model suffice to reproduce the entire uptake of liquid water with the model.

As the vapour diffusion model still leaves room for improvement, it cannot be excluded that the re-saturation of a bentonite may mainly take place due to vapour diffusion and not as a result of the propagation of liquid water in the pore space. In this case, it has to be assumed that there is no two-phase flow during the re-saturation of bentonite.

Literature

[1]   Biot, M.A.: General theory of three-dimensional consolidation. J. Appl. Phys., 12,1941.

[2]   Bishop, A.W.: The principle of effective stress. Tek. Ukebl., 106(39), 1959.

[3]   Börgesson, L.: Water Flow and Swelling Pressure in Non-Saturated Bentonite-Based Clay Barriers. Clay Barriers for Isolation of Toxic Chemical Wastes, International Symposium, May 28-30, Stockholm, 1984.

[4]   Börgesson, L.: Compilation of laboratory data for buffer and backfill materials in the Prototype Repository. SKB, International Preogress Report IPR-01-34, 2001.

[5]   Börgesson, L., Johannesson, L.-E., Sanden, T., Hernelind, J.: Modelling of the physical behaviour of water satured clay barriers. SKB, Technical Report 95-20, 1995.

[6]   Börgesson, L., Karnland, O., Johannesson, L.-E.: Modelling of the physical Behaviour of Clay Barriers Close to Water Saturation. Engineering Geology, 41, 127-144, 1996.

[7]   Bucher, F., Spiegel, U.: Quelldruck von hochverdichteten Bentoniten. Nagra NTB 84-18, Nagra, 1984.

[8]   Bucher, F., Müller-Vonmoos, M.: Bentonite als technische Barriere bei der Endlagerung hochradioaktiver Abfälle. Mitteilungen des IGB der ETH Zürich, Heft 133, S 51-64, 1987.

[9]   Carslaw, H.S. and Jaeger, J.C.: Conduction of Heat in Solids. 2. Auflage, Oxford University Press, 1959.

[10]   Cleall, P., Melhuish, T.A., Thomas, H.: Vapour transfer in clay based engineered barriers in high level nuclear waste disposal. Workshop on Clay microstructure and its importance to soil behaviour, Lund, Sweden, Oktober, 2002.

[11] D'Ans, Lax: Taschenbuch für Chemiker und Physiker, Band I Physikalisch-chemische Daten. Springer-Verlag, 1992.

[12] Dixon, D.A.: Porewater salinity and the developement of swelling pressure in bentonite-based buffer and backfill materials. POSIVA-Bericht 2000-04, Helsinki, 2000.

[13] Dullien, F.A.L.: Porous Media - Fluid Transport and Pore Structure. Academic Press, Inc., 1991.

[14] Gärtner, S.: Zur diskreten Approximation kontinuumsmechanischer Bilanzgleichungen. Bericht Nr. 24/1987 einschließlich Habilitationsschrift, Institut für Strömungsmechanik und Eleketronisches Rechnen im Bauwesen, Universität Hannover, 1987.

[15] Helmig, R.: Multiphase Flow and Transport Processes in the Subsurface. Springer Verlag, 1997.

[16] Helmig, R., Class, H., Huber, R., Sheta, H., Ewing, J, Hinkelmann, R., Jakobs, H., Bastian, P.: Architecture of the Modular Program System MUFTE_UG for Simulating Multiphase Flow and Transport Processes in Heterogeneous Porous Media. In: Mathemathische Geologie, Vol2, (1998).

[17] Herbert, H.-J.: Persönliche Mitteilung, 2000.

[18] Hölzemann, S., Class, H., Helmig, R.: A new Concept for Numerical Simulation and Parameter Identification of Multiphase Flow and Transport Processes in Cohesive Soils. (Veröffentlichung in Vorbereitung) International conference on unsaturated soils, Weimar, 2003.

[19] Horseman, S.T., Higgo, J.J.W., Alexander, J., Harrington, J.F.: Water, gas and solute movement through argillaceous media. NEA Report CC-96/1, 1996.

[20] Huertas, F., Farias, J., Griffault, L., Leguey, S., Cuevas, J., Ramirez, S., Vigil de la Villa, R., Cobena, J., Andrade, C., Alonso, M.C., Hidalgo, A., Parneix, J.C.,

Rassineux, F., Bouchet, A., Meunier, A., Decarreau, A., Petit, S., Vieillard, P.: Effects of cement on clay barrier performance - Ecoclay project. European Commission, Final Report EUR 19609 EN, 2000.

[21] International Formulation Committee: A Formulation of the Thermodynamic Properties of Ordinary Water Substance. IFC Sekretariat, Düsseldorf, 1967.

[22] Jasmund, K.; Lagaly, G.: Tonminerale und Tone. Steinkopff Verlag Darmstadt, 1993.

[23] Jing, L., Stephansson, O., Börgesson, L., Chijimatsu, M., Kautsky, F., Tsang, C.-F.: DECOVALEX II Project, Technical Report - Task 2C. SKI, SKI Report 99:23, 1999.

[24] JNC - Japan Nuclear Cycle Developement Institute: H12 Project to Establish Technical Basis for HLW Disposal in Japan, Supporting Report 2, Repository Design and Engineering Technology. JNC-Bericht JNC TN1 400 99-012, Draft, May 1999.

[25] JNC - Japan Nuclear Cycle Developement Institute: H12 : Project to Establish the Scientific and Technical Basis for HLW Disposal in Japan - Project Overview Report. JNC Report JNC TN1410 2000-001, 2000.

[26] Jockwer, N., Miehe, R., Müller-Lyda, I.: Untersuchungen zum Zweiphasenfluss und diffusiven Transport in Tonbarrieren und Tongesteinen. GRS-167 Abschlussbericht, 9/2000.

[27] Johannesson, L.-E., Börgesson, L., Torbjörn, S.: Backfill Materials Based on Crushed Rock (Part 2), Geotechnical Properties Determined in Laboratory. SKB, International progress report SKB-IPR-99-23, 1999.

[28] Kahr, G., Kraehenbuehl, F., Müller-Vonmoos, M., Stoeckli, H.F.: Wasseraufnahme und Wasserbewegung in hochverdichtetem Bentonit. NAGRA, Technischer Bericht 86-14, 1986.

[29]   Karnland, O.: Bentonite swelling pressure in strong NaCl solution. Posiva, 1998.

[30]   Karnland, O., Sanden, T., Johannesson, L.-E., Eriksen, T.E., Jansson, M., Wold, S., Pedersen, K., Motamedi, M., Rosborg, B.: Long term test of buffer material, Final report on the pilot parcels. SKB, Technical Report TR-00-22, 2000.

[31]   Kolditz, O., Kaiser, R., Habbar, A., Kohlmeier, M., de Jonge, J., Beinhorn, M., Xie, M., Kalbacher, T., Ungruh, G., Bauer, S., Wang, W., McDermott, Ch., Chen, C., Beyer, C., Gronewolr, J., Kemmler, D.: RockFlow Manual, RFD Input Description, Version 3.9, First Draft. Center for Applied geosciences, Unversity of Tübingen, and Institute of Fluid Mechanics and Computer Applications in Civil Engineering, University of Hannover, 2003.

[32]   Kröhn, K.-P.: New conceptual models for the resaturation of bentonite. Proceedings of the Workshop on "Clay Microstructure and its Importance to Soil Behaviour" held in Lund, Applied Clay Science, Vol. 23, 2003.

[33]   Kröhn, K.-P.: Results and interpretation of bentonite resaturation experiments with liquid water and water vapour. Accepted for the Proceedings of the International conference on unsaturated soils, Weimar, 2003.

[34]   Liu, J., Kozaki, T., Yusuke, H., Sato, S.: Microstructure of montmorillonite/silica sand mixture and its effects on the diffusion of strontium ions. in: Workshop on clay microstructure and its importance to soil behaviour, Pusch, R. (ed.), Lund, Schweden, 2002.

[35]   Mooney, R. W., A., G. Keenan und L. A. Wood: Adsorption of Water Vapour by Montmorillonite; I: Heat of Desorption and Applicatioin of BET Theory. Journal of the American Chemical Society, Nol. 74, No. 6, 1952.

[36]   Neumüller, O.-A.: Römpps Chemielexikon. Franckh'sche Verlagshandlung, Stuttgart, 8. Auflage, 1979.

[37]   Pusch, R.: Water uptake, migration and swelling characteristics of unsaturated and saturated, highly compacted bentonite. KBS Report 80-11, SKBF, Stockholm, 1980.

[38]   Pusch, R.: Swelling Pressure of Highly Compacted Bentonite. KBS Report 80-13, SKBF, Stockholm, 1980.

[39]   Pusch, R.: Permeability of Highly Compacted Bentonite. KBS Report 80-16, SKBF, Stockholm, 1980.

[40]   Pusch, R.: Buffer Mass Test "Buffer Materials". IR 82-06, SKBF, Stockholm, 1982.

[41]   Pusch, R.: Waste Disposal in Rock. Dveleopements in Geotechnical Engineering, 76. Elsevier, 1994.

[42]   Pusch, R. (ed.): Äspö Hard Rock Laboratory, Prototype Repository, Selection of THMCB models. International Progress Report IPR-01-66, SKB, Stockholm, 2001.

[43]   Pusch, R., Karnland, O., Sanden, T.: Final report of physical test programm concerning spanish clays (Saponites and Bentonites). enresa, Publicacion Tecnica Num. 02/96, 1996.

[44]   Pusch, R., Karnland, O., Hökmark, H.: GMM -A general microstructural model for quantitative studies of smectite clays. SKB, Technical Report 90-43, 1990.

[45]   Pusch, R., Muurinen, A., Lehikoinen, J., Bors, J., Erikson, T.: Microstructural and chemical parameters of bentonite as determinants of waste isolation efficiency. EUR 18950 EN, Luxemburg 1999.

[46]   Pusch, R., Svemar, Ch.: Prototype Repository Project: WP3 Modelling Meeting - Minutes of the Meeting in Lund. SKB, 2000.

[47] Pusch, R., Kasbohm, J.: Can the Water Content of Highly Compacted Bentonite be Increased by Applying a High Water Pressure? SKB, Technical Report 01-33, 2001.

[48] Pusch, R., Weston, R.: Microstructural stability controls the hydraulic conductivity of smectite buffer clay. in: Proceedings of a Workshop held in Lund, Applied Clay Science, Vol. 23, 2003.

[49] Pusch, R., Yong, R.: Water saturation and retention of hydrophilic clay buffer - microstructural aspects. in: Proceedings of a Workshop held in Lund, Applied Clay Science, Vol. 23, 2003.

[50] Rodwell, W.R., Harris, A.W., Horseman, S.T., Lalieux, P., Müller, W., Ortiz Amaya, L., Pruess, K.: Gas Migration and Two-Phase Flow through Engineered and Geological Barriers for a Deep Repository for Radioactive Waste. A Joint EC/NEA Status Report, EUR 19122 EN, 1999.

[51] Stephansson, O., Jing, L., Tsang, Chin-Fu : Coupled Thermo-Hydro-Mechanical Processes of Fractured Media. Developments in Geotechnical Engineering, 79, Elsevier, 1996.

[52] Studer, J., W. Ammann, P. Meier, Ch. Müller, E. Glauser: Verfüllen und Versiegeln von Stollen, Schächten und Bohrlöchern, Band 2: Anhänge. Technischer Bericht der Nagra NTB 84-33, 1984.

[53] Sugita, Y., Ito, A., Chijmatsu, M., Kurikami, H.: Äspö Hard Rock Laboratory, Prototype Repository, Prediction analysis A for PRP with the numerical code THAMES. IPR-02-24, SKB, 2002.

[54] Terzaghi, K.: Erdbaumechanik auf bodenphysikalischer Grundlage. F. Deutike, Leipzig, 1925.

[55] Vargaftik, N.B.: Tables on the Thermophysical Properties of Liquids and Gases. Whiley and Sons, New York, 1975.

[56]   Weast, R.C., Astle, M.J., Beyer, W.H. (eds.): CRC Handbook of Chemistry and Physics. CRC Press, Inc., Boca Raton, Florida, 1986.

[57]   Zhang, C.-L., Kröhn, K.-P., Rothfuchs, T.: Applications of CODE-BRIGHT to Model Thermal-Hydro-Mechanical Experiments on Clays. (Veröffentlichung in Vorbereitung) International conference on unsaturated soils, Weimar, 2003

List of figures

List of tables

Appendix A Effective vapour diffusion coefficient

A.1   Diffusion mechanisms and their scope

In porous media, gas diffusion can be seen as free gas diffusion as long as the collision of a gas molecule with another molecule is considerably more likely than a collision with the pore wall. This is the case when the mean free path length λ of a gas molecule is clearly smaller than the pore diameter d. In contrast, Knudsen diffusion takes place when there is a considerably higher number of collisions with the pore wall than with other molecules meaning that $\lambda \gg d$ holds true. In a transition area in which the mean free path length lies in the same order of magnitude as the pore diameter, both kinds of diffusion take place.

As a measure for the determination of the relevant transport mechanism, the Knudsen number Kn can be used:

$$Kn = \frac{d}{\lambda} \qquad\qquad (\text{A.1})$$

Kn - Knudsen number [-]
d - pore diameter [m]
λ - mean free path length [m]

The mean free path length of a molecule of an ideal gas is calculated from the mean kinetic energy of the particles as:

$$\lambda = \frac{1}{\sqrt{2}\pi\delta^2 N_A \rho_g} \qquad\qquad (\text{A.2})$$

δ -   molecule diameter [m]; according to [35]:
   $\delta = 2.8\cdot10^{-10}$ m for water,
   $\delta = 3.0\cdot10^{-10}$ m for oxygen and
   $\delta = 3.2\cdot10^{-10}$ m for nitrogen.
N_A - Avogadro constant [1/mol]; $N_A = 6.02252\cdot10^{+23}$ 1/mol
ρ_g - gas density [mol/m^3]

Although strictly seen this formula does not apply to gas mixtures, it is still used here because the molecule diameters of the essential components nitrogen, oxygen and water are comparable. For the estimation, the molecule diameter of oxygen is applied in approximation, as is the density of the air as gas density. The density of the air ensues from the simplified assumption that the equation of state for ideal gases also applies to air:

$$\rho_g = \frac{p_g}{RT}$$

(A.3)

p_g - gas pressure [Pa]

At a pressure of p_g = 101300 Pa and a temperature of 293.15 K, a density of ρ_g = 41.56 mol/m^3 ensues and therefore an mean free path length of λ = 100 nm. The mean free path length thus lies on the order of magnitude of the diameter of a clay mineral particle (cf. Chapter 2.2).

For a determination of the kind of diffusion, the bandwidth of the transition area is yet to be put in concrete terms. According to [15], the influence of Knudsen diffusion can be neglected for Knudsen numbers of $Kn > 10$. Here, $Kn = 0.1$ is used ad-hoc as lower limit for the transition area. As a result, the scope of the two transport mechanisms is as follows:

free diffusion   for $Kn > 10$,
transition area   for $0.1 < Kn < 10$ and
Knudsen diffusion for $Kn < 0.1$.

A.2   Diffusion coefficients on microscopic level

A.2.1   Binary gas diffusion

For practical purposes the coefficient of binary gas diffusion D_f can be calculated with the semi-empirical approach according to [55] in [15]:

$$D_b = D_{b_0} \frac{p_{g0}}{p_g} \left(\frac{T}{T_0} \right)^{\theta}$$

(A.4)

D_b - coefficient of binary gas diffusion [m^2/s]

$D_{b0,}\, p_{g0,}\, T_0$ - diffusion coefficient, pressure and temperature under reference conditions

θ - constant fit parameter [-]; according to [53] in [15],

θ =1.8 and

D_{f0} = 2.13·10^{-5} m^2/s for water vapour in air with

p_0 = 101300 Pa and

T_0 = 273.15 K.

A.2.2   Knudsen diffusion

It follows from the theory of gas kinetics that the coefficient of Knudsen diffusion D_k is proportional to the pore diameter d [13]:

$$D_k = \frac{1}{3} d v_m \qquad\qquad (A.5)$$

D_k - coefficient of Knudsen diffusion [m^2/s]

v_m - mean molecular velocity [m/s]

The mean molecular velocity also follows from the theory of gas kinetics:

$$v_m = \sqrt{\frac{8RT}{\pi M_w}} \qquad\qquad (A.6)$$

M_w - molar weight [kg/mol]; for water: M=0.018016 kg/mol

The coefficient of Knudsen diffusion depends on the temperature as well as on the pore diameter, but not on the pressure:

$$D_k = \frac{1}{3} \sqrt{\frac{8R}{\pi M_w}} d \sqrt{T} \qquad\qquad (A.7)$$

A.2.3   Diffusion coefficient in the transition area

According to [15], the fractions of free diffusion and Knudsen diffusion in the transition area can be summarised to form an mean diffusion coefficient D_m in the following manner:

$$\frac{1}{D_m} = \frac{1}{D_b} + \frac{1}{D_k} \qquad\qquad\qquad\qquad\qquad (\,A.8\,)$$

D_m -   mean diffusion coefficient on microscopic level [m²/s]

However, if a variable pore diameter is considered, this approach is not sufficient as it leads to an abrupt change of the diffusion coefficient at the boundaries of the transition area. For this reason, an ad-hoc factor κ is proposed that weights the influence of the fractions from free diffusion and from Knudsen diffusion as a function of the Knudsen number:

$$\frac{1}{D_m} = \kappa\frac{1}{D_b} + (1-\kappa)\frac{1}{D_k} \qquad\qquad\qquad (\,A.9\,)$$

κ -   weighting factor [-]

with

$\kappa = 1$ for $Kn > 10$

$\kappa = 1/2\ (1 + \log10(Kn))$ for $0.1 < Kn < 10$

$\kappa = 0$ for $Kn < 0.1$

A.3   Identification of the relevant diffusion processes

The following considerations rest on the assumption that the expected most frequent pore diameter $\overline{d}$ in a bentonite body is decisive for the diffusion behaviour on macroscopic level. One indication for this value is provided by the grading curve in [27] under the assumption that the size of the pores between the clay particles corresponds to the size of the particles themselves. In this case, 85 % of the clay particles have a diameter of less than one micrometre.

A further indication is provided in a theoretical study concerning re-saturated bentonite in [49] which is based on investigations performed in [45]. This study contains a rough statistic on the frequency of pores in a fully saturated bentonite in dependence on their diameter and the final density of the bentonite. However, frequencies for diameters below one micrometre are not included even though the distribution function comprises this di-

ameter range down to 100 nm. According to the statistical data, the expected value for the pore diameter in a re-saturated bentonite with a dry density of 1350 kg/m^3 and with a normally distributed probability of the pore diameters is below one micrometre. In a log-normal distribution, which is also considered in [45], this value is further reduced. On the basis of these investigations, the view is presented elsewhere in [45] that in highly compacted bentonites and at full re-saturation, pore diameters within a range of 10 nm and 10 µm can be expected.

At an mean pore diameter of d=100 nm and thus an mean free path length of λ=100 nm, the fraction of Knudsen diffusion according to (A.9) cannot be neglected for pores with a diameter in the micrometre range. At full saturation of the bentonite via vapour there consequently follows a Knudsen number in the transition area, and free diffusion as well as Knudsen diffusion occurs.

A.4 Expected value for the pore diameter as a function of porosity

The expected most frequent pore diameter $\overline{d}$ determines the diffusion coefficient. This, however, is a microscopic parameter. For the purpose of modelling, the connection with a macroscopic parameter has to be established. The macroscopic parameter corresponding to the pore diameter $\overline{d}$ could be the porosity as with the swelling of the bentonite, the pore space and thus also the diameter of the pore channels is reduced. Porosity and pore diameter are therefore proportional to each other. Ad hoc, a linear connection is assumed:

$$\overline{d} = \varphi d_{max} + (1-\varphi)d_{min} \qquad\qquad\text{(A.10)}$$

$\overline{d}$ - expected value of the pore diameter [m]
d_{max}- maximum pore diameter [m]
d_{min}- minimum pore diameter [m]
φ - weighting factor [-]

with

$$\varphi = \frac{\Phi - \Phi_e}{\Phi_0 - \Phi_e} \qquad\qquad\text{(A.11)}$$

Φ -   porosity [-]

Φ_0 -   initial porosity [-]

Φ_e -   final porosity [-]

The value of $\bar{d}$ thus determined then provides - dependent on the Knudsen number Kn and the approach for κ - the diffusion coefficient D_m on macroscopic level.

A.5   Diffusion coefficient on macroscopic level

At the transition to the macroscopic level it has to be taken into account that the diffusive flow does not take place over the entire cross-section of the porous medium but only in part of this area that corresponds to the porosity. Furthermore, tortuosity leads to the fact that the travel path of the diffusing particles is curved.

From a macroscopic point of view, both effects apparently slow down the diffusion and can be described by an effective diffusion coefficient D_{eff}:

$$D_{eff} = \Phi \tau D_m \tag{A.12}$$

D_{eff} -   effective diffusion coefficient on the macroscopic level [m^2/s]

Appendix B Numerical solution of the vapour diffusion equation

In order to solve the balance equation (7.28) numerically, the continuous solution area is divided into finite elements - i. e. one-dimensional sections - which are interconnected by nodes. This way, the partial differential equation can be transformed into a system of algebraic equations, the unknown quantity of which provides the approximation solution at the nodes.

In the solution of (7.28), an explicit time step procedure was applied which calculates the node values following the elapse of a time interval Δt with the help of the node values from the old time level. Subsequently, the approximation of the individual terms is indicated. Here, the following conventional notation is applied: the superscript + stands for the new time level and the superscript - for the old one. The subscript index 0 marks the node i for which the unknown quantity is to be calculated, and the subscript indices + and - stand for the associated neighbouring nodes. To simplify the notation, the indices v and m are omitted in the case of the discrete node values of the partial vapour pressure and the vapour diffusion coefficient.

$$\Phi \frac{\partial \rho_v}{\partial t} \approx \Phi_0^- \frac{\rho_0^+ - \rho_0^-}{\Delta t} \tag{B.1}$$

$$\rho_v \frac{\partial \Phi}{\partial t} \approx \rho_0^- \frac{\Phi_0^+ - \Phi_0^-}{\Delta t} \tag{B.2}$$

$$\Phi D_m \frac{d^2 \rho_v}{dx^2} \approx \Phi_0^- D_0^- \frac{\rho_+^- - 2\rho_0^- + \rho_-^-}{(\Delta x)^2} \tag{B.3}$$

$$\Phi \frac{\partial D_m}{\partial x} \approx \Phi_0^- \frac{D_+^- - D_-^-}{2\Delta x} \tag{B.4}$$

$$D_m \frac{\partial \Phi}{\partial x} \approx D_0^- \frac{\Phi_+^- - \Phi_-^-}{2\Delta x} \tag{B.5}$$

$$\frac{\partial \rho_v}{\partial x} \approx \frac{\rho_+^- - \rho_-^-}{2\Delta x} \tag{B.6}$$

$$\rho_d \dot{m}_{ref} \ln \frac{\rho_v}{\rho_{sat} \, r_{h \, eq}(w)} \approx \rho_b \dot{m}_{ref} \ln \frac{\rho_-^-}{\rho_{sat} \, r_{h \, eq}(w)} \tag{B.7}$$

With the approximations (B.1) to (B.7) it is possible to set up a system of equations for the determination of the partial vapour pressures ρ_0^+. What is awkward here is the time derivation of the porosity, which as a further unknown quantity introduces the porosity Φ_0^+ at the new time level. This depends eventually on the mass sink r, so that Φ_0^+ would have to be determined by means of an iteration. It turns out, however, that the variation of the porosity upon the re-saturation with vapour is slight compared with the variation in the partial vapour density, so that the term (B.2) can be neglected. Equation (7.28) is thus approximated under the assumption of constant element length and a constant cross-sectional area of the element by

$$
\Phi_0^- \frac{\rho_0^+ - \rho_0^-}{\Delta t} - \tau \left[\left(\Phi_0^- \frac{D_+^- - D_-^-}{2\Delta x} + D_0^- \frac{\Phi_+^- - \Phi_-^-}{2\Delta x} \right) \frac{\rho_+^- - \rho_-^-}{2\Delta x} + \Phi_0^- D_0^- \frac{\rho_+^- - 2\rho_0^- + \rho_-^-}{(\Delta x)^2} \right]
$$

$$
= \rho_d \dot{\overline{m}}_{ref} \ln \frac{\rho_-^-}{\rho_{sat}\, r_{h\ eq}(w)} . \tag{B.8}
$$

The special form of the right-hand side of (B.8) is the reason for the choice of the explicit procedure. It contains the water-content-dependent equilibrium humidity $r_{h\ eq}(w)$ which can only be calculated from the solution of (B.8). In an implicit procedure, this would require an iteration; in the explicit procedure, it is sufficient to update the source term before the next time step can be calculated. A conversion to the known parameter ρ_0^+ yields the node equation

$$
\rho_0^+ = \rho_0^-
$$

$$
+ \frac{\Delta t}{(\Delta x)^2} \frac{\tau}{\Phi_0^-} \left(\frac{1}{4} \{ \Phi_0^-[D_+^- - D_-^-] + D_0^-[\Phi_+^- - \Phi_-^-] \} (\rho_+^- - \rho_-^-) \right)
$$

$$
+ \frac{\Delta t}{(\Delta x)^2} \frac{\tau}{\Phi_0^-} (\Phi_0^- D_0^-[\rho_+^- - 2\rho_0^- + \rho_-^-])
$$

$$
+ \frac{\Delta t}{(\Delta x)^2} \left(\rho_b \dot{\overline{m}}_{ref} \ln \frac{\rho}{\rho_{sat}\, r_{h\ eq}(w)} \right) \tag{B.9}
$$

Appendix C Estimation of the density of the interlayer water

C.1   Description of the re-saturation steps

According to [28], the re-saturation of a smectite with water takes place in a maximum of five steps. As a measure of the swelling of a clay material, the thickness of an elementary layer including one interlayer is applied in the literature as the so-called "basal spacing". The starting point of the model is a fully water-free state of the bentonite minerals - which is only possible in theory. For this state, a basal spacing of 0.96 nm is indicated. In the first step of water uptake, water molecules are sorbing above the centres of charge in the hexagonal openings of the outer-lying tetrahedron layers and thereby lead to a basal spacing of about 1.02 nm. The second step is marked by the fact that depending on the kind of the interlayer cations that are still around in the hexagonal openings in this state, 2 or 4 water molecules arrange themselves above these openings. The basal spacing is then 1.16 - 1.18 nm. A continuous water supply causes further water molecules to group around the cations, lifting these from the openings and forming a monomolecular layer mid-level between two elementary layers. This state represents the third re-saturation step with a basal spacing of 1.24 nm. After further water uptake, the water molecules organise themselves in the fourth step to form a bimolecular layer extending the separation distance to 1.50 to 1.52 nm. Montmorillonites with sodium or magnesium cations reach furthermore a fifth resaturation step with a trimolecular water layer and a basal spacing of 1.9 to 2.0 nm. In principle it has to be assumed that a molecular layer first has to be formed completely before another layer starts to form. As different hydration states are also possible due to different cations in the interlayers and thus to different charge distributions, the transition between the hydration steps is vague.

The basal spacings of the third to the fifth step are indicated in [22] as being 1.18 - 1.24 nm, 1.45 - 1.55 nm and 1.9 - 2.0 nm. However, they relate not only to smectites but also to all 2:1 clay minerals, so the range of the values is slightly wider than indicated in [28]. A detailed list of the layer thicknesses of dehydrated montmorillonite crystals and of the hydration water layers, itemised by the cations Mg, Ca, Na and K, can be found in [44]. All data are summarised in Tab. C.1. In addition, the water content pertaining to each re-saturation step and the associated number of water molecules per counter-cation are also indicated in [28]. These values, too, can be found in Tab. C.1.

Tab. C.1   Data on the step-wise interlayer saturation with water

according to [28], [22] and [44]

State	Basal spacings d [nm]						Water molecules per counter-cation N_G		Water content [%]	Remarks
	Smectites by [28]	2:1 clays by [22]	Montmorillonites by [44]							
			Ca	Na	K	Mg	Ca-montmo-rillonite	Na-montmo-rillonite		
dry	0.96		0.961	0.962	1.008	0.952	-	-	-	
1st step	1.02						-	-	< 1	some molecules in the hexagonal openings
2nd step	1.16-1.18						4	2	1 - 2.5	begin of hydration of cations
3rd step	1.24	1.18-1.24	1.250	1.265	1.250	1.252	12	6	< 10	monomolecular layer
4th step	1.50-1.52	1.45-1.55	1.525	1.588	1.623	1.555	24	12	< 20	bimolecular layer
5th step	1.9 - 2.0	1.9-2.0	-	1.936	-	1.860	-	>12	~ 20	trimolecular layer; only Na- and Mg-bentonites

C.2   Water density in the interlayers

For a quantitative description of the hydration process, the density with which the water molecules are stored in the interlayers is of importance. The space required by a cation in the interlayer depends on the charge density of the smectite. For montmorillonites, values between 0.3 and 0.4 are indicated for the charge per formula unit L [22]. The side lengths of an elementary cell in the SiO_4 tetrahedron layer parallel to the interlayer are a_0 = 0.517 nm and b_0 = 0.894 nm per formula unit [22], which corresponds to an area of 0.462 nm^2. With the help of

$$D_L = \frac{2L}{a_0 b_0}$$

(C.1)

there ensues a "charge density" D_L of 1.3 - 1.73 charges/nm^2 as two interlayers per formula unit have to be considered (upper and lower SiO_4 tetrahedron layer of the three-sheet mineral). From the charge density and the charge of the interlayer cation z_i, the space required by the counter-cation is derived as z_i/D_L:

-    z_i/D_L = 0.58 - 0.77 nm^2/Na$^+$ ion and
-    z_i/D_L = 1.16 - 1.54 nm^2/Ca^{2+} ion.

With consideration of the water molecules per counter-cation N_G, the number of water particles per area N_F in the interlayer ensues from Tab. C.1 according to

$$N_F = \frac{N_G}{z_i/D_L} \quad \text{[water molecules /nm2]}$$

(C.2)

and can be converted into an area-related water uptake capability N_m with the help of Lohschmidt's constant N_L:

$$N_m = \frac{N_F}{N_L} \quad \text{[mol/nm}^2\text{]}.$$

(C.3)

The water density in the interlayer N_V then ensues when N_m is divided by the interlayer thickness Δd

$$N_V = \frac{N_m}{\Delta d} \ [\text{mol/nm}^3]. \tag{C.4}$$

With the help of the molecular weight for water M_w, the density can eventually also be expressed in kg/m^3:

$$\rho_{w\,Z} = M_w N_V 10^{+27} \ [\text{kg/m}^3]. \tag{C.5}$$

The data for the calculation of the water density in the interlayer are summarised in Tab. C.2. The values for the interlayer thickness were calculated from a difference of the separation distances of the layers and averaged where necessary.

The data according to [28] show that the density of the interlayer water is on average the same as that of freshwater. This is in line with the values given in the literature according to [44], albeit with the range being somewhat wider with values between 700 and 1400 kg/m^3. If one applies the measured values of [44], however, a slightly lower density ensues. Under consideration of the comparably wide ranges and the uncertainties associated with the measurements that are not further explained in [44], the change in the density of the water following the transfer to the interlayer is neglected in the context of the work documented in this report.

Tab. C.2   Data for the calculation of the water density in the interlayer

	Δd [nm]	NF [Particle/nm2]	N_V [10^{-4}mol/m^3]	ρ_{wZ} [kg/m^3]	$\bar{\rho}_{wZ}$ [kg/m^3]
Smectites by [28]:					
3rd step	0.28	7.8 - 10.3	4.62 - 6.16	832 - 1110	980
4th step	0.55	15.6 - 20.7	4.70 - 6.27	847 - 1130	
Ca-montmorillon-ite by [44]:					
3rd step	0.29	7.79 - 10.39	4.48 - 5.97	806 - 1075	952
4th step	0.56	15.58 - 20.77	4.59 - 6.11	826 - 1102	
K-montmorillonite by [44]:					
3rd step	0.24	7.79 - 10.39	5.34 - 7.13	963 - 1284	1004
4th step	0.62	15.58 - 20.77	4.2 - 5.61	758 - 1010	
Na-montmorillon-ite by [44]:					
3rd step	0.30	7.79 - 10.39	4.27 - 5.69	769 - 1025	883
4th step	0.63	15.58 - 20.77	4.13 - 5.51	744 - 993	
Mg-montmorillon-ite by [44]:					
3rd step	0.30	7.79 - 10.39	4.31 - 5.75	777 - 1036	904
4th step	0.60	15.58 - 20.77	4.29 - 5.72	773 - 1030	

Appendix D Density and porosity as a function of the water content

D.1 Parameters, indices and definitions

The following parameters are associated with each other:

- m mass [kg]
- V volume [m^3]
- ρ density [kg/m^3],
- w water content related to the mass of the oven-dry bentonite [-],
- $\overline{w}$ water content related to the mass of the air-dry bentonite [-],
- Φ porosity [-] and
- e pore number [-].

In this context, the following indices are used for the state of saturation:

- d oven-dry condition,
- 0 air-dry condition,
- max condition of maximum saturation with water vapour, and
- e condition of maximum saturation with liquid water.

The following indices describe subsets in the bentonite body:

- p pores,
- i interlayers,
- s solid-matter fraction,
- w water, and
- b entire bentonite body.

The graphs in this Appendix are based on a water density of ρ_w = 1000 kg/m^3 and a solid-matter density of ρ_s = 2780 kg/m^3. Expressed in formulas, the definitions of water content, porosity and solid-matter density are:

water content:
$$w = \frac{m_w}{m_s} \qquad\qquad (\text{ D.1 })$$

porosity:
$$\Phi = \frac{V_p}{V_b} \qquad\qquad (\text{ D.2 })$$

solid-matter density:
$$\rho_s = \frac{m_s}{V_s} \qquad\qquad (\text{ D.3 })$$

D.2 Introduction

At present, there exists no standard method for the characterisation of a bentonite body. The literature refers to the use of the most various different sets of parameters for this purpose, with density, water content and porosity of the bentonite being most commonly used. Only two of the three parameters are needed for a clear description.

The state of saturation of the bentonite - to which these parameters refer - is also chosen differently. There are three distinct conditions:

- the oven-dry condition,
- the air-dry condition, and
- the fully saturated condition.

The aim of this appendix is to make measuring results and other details from the literature comparable. For this purpose, the density, water content and porosity are set in relation to each other under simplifying assumptions in a way that allows the conclusion of all parameters of any condition from the indication of two parameters of a known re-saturation state.

The following considerations assume that the volume V_b of the bentonite body concerned keeps constant during swelling. It is composed of the solid-matter volume V_s, the pore volume V_p and the volume of the interlayers V_s:

$$V_b = V_s + V_p + V_i = const.$$ (D.4)

The fraction of hydrated water that cannot be driven out by oven drying is added to the solid-matter volume V_s. Changes in the solid-matter volume should be negligible. From these considerations, it follows with equation (D.4) that the sum formed of the pore volume and the interlayer volume is constant upon the uptake of water:

$$V_p + V_i = const.$$ (D.5)

The following are assumed as being known:

- the solid-matter density ρ_s,
- the density of the liquid water ρ_w and
- the residual porosity Φ_e remaining at full re-saturation.

Further reference values that are used in all other equations ensue in Chapter D.3 from the considerations with respect to the oven-dry condition. Subsequently, the equations in Chapter D.4 are brought into the most general form, with consideration of a variable water content at partial saturation. This includes the air-dry condition as a special case which can only be reproduced with moderate accuracy. The equations are applied to the saturated condition in Chapters D.5 and D.6. In Chapters D.7 and D.7.2, the range of possible conversions is extended by conversion formulas and diagrams for various different definitions of the water content and for the pore number.

D.3 Oven-dry condition

According to the definitions in Chapter D.2, there is no water in the pore space or in the interlayers in oven-dry condition. In this case, the interlayers disappear:

$$V_i = 0$$ (D.6)

The dry density ρ_d ensues from the solid-matter fraction m_s and the bentonite volume V_b

$$\rho_d = \frac{m_s}{V_b} \qquad\qquad (\text{D.7})$$

The connection with the solid-matter density ρ_s is established via the porosity in oven-dry condition Φ_d and definition (D.4):

$$\rho_d = (1 - \Phi_d)\rho_s \qquad\qquad (\text{D.8})$$

Equation (D.8) therefore also is a conditional equation for the porosity, which only depends on the dry density:

$$\Phi_d = 1 - \frac{\rho_d}{\rho_s}. \qquad\qquad (\text{D.9})$$

The connection (D.9) is shown in a diagram in Fig. D.1.
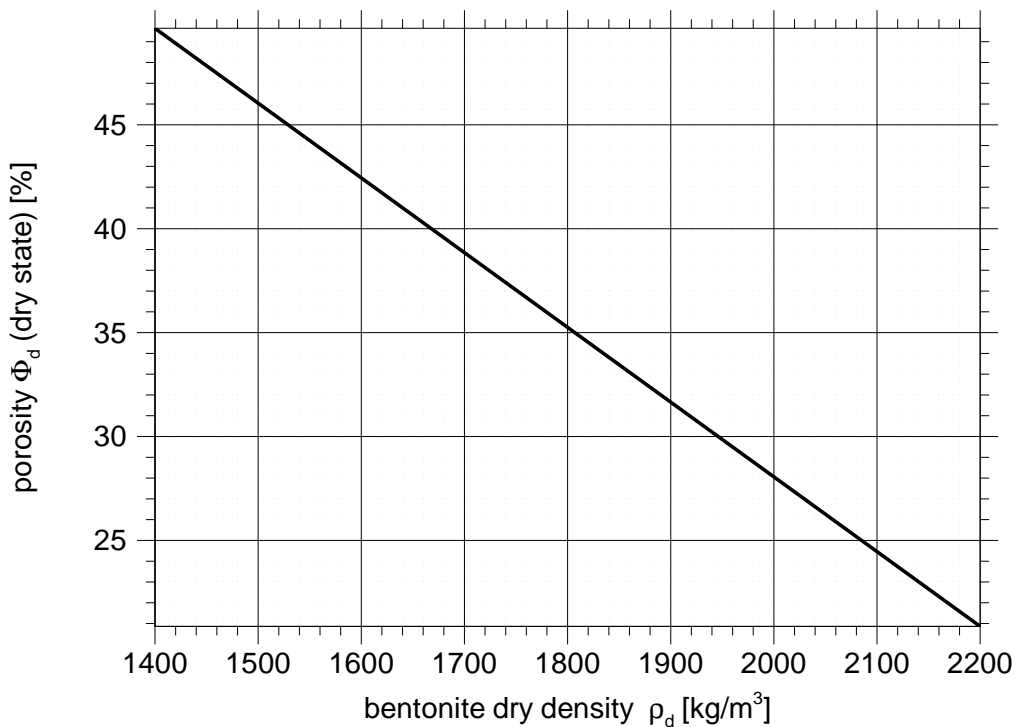

Fig. D.1   Porosity in oven-dry condition as a function of the dry density

D.4 Partial saturation

A special state of saturation of the bentonite is the air-dry condition in which the interlayers in the bentonite are filled with hydrated water in line with the ambient humidity. This condition is considered as a representative of all other partially saturated conditions. At an even distribution of the water in the bentonite, the following considerations apply to the entire body. Otherwise, they only apply locally.

Compared with the dry mass m_s, the mass of the partially saturated bentonite m_b increases by the absorbed water m_w:

$$m_b = m_s + m_w \qquad\qquad (\text{D.10})$$

A division by the bentonite volume and the insertion of definition (D.1) for the water content yields the density of the partially saturated bentonite ρ_b as

$$\rho_0 = (1 + w_0)\rho_d \qquad\qquad (\text{D.11})$$

The porosity in air-dry condition ensues starting from definition (D.2) and the geometric consideration

$$V_p = V_s - V_i \qquad\qquad (\text{D.12})$$

The insertion of equation (D.7) then yields

$$\Phi_0 = \Phi_d - \frac{V_i}{V_b} \qquad\qquad (\text{D.13})$$

As explained in Chapter 3.2.4.1, in a thermodynamic equilibrium the entire amount of water is present in the interlayers, with the exception of a negligible vaporous fraction. In this case, the following applies:

$$V_i \cong V_w \qquad\qquad (\text{D.14})$$

123

If the volume of water is replaced by the quotient m_w/ρ_w and the definition (D.1) of the water content is inserted, one eventually obtains the following for the porosity in the partially saturated equilibrium condition:

$$\Phi_0 = \Phi_d - \frac{\rho_d}{\rho_w} w_0 \qquad\qquad (D.15)$$

D.5 Maximum re-saturation via vapour in the gas phase

The equations derived in Chapter D.4 also apply analogously to the state of maximum re-saturation via water vapour. The index 0 merely has to be replaced with the index max. Here, porosity has reduced to its minimum value Φ_e. From equation (D.15), this results in the water content at maximum re-saturation via water vapour w_{max} as

$$w_{max} = (\Phi_d - \Phi_e)\frac{\rho_w}{\rho_d} \qquad\qquad (D.16)$$

The application of equation (D.16) can be further simplified with the help of equation (D.9) by eliminating the dry porosity:

$$w_{max} = \rho_w\left(\frac{1}{\rho_d} - \frac{1}{\rho_s} - \frac{\Phi_e}{\rho_d}\right) \qquad\qquad (D.17)$$

The maximum water content that can be achieved via water vapour is thus a function of the dry density and the final porosity. The maximum bentonite density ρ_{max} follows by the insertion of w_{max} from equation (D.17) in equation (D.11)

$$\rho_{max} = \rho_d + \rho_w\left(1 - \frac{\rho_d}{\rho_s} - \Phi_e\right) \qquad\qquad (D.18)$$

D.6　　　　Maximum re-saturation via liquid water

The state of maximum re-saturation with liquid water differs from that of re-saturation via water vapour at 100 % humidity only in the fact that in addition to the interlayers, the remaining pore space is filled with water, too. For the determination of the final density ρ_e it is therefore no longer necessary to distinguish between the pore volume and the interlayer volume:

$$V_w = V_p + V_i \tag{D.19}$$

Analogous to equations (D.17) and (D.18), the following applies for the final water content

$$w_e = \rho_w \left(\frac{1}{\rho_d} - \frac{1}{\rho_s} \right) \tag{D.20}$$

and for the bentonite density at full saturation

$$\rho_e = \rho_d + \rho_w \left(1 - \frac{\rho_d}{\rho_s} \right) \tag{D.21}$$

For conversion purposes, the conditional equations for the dry density as a function of the final saturation and the final water content, respectively, i. e. the inverse forms of equations (D.20) and (D.21) are of interest:

$$\rho_d = \frac{\rho_s \rho_w}{\rho_s w_e + \rho_w}, \tag{D.22}$$

$$\rho_d = \frac{\rho_e - \rho_w}{\rho_s - \rho_w} \rho_s \tag{D.23}$$

The interdependencies (D.20) and (D.21) are shown in Figs E.3 and E.2.
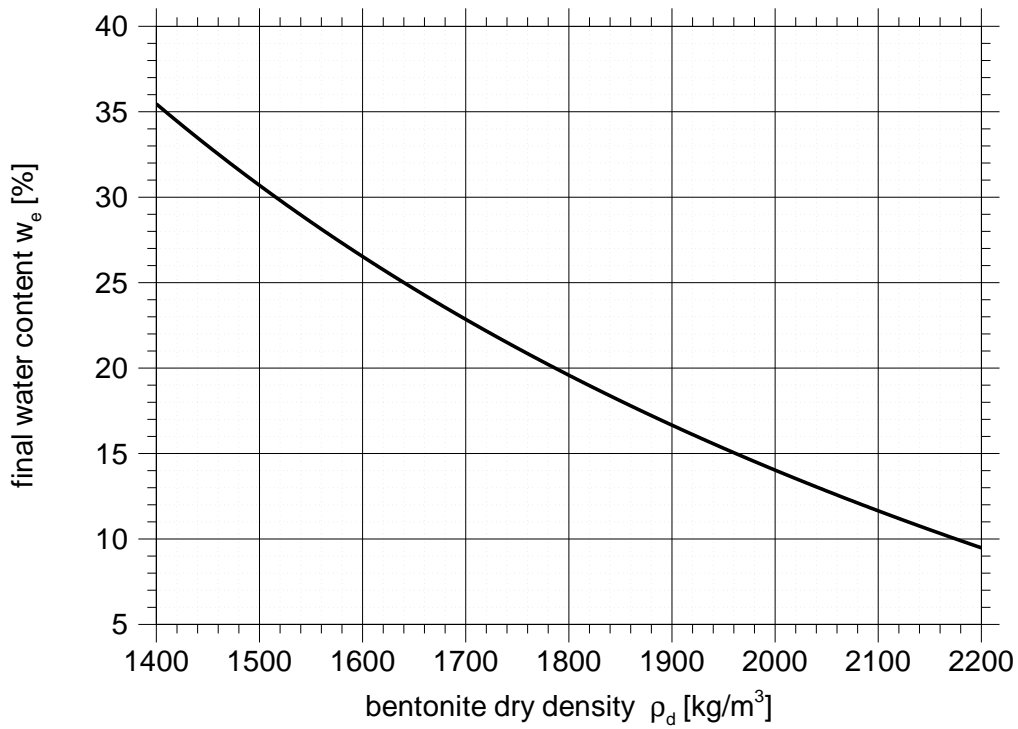
Fig. D.2   Solid-matter-related final water content as a function of the dry density
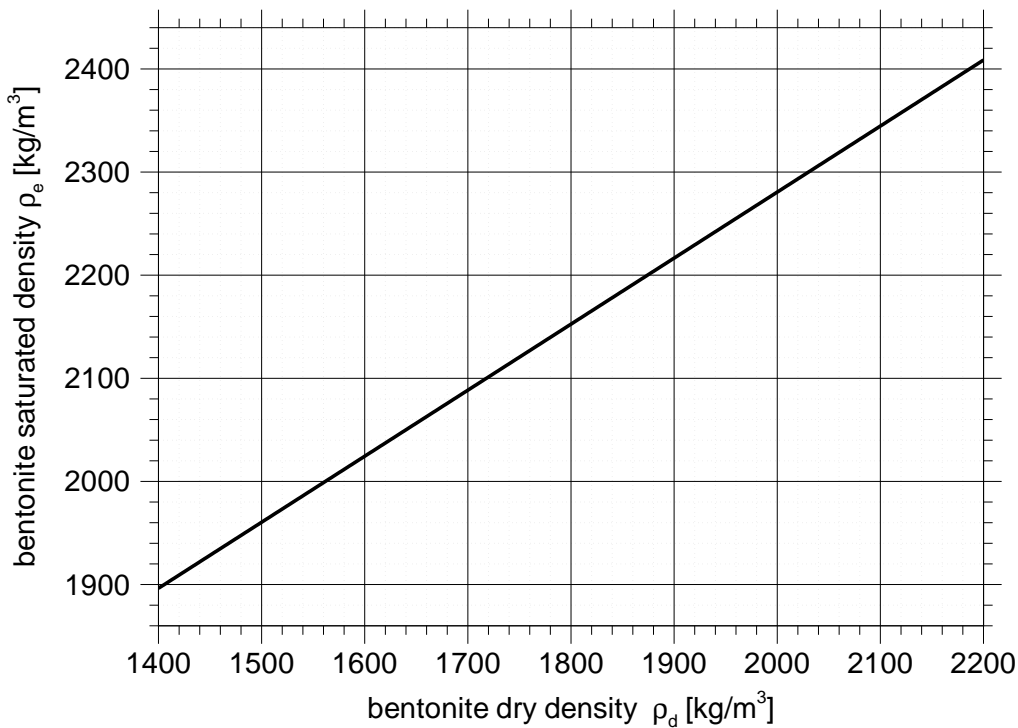

Fig. D.3   Saturation density as a function of the dry density

D.7 Conversions

D.7.1 Water content

For simplification it happens frequently that in laboratory measurements the water content is not related to the mass of solid matter but to the mass in air-dry condition:

$$\overline{w} = \frac{m_w}{m_{w_0} + m_s} \qquad (\text{D.24})$$

The following ensues from the relation of the water contents $\overline{w}$ according to definition (D.24) and w according to definition (D.1):

$$\frac{w}{\overline{w}} = \frac{m_{w_0} + m_s}{m_s} \qquad (\text{D.25})$$

In this equation, it is possible to eliminate with the help of equation (D.24) the amount of water $m_{w\,0}$ contained in air-dry condition, thus yielding

$$w = \frac{1}{1 - \overline{w}_0}\overline{w} \qquad (\text{D.26})$$

For a transformation in the other direction, the procedure has to be applied analogously. In equation (D.25), m_{w0} is eliminated with the help of definition (D.1):

$$\overline{w} = (1 + w_0)w \qquad (\text{D.27})$$

With the help of equation (D.26), equations (D.11) and (D.15) can now be transformed for the density and the porosity of the bentonite:

$$\rho_b = \left(1 + \frac{\overline{w}}{1 - \overline{w}_0}\right)\rho_d \qquad (\text{D.28})$$

127

$$\Phi_b = \Phi_d - \frac{\overline{w}}{1 - \overline{w}_0} \frac{\rho_d}{\rho_w}$$
(D.29)

D.7.2　　Pore number and porosity

The pore number e is defined as the ratio between the pore volume and the solid-matter volume:

$$e = \frac{\Phi}{1 - \Phi}$$
(D.30)

e　-　pore number [-]

For the transformation of the equations from the preceding chapters from porosity as in-dependent variable to the pore humber, equation (D.30) has to be adapted as follows:

$$\Phi = \frac{e}{1 + e}$$
(D.31)

The connection of dry density and pore number - shown in Fig. D.4 - then ensues from equation (D.9):

$$e = \frac{\rho_s - \rho_d}{\rho_d} \quad \text{or} \quad \rho_d = \frac{\rho_s}{1 + e}$$
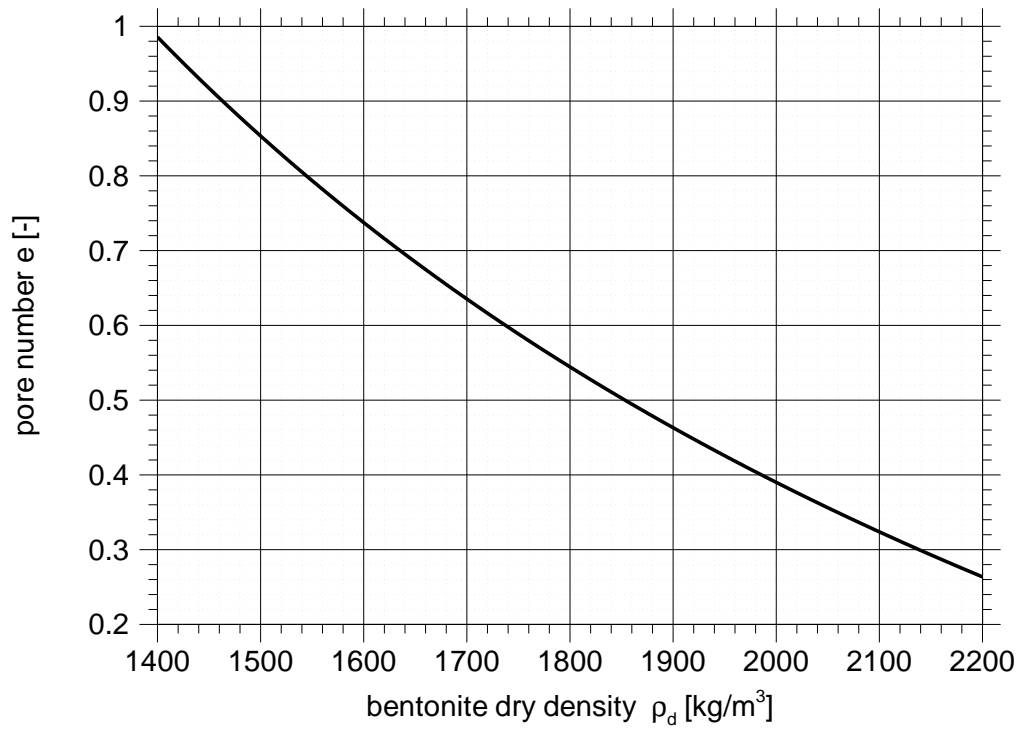(D.32)

Fig. D.4   Pore number as a function of the dry density

Appendix E Empirical diffusion model

In the simplified case of isothermal re-saturation under atmospheric pressure, the uptake of water in the one-dimensional space can be described using Fick's approach and a constant coefficient:

$$\frac{\partial w}{\partial t} + D_{emp} \frac{\partial^2 w}{\partial x^2} = 0 \qquad\qquad (\text{E.1})$$

D_{emp} -   coefficient of the empirical diffusion model [m^2/s]

w -   water content [-]

Due to the analogy to the mathematical description of diffusion processes, the coefficient D_{emp} is referred to as "diffusion coefficient" even though the approach is purely empirical. This relation is generally accepted as the values determined for the coefficient lie within a narrow range between $1 \cdot 10^{-10}$ m^2 and $3 \cdot 10^{-9}$ m^2:

- $2.2 \cdot 10^{-10}$ to $3 \cdot 10^{-10}$ m^2 [3],
- $3.4 \cdot 10^{-10}$ m^2 [28],
- $3.5 \cdot 10^{-10}$ m^2 [8],
- $1 \cdot 10^{-9}$ m^2 [37], and
- $1 \cdot 10^{-10}$ to $3 \cdot 10^{-9}$ m^2 [25].

Three time-dependent parameters are of interest in connection with the re-saturation of the bentonite:

- the inflow rate,
- the amount of water contained in the bentonite, and
- the spatial distribution of the water content.

The mathematical formulation as a diffusion problem leads to the solution for a one-dimensional finite bar of the length l with an initial water content w_0 for which the water content at the inflow boundary increases instantaneously to the value w_{Rand}. Here, the outflow boundary is problematic because the water content at this place depends on the time-dependent solution.

By approximation, the solution is therefore used for a bar of a length of $2l$ where the increased concentration is assumed to occur at both ends. Subsequently, half of the system is considered, so that the plane of symmetry forms a closed boundary. For this problem there exists an analytic solution for each of the above-mentioned parameters [9]. Equations (E.2) to (E.4) apply in cases where the inflow occurs in the position $x=l$:

- water content w as a function of space and time

$$w = w_0 +$$

$$(w_{Rand} - w_0)\left(1 - \sum_{n=0}^{\infty} (-1)^n \left\{ erfc\frac{(2n+1)l - x}{2\sqrt{D_{emp}t}} + erfc\frac{(2n+1)l + x}{2\sqrt{D_{emp}t}} \right\}\right)$$

(E.2)

w_{Rand}	-	water content at the inflow boundary [-]
w_0	-	initial water content [-]
l	-	length of the bentonite body [m]

- average water content $\overline{w}$ in the bentonite body

$$\overline{w} = 1 + \left(-\frac{8(w_{Rand} - w_0)}{\pi^2}\right)\left(\sum_{n=0}^{\infty} \frac{1}{(2n+1)^2}\left\{ e^{-\frac{D_{emp}(2n+1)^2\pi^2 t}{4l^2}} \right\}\right) + w_0$$

(E.3)

and

- flow w' through the inflow boundary

$$w' = \frac{D_{emp}(w_{Rand} - w_0)}{\sqrt{\pi D_{emp}t}}\left(1 + 2\sum_{n=1}^{\infty} (-1)^n e^{-\frac{n^2 l^2}{D_{emp}t}}\right)$$

(E.4)

Glossary of symbols

A - cross-sectional area of the bentonite [m²]

B - volume of a moving body [m³]

D - diffusion coefficient [m²/s]

D_b - coefficient of binary gas diffusion [m²/s]

D_{eff} - effective diffusion coefficient on the macroscopic level [m²/s]

D_{emp} - coefficient of the empirical diffusion model [m²/s]

D_k - coefficient of Knudsen diffusion [m²/s]

D_m - diffusion coefficient on microscopic level [m²/s]

G - solution area (control volume) [m³]

$\boldsymbol{J}$ - mass flow density due to diffusion on a macroscopic level [kg/(m² s)]

J_m - mass flow density due to diffusion on microscopic level [kg/(m² s)]

J_A - mass flow density from the advection model [kg/(m² s)]

J_D - mass flow density from the diffusion model [kg/(m² s)]

K - hydraulic conductivity [m/s]

Kn - Knudsen number [-]

M - molecular weight [kg/mol]

N_A - Avogadro constant [1/mol]; $N_A = 6.02252 \cdot 10^{+23}$ 1/mol

R - universal gas constant [J/(mol K)]; $R=8.314$ J/(mol K)

T - absolute temperature [K]

T_c - temperature [°C]

V - volume [m³]

$\overline{V}_w$ - partial specific volume of water; pure water: $\overline{V}_w=10^{-3}$ m³/kg

Z - extensive state variable [?]

a - proportionality factor [(kg$_{water}$ s)/(kg$_{bentonite}$ m²)]

d - pore diameter [m]

$\overline{d}$ - expected value of the pore diameter [m]

d_{max} - maximum pore diameter [m]

d_{min} - minimum pore diameter [m]

g - acceleration of gravity [m/s²]

k - permeability [m²]

l - length of the bentonite body [m]

m_b - dry mass of the bentonite [kg]

m_w - mass of the water [kg]

$m_{w\,auf}$ - absorbed amount of water [kg]

$\dot{m}$ - specific hydration rate [kg$_{water}$/(kg$_{bentonite}$ s)]

133

$\dot{\overline{m}}_{ref}$ - reference hydration rate [kg$_{water}$/(kg$_{bentonite}$ s)]

p_g - gas pressure [Pa]

p_l - liquid pressure [Pa]

p_s - total suction [Pa]

p_{sat} - saturation vapour pressure [Pa]

p_v - partial vapour pressure [Pa]

r - mass source density [kg/(m^3 s)]

r_h - relative humidity [-]

$r_{h\,eq}$ - relative humidity in equilibrium with the water content [-]

t - time [s]

t_0 - beginning of re-saturation [s]

$\mathbf{v}$ - velocity [m/s]

v_F - propagation velocity of the liquid front [m/s]

v_f - filter velocity [m/s]

v_m - average molecular velocity [m/s]

w - water content [-]

w_0 - initial water content [-]

w_e - final water content at re-saturation with liquid [-]

w_{max} - fictitious water content at 100% relative humidity (parameter in eq. (7.9)) [-]

Δw_{max} - increment from w_{max} to the actual maximum water content [-]

w_{Rand} - water content at the inflow boundary [-]

x - distance from the inflow boundary [m]

Δx_i - progress of the front in time step i [m]

x_F - location of the liquid front [m]

z - field variable [?/m^3]

δ - molecule diameter [m]

η - dynamic viscosity [Pa s]

θ - constant fit parameter [-]

κ - weighting factor [-]

λ - average free path length [m]

Π_p - chemical potential of the vapour in the pore space [J/kg]

Π_i - chemical potential of the interlayer water [J/kg]

ρ_d - dry density of the bentonite [kg/m^3]

ρ_g - gas density [mol/m^3]

ρ_s - density of the clay particles [kg/m^3]

ρ_{sat} - partial saturated vapour density [kg/m^3]

ρ_v - partial vapour density [kg/m^3]

ρ_w - density of the liquid water [kg/m^3]

τ - tortuosity [-]

Φ - porosity [-]

Φ_0 - initial porosity [-]

Φ_e - final porosity [-]

φ - weighting factor [-]

Indices

B - cask

b - bentonite

i - interlayer

m - clay mineral

nq - non-expandable material

o - open (ref. to volumes)

p - pores of the bentonite

q - expandable material

s - solid fraction on the bentonite